POLITECNICO

MILANO 1863

SCUOLA DI INGEGNERIA INDUSTRIALE E
DELL'INFORMAZIONE

Tesi di Laurea Magistrale in
Mechanical Engineering - Ingegneria Meccanica

Verification of two Operational Modal Analysis tools on Simulated and Full-Scale OWTs

Advisor: Prof. Alberto Zasso
Co-advisor: Dr. Alessandro Fontanella

Author: **Bruno Rodrigues FARIA**
Student ID: 935930

Academic Year 2021-22

Abstract

Offshore wind turbines (OWT) are rather complex structures to dynamically analyze in terms of accessibility and load modeling. The usage of output-only methods, such as operational modal analysis (OMA), represents a powerful solution. Two OMA tools with distinct complexity levels are chosen to be validated: a simpler and partially manual tool for a single accelerometer measure (OMA Sing); and a more mathematically complex and fully automated solution, so-called Covariance driven Stochastic Subspace Identification (OMA SSI-COV). They are applied in simulated and full-scale Alpha Ventus 5MW OWTs data. The FAST model provides a great source of validation since it guarantees OMA strong assumptions of linearity and white noise excitation. The OMA tools aimed to identify the closely spaced fore aft (along wind) and side to side (cross wind) tower bending modes. Significant different damping orders of magnitude are observed for the orthogonal modes in both extraction methods. Moreover, the automated solution presented a worsened identification performance for highly damped responses, with evident larger variability for above rated wind speed seeds. The procedures pursued in the given thesis is based on the National Renewable Energy Laboratory (NREL) OC5 project procedures. From the FAST model verification and tuning to the load cases (LCs) generation, the methodology provided the means to validate the OMA tools and identify the tower modes.

Keywords: Offshore Wind Turbine (OWT), Operational Modal Analysis (OMA), FAST model, full scale data, Single Accelerometer method (OMA Sing), Covariance driven Stochastic Subspace Identification method (OMA SSI-COV), along wind and cross wind tower motion

Abstract in Lingua Italiana

Le Turbine Eoliche Offshore (OWT) sono strutture piuttosto complesse da analizzare dinamicamente in termini di accessibilità e modellazione del carico. L'utilizzo di soli-output metodi, come l'Analisi Modale Operativa (OMA), rappresenta una soluzione potente. Due strumenti OMA con livelli di complessità distinti sono scelti per validazione: uno strumento più semplice e parzialmente manuale per l'accelerometro singolo (OMA Sing); e una soluzione matematicamente più complessa e completamente automatizzata, la identificazione Stocastica del Sottospazio guidata dalla Covarianza (OMA SSI-COV). Sono applicati in dati delle Alpha Ventus 5MW OWT sia simulati dati che su larga scala data. Il modello FAST fornisce un'ottima fonte di convalida poiché garantisce i OMA forti ipotesi di linearità ed eccitazione del rumore bianco. Gli strumenti OMA vengono applicati con l'obiettivo di identificare i vicini modalità di vibrazione della torre di prua a poppa (lungo vento) e da lato a lato (vento trasversale). Si osservano significativi diversi ordini di grandezza di smorzamento per le modalità ortogonali in entrambi i metodi di estrazione. Tuttavia, la soluzione automatizzata ha presentato un peggioramento delle prestazioni di identificazione per una risposta altamente smorzata, con un'evidente maggiore variabilità per i semi di velocità del vento superiori a quelli nominali. La metodologia perseguita nella tesi si basa sulle procedure del progetto OC5 del National Renewable Energy Laboratory (NREL). Dalla verifica e messa a punto del modello FAST alla generazione dei casi di carico (LC), fornendo i mezzi per convalidare gli strumenti OMA e identificare le modalità della torre.

Parole chiave: Turbina Eolica Offshore (OWT), Analisi Modale Operativa (OMA), modello FAST, dati a fondo scala, metodo dell'accelerometro singolo (OMA Sing), metodo di Identificazione del Sottospazio Stocastico guidato dalla Covarianza (OMA SSI-COV), movimento della torre vento lungo e trasversale

Contents

Introduction

The present master thesis is a work that has been carried out at Politecnico di Milano, in the Mechanical department - Wind Energy section.

OWTs represent a great technological solution toward the green energy grid transition. This thesis work aims to further allow the extraction of meaningful data from operating wind turbines and the analysis of relevant tower modal parameters.

OMA tools have been widely used in civil engineering applications however, there is still a research gap on their limitations and capabilities when applied to OWTs. Two different OMA methods are sought to be validated: OMA Sing as a partially automated solution, presenting a classical peak-picking routine and an optimized version; and OMA SSI-COV as a fully automated method with more complex identification. FAST model data and full-scale measurements of the 5MW OWTs from Alpha Ventus wind park are identified. The usage of FAST model provides an extra source of proof to the OMA performance as the stationarity of the load excitation is numerically guaranteed and there is no measurement noise included.

In parallel to that, many wind simulation standards do not distinguish between recommended total damping values for tower orthogonal direction modes [1]. Such assumption should be further studied since different levels of damping could play a major role in the OWT's controller strategy and overall fatigue life. The along wind and cross wind closely spaced tower modes will be the focus of the OMA identification tools.

1 | Researching Gaps, Objectives and Methodology

In this chapter, researching gaps in the track of OWT's modal identification will be exhibited, which inspired this thesis to contribute with meaningful results, as shown in Sec.1.1. In order to properly meet the proposed objectives and answer the questions, a stepwise procedure of research is mandatory. In Sec.1.2, the methodology generated to achieve a robust work is explained in detail. Furthermore, in order to simplify the understanding of the thesis structure, in Sec.1.3, the chapters' content are overviewed.

1.1. Motivations of the work

Meaningful insights should be chased from available database of several operating wind park all over the world in order to push and achieve remarkable technologically-improved OWT designs. An appealing track into the Data Analytics of large structures database is the extraction of modal parameters through operational modal analysis (OMA) tools, which do not depend on techniques to artificially load the structure as in many classic modal analysis [2]. The identification of main parameters as eigen frequencies and modal damping from OWTs could lead to a better understanding of steady and unsteady aerodynamics on the response motion, their consequent aerodynamic damping contributions and therefore more efficient health monitoring campaigns and controller strategies.

However, the extraction of reliable OWT's modal parameters is quite challenging. Identifying modal parameters, as the damping ratio, showed to be rather complicated in several studies due to its significantly bias on the operational conditions, such as wind speed, vibration amplitude and rotor speed. As discussed in Ch.3, one of the principal assumptions that has to be respected to perform OMA is the zero mean Gaussian white noise load assumption [3]. Long recording times on offshore

installations, necessary for the identification of low frequency modes, is probably linked with a compromise to the stationary nature of the excitation, as meteorological conditions are often changing (check Fig.5.7). The question that submerges is: are the OMA tools chosen in this thesis able to properly identify the OWT's modes, even though the load assumptions can not be fully guaranteed? This thesis works aims to validate two OMA techniques, with different degrees of complexity, allowing the identification of relevant modal parameters from operating OWTs.

In the same direction, a broad study on the reliability and principal maintenance features of a state-of-the-art 2MW WT was pursued by the Community Research and Development Information Service (CORDIS-EU) [4] and one of the conclusions taken was that the tower had the highest relative component cost on the project at 28.4%, followed by the blade at 24.9% and the gearbox at 14.5%. The understanding of the dynamic excitation forces and their respective stress applied to the tower become essential whether costly efficient and longer lifetime designs are pursued.

More than that, in 2013, a novel work [5] concluded that the orthogonal tower bending modes, along wind and cross wind, had similar eigen frequencies but presented discrepant damping ratio result, together with different OMA identification variability (performance criterion). The same was found in [1], emphasizing the lack of standard recommendations, for simulation purposes, on the distinguished tower damping ratios based on the direction. Understanding the difference between along wind and cross wind modal parameters dependence on the wind speed ought to be more researched. Can the chosen OMA tools distinguish this closely frequency-spaced orthogonal modes? Furthermore, in the case of Alpha Ventus OWTs, along wind and cross wind motion present significant different damping ratios? The confirmation of a lower level of cross wind damping for the tower could provide good insights and encourage solutions aiming to decrease fatigue stresses [6] and improve power control strategies. On the other hand, along wind motion higher damping ratio values and variability have to be discussed in more detail. Is there a limitation on the selected OMA tools for along wind motion damping ratio extraction? If there is a limitation, is the restraint related to specific operating conditions or are the chosen OMA tools intrinsically limited to identify highly damped modes?

1.2.   Methodology

This thesis work aims to address the given researching gaps and questions introduced in Sec.1.1. For that, a methodology is sought to be developed in order to allow the modal identification validation, while generating relevant results and a well-structured process that could be applied to a generic OWT.

The validation of the OMA tools is a rather complex task, depending on many uncontrollable features as wind conditions and strong assumptions, which will be discussed in detail in Sec.3.1. One of the solutions taken was to apply the chosen OMA tools on both a numerically simulated model and full scale measurements. The first guarantees OMA assumptions and avoids measurement's noise and unpredictable turbulent stochastic behavior. The second puts the OMA tools to proof on real data, which is the essence of output-only techniques, but also points to understanding their performance when OMA wind load assumptions are not completely respected. First, the Av04 FAST model has to be dynamically validated, following the OC5 Phase III [7] standards of performance. The real wind measurements and accelerations records are selected from Alpha Ventus RAVE database. These datasets is quality-checked in Sec.5.3 and in Sec.5.4.

Concerning the OMA tools selection, two OMA techniques were chosen in this thesis. A partially automated solution that considers only one measuring point and peak-picking based, the OMA Sing, and a fully automated and more mathematical complex solution that considers several measuring points, the OMA SSI-COV. Both have been previously validated in the analysis of bridge dynamics [8]. For the sake of robustness and quantitative comparison, before applying the OMA tools, a classical mean logarithmic decay (MLD) method is performed in specific Av04 FAST load cases.

The overall OMA validation methodology is based on a stepwise increase of complexity procedures, from the manually MLD method, to the partially automated OMA Sing and finally the fully automated OMA SSI-COV.

In order to extract meaningful tower modal parameters on both along wind and cross wind motion, while including the effect of lightly and highly aerodynamic damped responses, the OMA tools were applied in below and above rated wind speeds LCs, based on OC5 Phase III [9]. This should endorse the analysis of the two orthogonal modes sensibility to different wind conditions and also check the OMA techniques' performance.

1.3.   Outline of the thesis

The thesis is segmented as described below:

Chapter 1. The structure of the thesis is introduced. The research gaps that generated the key questions and the thesis motivation are illustrated. Afterwards, the subsequent work methodology is commented, stating how the missing researching results ought to be addressed.

Chapter 2. An overview of the wind energy on current and forecasted European power grid generation is carried out, while trying to answer main questions: How much wind energy could contribute to the green energy transition? And which design approaches could produce significant technological improvements?

Chapter 3. A literature review is pursued on significant OMA usages, limitations and main assumptions for OWT. The two OMA techniques chosen on the given thesis have their respective routines sequentially explained.

Chapter 4. The aeroelastic and wind simulation tools are presented together with NREL OC5 pursued code validation methodology and the stepwise model check of the Av04 FAST model.

Chapter 5. The Alpha Ventus wind park capabilities are exhibited, followed by its OWTs detailed description. In agreement to OC5 methodology, the wind seeds are checked and acceleration records of Av07 are selected.

Chapter 6. The modal parameters extracted from Av04 and Av07 tower bending modes are shared and discussed. Besides OMA Sing and OMA SSI-COV, a classical Mean Logarithmic Decay (MLD) method is applied in Av04 model for the sake of a quantitative reference.

Chapter 7. Relevant conclusions, uncertainties and future work possibilities are summarized in the last chapter.

2 | Wind Energy Novelty

A brief introduction to the wind energy current and forecasting capabilities will be shared in this chapter. The green power grid transition is imperative to achieve a more sustainable world. Principal goals from European governmental campaigns are shared in Sec.2.1, calling attention to the wind energy's protagonism, in Sec.2.2. The offshore solutions' optimistic trends are inevitable. Several advantages are described in Sec.2.3, together with consequent inherent challenges in their design and O&M.

2.1.   Global Energy Transformation

Several coalitions in Europe and all over the world have been formed in the past decades to efficiently break the impacts of climate change. At the Paris Agreement, in 2016, 195 Parties accepted to develop, in a 5-year cycle, nationally determined contributions (NDCs), describing which actions will be locally made to reduce their Greenhouse Gas emissions, and as a consequence, achieve the major goal of limiting global warming to 1.5 degrees Celsius. European Green Deal in 2019 similarly committed to such a goal but focused on the future European energy grid composition, becoming a climate-neutral continent by 2050.

The necessity to strongly invest in the green energy transition is a global consensus. The beneficial outcomes are many and as deeply discussed by the International Renewable Energy Agency (IRENA), in its Global Energy Transformation paper of 2019 [10], can be split into 5 main groups.

Renewable Energy Cost Reduction Unfortunately, green energy is still less affordable compared to fossil derived fuels. Government pressure and investment packs can influence it. This has already been done. The cost of electricity for onshore wind parks has reached and even crossed in some cases the lower end of the fossil fuel cost. Solar photovoltaic energy's cost declined by 77% from 2010 to 2018. As for the onshore wind parks, in 2017 there was an promising

35% lower cost than in 2010;

Air quality improvement Year by year, the world population suffers from different diseases caused in part by the energy sources mismanagement. Air pollution plays a big role in the public health crisis. Renewable energies improve the air quality of cities, preserve the environment and lead to considerable savings in the health system. Prevention is better than cure.

Decrease of Carbon Emissions If the Paris Agreement is to be respected, wider energy-related emissions reduction is needed. At least 70% compared to current levels. In which way energy is generated has a big impact on it.

Universal and Accessible Energy In countries where there is a strict dependence on the importation of fossil fuels, renewable sources can provide a clean, constant and safe alternative. The green grid spread to rural areas represents a further great strategy towards weakening local inequalities inside a territory.

Socio-Economic Benefits Renewable energy is a booming market, characterized by high availability of job offers, in search for skilled workers and dense background. That is a solid opportunity to develop a country's economy by generating technological innovations.

2.2.   The Role of the Wind Energy

IRENA report extensively and numerically argues the relevance of Wind Energy in a short and long period transition. Its capacity can be easily scaled-up with the current and mature applied technology. The forecasted wind share on the total global power generation need to reach 35-40% by 2050 2.2, as also found by the World Wind Energy Association (WWEA), if the cited coalitions want to meet their objectives. By 2050, renewable energies should account for 86% of the total electricity generation in the European Union (EU). Out of those, wind energy alone would share 40% and be the leading source.

Even before foreseeing it, analyzing the massive recording database provided by Eurostat, the statistical office of the EU, it can be said that a relevant attention not only to Renewable Energy, with an 60% capacity share increase in European Union from 2011 to 2020, but especially to Wind Energy has already been drawn in the past decade, as shown in 2.1. Wind and Solar Energy capacity rise at a constant pace, with a slight advantage from the first over the second.
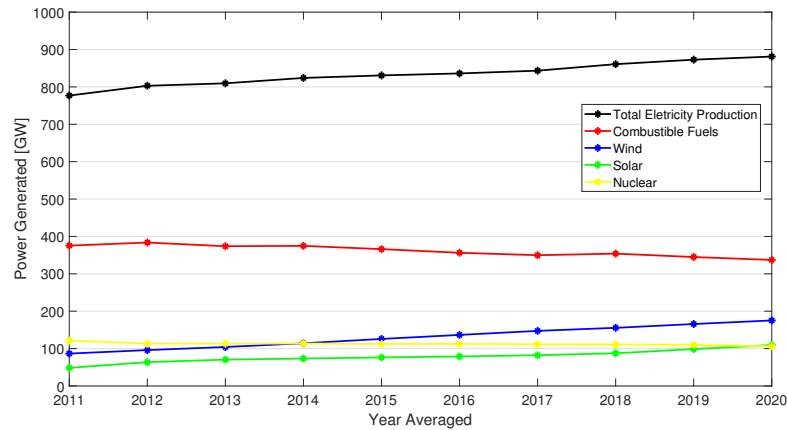
(a) Power Generation from Renewable and Combustible Fuels sources.
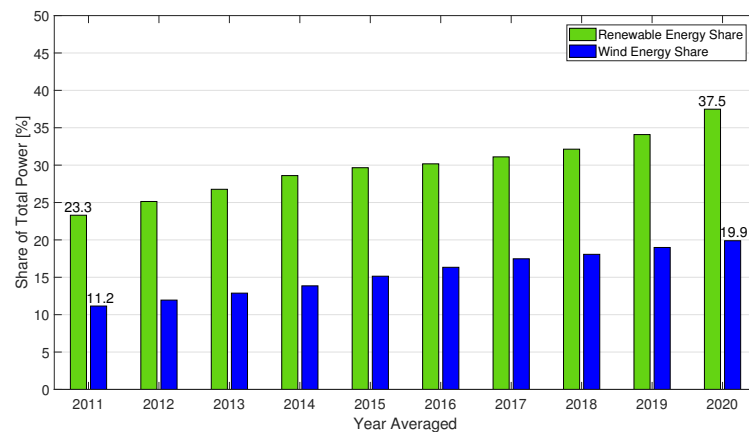
(b) Renewable Sources Share in Electricity.

Figure 2.1: Eurostat Database for the UE (27 countries) on the past decade.

Some countries can be discussed individually, as an extra source of comparison and proof of Wind Energy potential growth. Italy presented, in 2020, 10.8GW of operating capacity, a 57% increase facing 2011. Germany 62.2GW, an even sharper development of 117% in less than a decade. Even in early cases where the domestic electricity in 2011 was mainly composed of renewable energy as for Norway (90-100%) and Sweden(50-70%), gross financing on Wind Energy installations resulted in a 3.9GW (668% gain) and 9.9GW (260% gain) absolute values in 2020. Denmark, in 2019, generated 47% of the entire supplied electricity from wind, on a year-round average. Surprisingly, for a particular windy day, Denmark produced 140% of its electricity needs with wind energy, and thanks to robust interconnections with neigh-

boring countries, sold the remaining energy to Norway, Germany and Sweden.
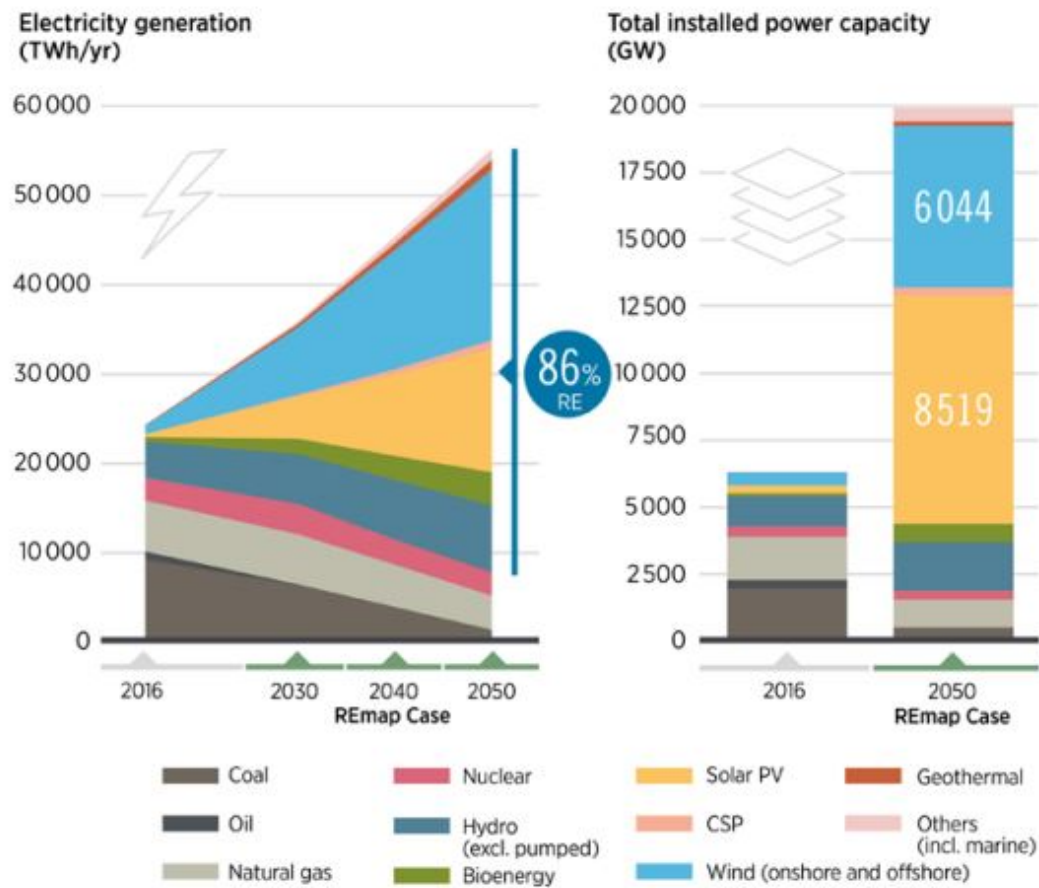

Figure 2.2: IRENA forecasting of Power Grid Composition (figure from [10]).

The positive capacity trend of onshore and offshore wind energy has never been so sharp all over the globe. Gansu, the largest onshore wind farm in the world, located in China, has an enormous planned capacity of 20GW, of which 7.96GW are already operating. In the United Kingdom, Hornsea Project One is the largest OffShore wind park at 1.22GW, formed by 174 Siemens Gamesa OWT of 7MW. Both off-shore and onshore technologies can represent optimum solutions to different scenarios.

2.3. The Offshore Technological Trend

The enthusiasm for offshore solution, however, is inevitable and it may have major technological advantages. More than that, in several cases, onshore design and projects are limited not only by technological boundaries but social acceptance and logistical challenges. Having nearby residents set numerous regulatory conditions. Transportation constraints inhibit onshore turbines in some locations to reach the size of offshore machines, of which components such as the individual blades can not be disassembled into smaller modular sections and need to be transported as one solid piece. The sizing of a WT on the conceptual design has a crucial role. Converting Kinetic Energy from wind to electricity (Electric Power) is the essence of WTs. Larger the rotor diameter, the higher the area, and by so, the higher the potential captured wind, the higher the power production, and the lower can be the cost of electricity generated as the literals economies of scale appear. Furthermore, pushing the limits of hub height improves the operating conditions of a WT, framing higher average wind speeds over the rotor and less turbulent flows. Empirically speaking, big WTs present greater capacity factors, the ratio of average power output and maximum power capability, compared to smaller ones. Due to greater regularity and strength of sea winds, offshore solutions once again stand out. In the USA, as shown by the Center for Sustainable Systems of the University of Michigan, the capacity factors of on-land applications range from 0.26 to 0.52, with a fleetwide average in 2019 of 35%. As for OffShore winds, the capacity factors for 2022 new projects are expected to reach 51%. Such differences expose some of the reasons why the OWTs are rapidly increasing their predominance in the market. As IRENA reported in Fig.2.3, offshore WTs will keep an approximate double to triple multiplier factor on rated power generation in front of onshore WTs by 2022-2025.
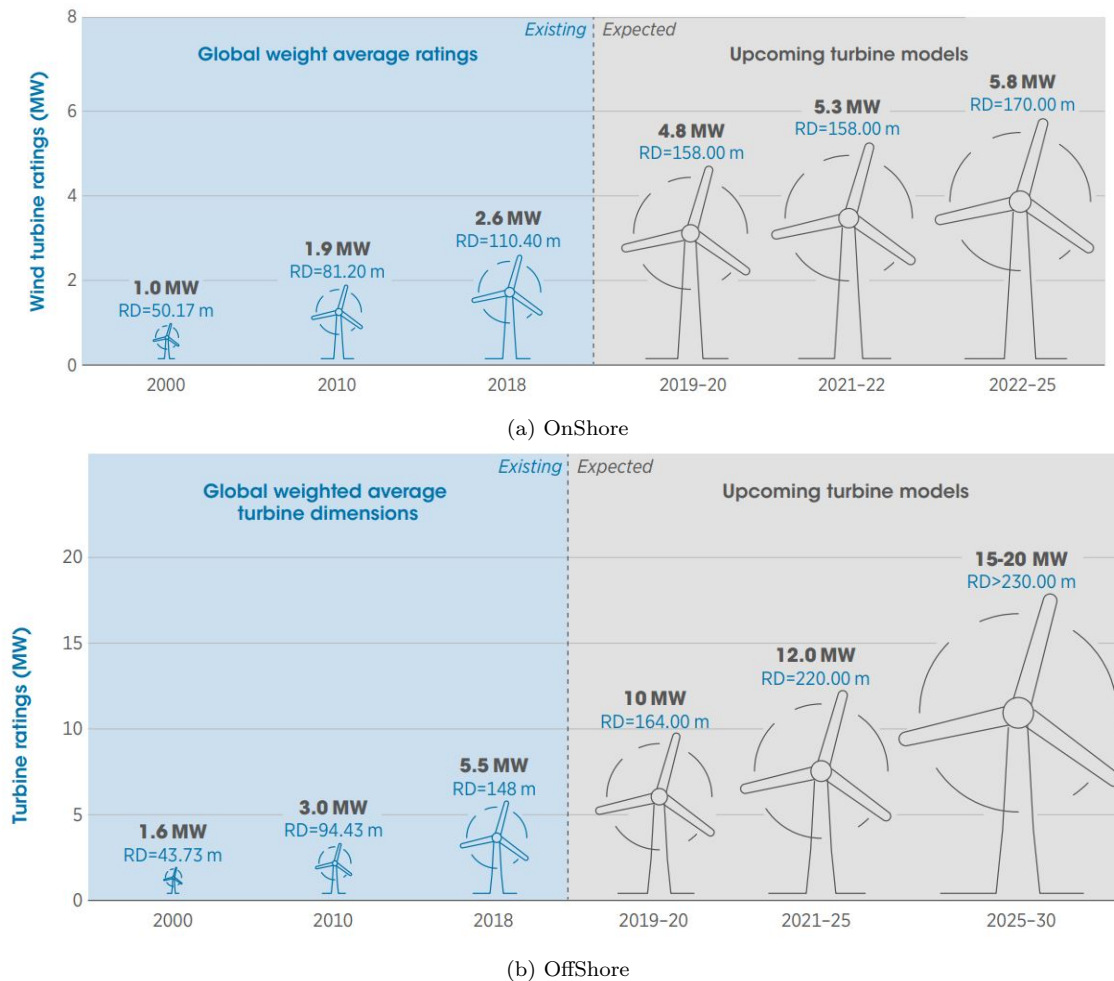
(a) OnShore

(b) OffShore

Figure 2.3: Rotor Diameter and Power Capability over the years (figure from [10]).

Once the focus narrows down to OffShore applications, there are 2 main categories to be commented, the Fixed-Bottom and the Floating OWTs foundations. The applicability of both depends firstly on the depth conditions of a given potential wind park. It is normally considered shallow waters, coast areas having depth conditions up to 50m, and deep waters, where the depth ranges from 50 to 100m.

Fixed foundations provide simpler and cheaper solutions for the lower end of shallow waters (up to 30m). China, for example, has around 42% of its total wind potential of 3860GW on water depths below 50m. Proving that there is a lot of energy demand to be suited from this OWT foundation category. Nevertheless, in UE, the shares of OffShore wind resources requiring a floating facility (depth of 60m or more) is of around 80%, as data clustered by Carbon Trust in 2015 has concluded. In the case of Norway, the director of the Bergen OffShore Wind Center (BOW), Finn Gunnar

Nielsen, emphasized that their ocean areas are predominantly deep waters and the path of moving towards floating solutions is mandatory to reach neighbor countries' achievements. Some of the most common foundations technologies in usage are Spar-Buoy, Tension Leg Platform and Spar-Submersible. Moreover, floating foundations often offer more ecologically driven designs, since there would be less-invasive activity on the seabed during the installation.

Anyhow, regardless of which foundation is chosen, offshore installations in overall introduce many accessibility limitations and consequently O&M challenges. Optimized designs and controller strategies are mandatory to decrease the LCOE, which is affected by high commissioning and O&M campaign costs.

The cutting-edge development of innovative, costly accessible and longer-lifetime OWT is intrinsically dependent on the availability of a huge amount of data. From meteorological, oceanic, structural to acceleration records. Data processing and analytics will only generate useful results in case all those data sets are used in parallel and are exclusively reliable. Light Detection And Ranging (LIDAR) is an example of technology that has been widely improved over the past years and it is the core of many research fields to guarantee the legit measure of wind parameters, like speed and direction. LIDAR is quickly becoming a wind industry standard, allowing the measuring and modeling of turbulent wind flow to be used in post simulations.

3 | Operational Modal Analysis

In this chapter, a literature review pointing out the state-of-the-art OMA technique usage is carried out in Sec.3.1. Followed by a more deeply description of the chosen OMA Sing in Sec.3.2 and OMA SSI-COV in Sec.3.3.

The usage of different OMA methodologies is a good practice, providing a more robust and engineering-aligned cross-analysis of the identified modal parameters.

3.1.   Literature Review

In many cases, vibrating structures turn out to be complex systems to be instrumented with different sensors. Acceleration (output) and excitation forces (input) recordings are necessary for the full description of standard modal analysis, which aims to identify fundamental modal parameters. However, for extremely large structures whether in civil engineering (bridges, dams and highways) or in aeromechanical engineering (horizontal and vertical rotor axis wind turbines), performing experimental modal tests, such as free-vibration test and hammer test, can be a challenging task.

One of the these modal analysis' classical methodologies was applied on a Vertical Axis Wind Turbine (VAWT), the step-relaxation technique, as shown in [11]. Results were satisfactory. Experimental and model data were coherent, with a reliable range until the second mode of vibration, as shown in Tab.3.1. The real and scaled VAWT analyzed in the paper can be seen in Fig.3.1. The same verification was pursued on a Experimental Modal Analysis (EMA) technique, as shown in [12] and a vast of well-revised papers.

(a) The 110-m tall E´ole wind turbine, photographed in 1986

(b) Sandia 2-m VAWT with instrumentation

Figure 3.1: VAWT analyzed with step-relaxation method (figure from [11]).

Mode Shape Description	Step Relaxation (Hz)	Wind Excitation
First tower out-of-plane	0.63	0.63
First tower in-plane	0.74	0.73
Second tower out-of-plane	0.93	0.94
Second tower in-plane	1.38	1.39
Third tower out-of-plane	1.79	-

Table 3.1: Comparison of modal frequencies using step relaxation and wind excitation (figure from [11]).

Nevertheless, there are notable limitations, for example, on the step-relaxation technique when used in the analysis of OWT. In the presented case of the VAWT, the device had to be reloaded for each input force given, the whole prototype being moved down to parked condition, an extremely time-consuming task. Such use of resources is unreachable in terms of time, money and manpower for offshore devices. *OMA* is used precisely in these particular conditions, in which artificially exciting the structure is an impediment or measuring the ambient forces is not an affordable option, such as aerodynamic loading coming from wind and gust phenomenon. Identifying the modal properties based on acceleration data collected when the structure itself is

under operating conditions is one of the main capabilities of the cited method. The usage of more convenient and efficient techniques was possible mainly because of the parallel progress of accelerometers technologies, being more sensitive to low-frequency ranges and noise, and the development of novel methods, in the time and frequency domain, parametric and non-parametric, of modal identification [13].

Again in [11], the application of OMA was put to the proof. This time in a vertical axis wind turbine (VAWT) model of 34m height, using simulated 9m/s turbulent average wind speed and 15% turbulence intensity. The results presented in Tab.3.2 reveal acceptable accuracy when reproducing modal frequencies and specified damping values. Such a positive conclusion raise the confidence in the application of OMA for operating WTs.

Mode Shape Description	Frequency (Hz)		Damping (%)	
	Simulated	NExT	Simulated	NExT
First flapwise anti-symmetric	1.27	1.31	0.2	0.4
First flapwise symmetric	1.35	1.32	0.2	0.3
First blade edgewise	1.59	1.59	0.3	0.3
First tower in-plane	2.02	2.01	0.3	0.4
Second flapwise symmetric	2.43	2.44	0.4	0.5
Second flapwise anti-symmetric	2.50	2.50	0.4	0.4
First tower out-of-plane	2.80	2.80	0.3	0.3
Second tower in-plane	3.46	3.45	0.5	0.4

Table 3.2: Comparison of modal frequencies and damping values computed with NExT and traditional techniques (figure from [11]).

Please note that NExT stands for Natural Excitation Technique, being at the report [11] a synonym of OMA, a term yet to be widespread.

OMA tools have been successfully applied for non-destructive assessment and health monitoring of large civil infrastructures such as tall buildings and long-span bridges, where aerodynamics loading plays a relevant role in the vibration response [14–17]. More recently, the wind-induced vibrations of the Lysefjord Bridge, located in South-Western Norway, were studied and conducted with both anemometers and Doppler wind LIDAR system in parallel to multiple accelerometers recordings [18]. The last cited work has a significant influence and highly motivated the given thesis methodology.

Promising results were achieved in [5], this time specifically into the distinguished fore aft and side to side tower bending modes of a wind turbine.
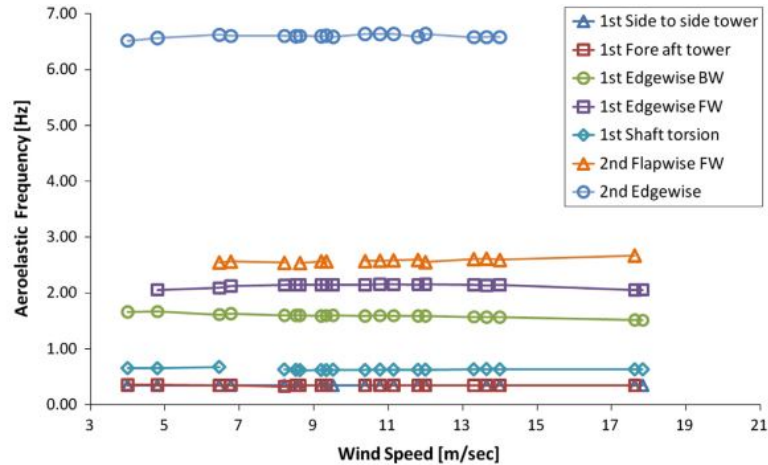
(a) Aeroelastic frequency ratios of the 1st tower mode.
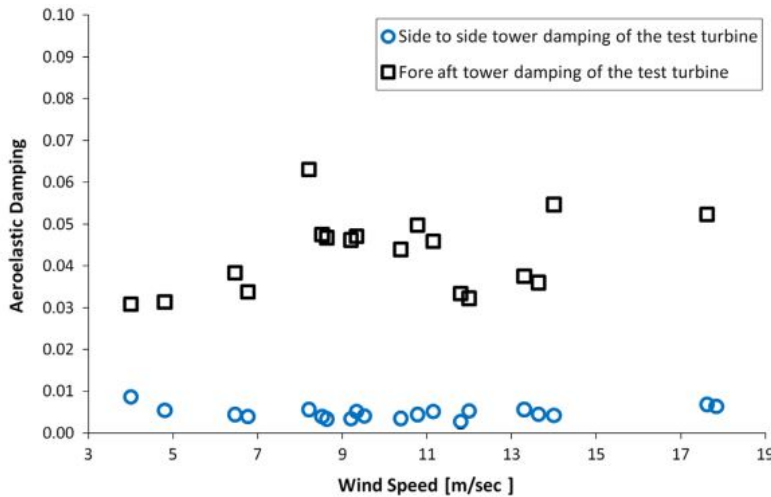
(b) Aeroelastic damping ratios of the 1st tower mode.

Figure 3.2: First Tower Bending Mode using OMA SSI-COV for Nordex N80 WT with rated power of 2.5 MW, located at the Energy Research Center of the Netherlands.

As shown in Fig.3.2, fore aft and side to side damping ratios have different orders of magnitude, highlighting the aerodynamic damping contribution to the tower response. It is commented by the author of the given work that analyzing the fore aft motion came to be more challenging than expected, since in measured samples, mean wind speed tends to slowly change, turning the fore aft motion recording into a varying average time series, compromising OMA assumptions. Side to Side damping ratio showed to be independent of the wind excitation, constant and below 1%, mainly formed by structural contribution from the tower. As for along wind, the

behavior is different. It is challenging to identify a pattern and a scatter distribution is produced. Such behavior is sought to be further studied in Ch.6.

As for any methodology, *OMA* presents advantages and disadvantages. The damping identification, for example, is commonly perceived to be amplitude-dependent, and ambient vibration levels for OWT ought to be at low levels. A major review has been conducted on the robustness of damping estimation for OWT towers while using OMA in [19]. Different relevant features were covered as the effect of signal noise, the effect of measurement duration, the effect of vibration amplitude and the effect of the stationarity of the response. Further on, these parameters will be taken into consideration when running the LC presented on Sec.3.2.

Finally, considering all of these four factors, the investigation concluded that the Covariance driven Stochastic Subspace Identification (COV-SSI) OMA algorithm is a strong candidate for the estimation of damping for OWTs, due to its lower mean squared error in comparison to the other 2 methodologies, as shown in the 2018 report [19]. Moreover, *SSI-COV* presents a considerably lower computational time, since it can be applied data-reduction with the Fast Fourier Transformation (FFT) An only output-data method is very advantageous in several scenarios. However, it should be noted that OMA SSI-COV relies upon strong assumptions that must be satisfied, and if not, can negatively impact results reliability [20].

The first regards the model *linearization.* Inertia, stiffness and damping are assumed to be in the linear elastic zone of the stress-strain diagram. For all the wind speeds studied, the model is assumed as a linear time-invariant dynamic system. This works well for small amplitude, however high wind speeds may excite large amplitudes and, as known, the structural damping ratio is amplitude-dependent.

Secondly, as presented in section 1.1, one of the strongest assumptions that should be satisfied for the application of OMA covariance methods is the *white noise loading.* Only by this means, the decomposition of the response covariance generates an estimation of the free vibration response (IRF), ensuring the conservation of the vibration record information and successive modal parameters identification, as will be explained more in detail in section 3.3. The white noise Gaussian mathematical proof will be extended below, based on the book [21].

- **White Noise Assumption Derivation**

Starting from the consideration of a **linear system** characterized by the impulse response function, it is possible to relate

$$h(t) \leftrightarrow H(s) \tag{3.1}$$

where $H(s)$ is the Laplace Transform and it is usually seem as the associated Fourier transform $H(i\omega)$. Such a function can be used to represent the energy of the system $g(t)$ in the frequency domain as the time function

$$g(t) \leftrightarrow |H(i\omega)|^2 = H(i\omega)H^*(i\omega) \tag{3.2}$$

using the time reversal and the convolution property

$$g(t) = h(-t) \circledast h(t) \tag{3.3}$$

For a single-input-single-output (SISO) scenario, output and input are related as in

$$y(t) = h(t) \circledast x(t) \tag{3.4}$$

similarly, on multiple -input-multiple-output (MIMO) case

$$y(t) = \mathbf{H}(t) \circledast \mathbf{x}(t) \iff \tilde{\mathbf{y}}(s) = \tilde{\mathbf{H}}(s)\tilde{\mathbf{x}}(s) \tag{3.5}$$

where $\tilde{\mathbf{H}}(s)$ is the transfer function matrix.
Now, presenting basic formulations of **auto/cross correlation** and **auto/cross spectral density** functions is needed to better understand further conclusions. The cross correlation function is defined as

$$R_{xv}(\tau) = E[x(t)y^T(t = \tau)] \tag{3.6}$$

being E the summation. Otherwise, it can be defined as the inverse Fourier transform of the cross spectral density function $G_{xy}(\omega)$

$$R_{xy} = \int_{-\infty}^{\infty} G_{xy}e^{i\omega\tau}d\omega \tag{3.7}$$

More specifically, the *Parseval's theorem* gives that for the case where $\tau = 0$,

cross correlation is

$$R_{xy}(0) = E[xy^T] = \int_{-\infty}^{\infty} G_{xy}(\omega)d\omega = C_{xy} \tag{3.8}$$

being C_{xy} called the covariance matrix of the (zero mean) signal.

The next topic that shall be overviewed before going into white noise applications, is the **SISO fundamental theorem**. Considering the output spectral density as

$$G_y = Y^*(\omega)Y(\omega) \tag{3.9}$$

and using both: equation 3.4 and the transform convolution property, it is possible to formulate

$$G_y(\omega) = Y^*(\omega)X(\omega)H(i\omega) = G_{yx}(\omega)H(i\omega)$$
$$G_{yx}(\omega) = Y^*(\omega)X(\omega) = G_x(\omega)H^*(i\omega) \tag{3.10}$$

rearranging the above equation, the final fundamental theorem is found as

$$G_y(\omega) = X^*(\omega)X(\omega)H^*(i\omega)H(i\omega) = G_x(\omega)|H(i\omega)|^2 \tag{3.11}$$

Important to note that the theorem works for general signal conditions, but here the steps were simplified for the periodic type data. The complete derivation can be found in [21]. Moreover, as done for SISO, MIMO also has its fundamental theorem, with a similar derivation. Only the final formulation is shown below

$$\mathbf{G_y}(\omega) = \tilde{\mathbf{H}}(-i\omega)\mathbf{G_x}(\omega)\tilde{\mathbf{H}}(i\omega) \tag{3.12}$$

Finally, walking specifically towards the **white noise** input signal. The main concept behind it regards to the fact that the auto correlation function of an white noise is null for any τ different from zero. The so called zero mean signal presents in addition a delta function in the auto correlation response as in

$$R_x(\tau) = E[x(t)x(t+\tau)] = 2\pi G_{x0}\delta(\tau) \tag{3.13}$$

where G_{x0} is a scaling parameter. Once the Fourier transform of a delta function is equal to $\frac{1}{2\pi}$, the covariance C_x is equal to G_{x0}. However, if continuous time interval is

used, the variance would tend to infinity. *Parseval's theorem* shows that equation 3.13 is only useful if a certain frequency band with maximum frequency B is considered. The variance then could be formulated as

$$\sigma_x^2 = 2G_{x0}B \tag{3.14}$$

and directly, the spectral density function is given by

$$G_{x0} = \frac{\sigma_x^2}{2B} \tag{3.15}$$

A white noise with variance σ_x^2 in the frequency band B is given by

$$R_x(\tau) = 2\pi\frac{\sigma_x^2}{2B}\delta(\tau) = \pi\frac{\sigma_x^2}{B}\delta(\tau) \tag{3.16}$$

the δ function shall be determined as a mathematical approximation since any signal will have a correlation function with finite initial value in the case of limited area under the spectral density. In this way, the spectral matrix of a white noise inside the given frequency band B will be constant, real, positive definite and symmetric; outside the band, it will be null

$$\mathbf{G_x}(\omega) = \begin{cases} \frac{C}{2B} & \text{inside the band} \\ 0 & \text{outside the band} \end{cases} \tag{3.17}$$

In the case of all components having the same variance σ_x^2, $G_x(\omega)$ becomes a identity matrix multiplied by $\frac{\sigma_x^2}{2B}$.

Considering Eq.3.11 and applying the derivations above, it can be derived

$$G_y(\omega) = G_x(\omega)H^*(i\omega)H(i\omega) = \frac{\sigma_x^2}{2B}H(-i\omega)H(i\omega) \tag{3.18}$$

The last derivation stands for the time reversal, using the convolution property, to find the correlation function of the response as

$$R_y(\tau) = 2\pi\frac{\sigma_x^2}{2B}h(-\tau) \circledast h(\tau) \tag{3.19}$$

In conclusion, it can be said that the correlation of the response in case of **white noise loading** Eq. 3.19 is **proportional** to the deterministic correlation function

given by Eq. 3.3, in another words, is proportional to the system energy or to the **IRF**.

The application of SSI-COV method, in which the white noise loading assumption is respected, not only preserve all the signal information, but also provides the means to extract fundamental parameters from the IRF, such as eigen frequencies, damping ratio and mode shape functions, while presenting higher computational efficiency, due to application of cross correlation functions instead of time-series data direct analysis, eliminating uncorrelated noise.

It should be mentioned that on operating OWTs, principal rotor rotation modes, the so-called P-harmonics, input harmonics influence in the vibration response and could violate the assumption concerning the nature of excitation [3]. However, the first order tower bending modes of Av04, shown in Tab.4.4, are between but fairly distant from the 1P 0.2Hz and 3P 0.6Hz [9] rotation modes, and then, it would initially avoid their harmonic influences on the *OMA* usage. However, the along wind and cross wind modes present close eigen frequency values and OMA tools shall be checked whether they can distinguish each mode in Sec.3.2 and in Sec.6.3.

In the following two sections, particularities from both OMA methods chosen in the given thesis will be exploited, justifying their usage for the Alpha Ventus OWT simulated and measured data.

3.2. OMA Single Accelerometer

One of the simplest OMA methods to estimate modal parameters is based on the so-called peak-picking routine. The selection of eigen frequencies is done by identifying the peaks corresponding to the resonant frequencies from the power spectrum response.

Peak-picking methods have already been validated in many applications. Nevertheless, it requires human intervention, making it a biased tool in cases of noisy data, weakly-excited modes and relatively close eigenfrequencies, as it becomes highly subjective [8].

The chosen routine used for the modal extraction from nacelle acceleration data (sections 4.3 and 5.4) had a similar algorithm validated in the identification of modal parameters from traffic-induced bridge vibration. And now, it will be further applied to the fore aft and side to side tower bending modes. It will be named OMA-Sing in this thesis for the sake of simplicity (full MatLab code available in [22]). OMA-Sing

was developed to extract eigen frequencies and modal damping ratios from line-like structures using only one measurement point, as for the nacelle accelerometer of an OWT.

One limitation of the peak picking method is that the PSD generation leads to a frequency resolution that is limited by the choice of the PSD estimate (typically the Welch method). Different from OMA SSI-COV, where the time domain analysis allows finer characterization. The peak picking method inside OMA Sing code is an optimization of classical ones to automatize the peak selection (provided by [23]). The subroutine is based on five main steps, as described below

1. A smoothing horizon is generated, initially as unitary. The bandwidth used may be different between a low-damped structure and a high-damped mode. A more segmented bandwidth and high-maximum values were used to guarantee several peak identification. As a drawback, the computational time might has increased inefficiently. From 1 Hz to 90 Hz, containing 33 log-spaced steps.

2. The spectrum response is smoothed using the created horizon (Fast Fourier Transform (FFT) based convolution)

3. Local extrema of the smoothed data are located

4. The found local extrema is linked to the previous iterations found local extrema. In the first moment, all peaks are stored. The logic afterward is that a peak location surviving the trajectory and gradual smoothing should be selected as an eigenvalue

5. Step *2.* is rerun but now with a larger horizon

The automated peak picking method is clearly preferred due to the avoidance of extensive and subjective workload. However, manual and classic peak picking is also available in the OMA-Sing. And as shown in 3.2, the last one, had to be used in some of the simulated seeds, since the automated solution was not finding any eigenvalues around 0.35Hz, even though there was an evident local extremum in the given spectrum plot.

OMA-Sing besides presenting an automated peak picking solution as an option, also subsequently compute the auto correlation function of each modal response, finding the IRF. It fits the IRF with a decay exponential curve to estimate the damping ratio and the eigen frequency. The last one is compared to the one found by the peak picking method, and if there is an error greater than 5%, a flag is announced.

3.3. OMA SSI-COV

OMA SSI-COV algorithm function is divided into six main routine tasks (the algorithm for MatLab application is entirely available at [24]). The only two mandatory input variables are y, time series of ambient vibrations matrix [MxN] (being N necessarily greater than 1), and dt, time step [s]. The algorithm was validated and found to be accurate enough when applied on a suspension bridge dynamic response [25], focusing mainly on the temperature effect of the modal properties. Surprisingly, it also performed well for the vehicle-induced bridge vibration modes identification [26].

A brief mathematical review on the covariance-driven basis of the used SSI tool will be derived below based on refs. [8, 18, 27]. It will facilitate the understanding of the subsequent description items *1-4*.

SSI-COV routine identify a stochastic state-space model of the structure, using a discrete-time formulation

$$x_{k+1} = Ax_k + w_k$$
$$y_k = Cx_k + v_k \tag{3.20}$$

where, x is the state vector, y is the measured output, A and C are the system matrix and the output matrix respectively, and at last, w and v are both considered zero mean white noise terms of excitation.

On the so called covariance driven SSI, covariance matrix for a given shift i is calculated as

$$R_i = E[y_{k+i}y_k^T] \tag{3.21}$$

the summation will not have its index tending to infinite but to $T_s/dt - 1$. Note that R_i is a MxM matrix, where M is equal to the number of accelerometers (at Av07, $M = 5$). An important derivation is that the R_i can be factorized as

$$R_i = CA^{i-1}G \tag{3.22}$$

being $G = E[x_{k+1}y_k^T]$ the state-output covariance matrix. Equation 3.22 reveals that by decomposing the correlation matrix, it is possible to find the state-spaces matrices. The complete justification that allows the above equation to be written can be found in ref.[8].

The goal here is to estimate A and C in order to extract modal parameters. To

achieve such a goal, a block-Toeplitz matrices is built

$$T = \begin{bmatrix} R_i & R_{i-1} & \cdots & R_1 \\ R_{i+1} & R_i & \cdots & R_2 \\ \vdots & \vdots & \ddots & \vdots \\ R_{2k-1} & R_{2k-2} & \cdots & R_i \end{bmatrix} \tag{3.23}$$

The known *extended observability* and *reversed extended stochastic controllability* matrices O and Γ can be derived from the singular value decomposition (SVD) of the block-Toeplitz matrix

$$T = USV^T \tag{3.24}$$

where $O = US^{1/2}$ and $\Gamma = S^{1/2}V^T$.

The system matrix or so called state-space matrix A can be found from O as follows

$$A = O_t^+ O_b^+ \tag{3.25}$$

where $+$ stands for the Moore-Penrose pseudo-inverse; O_t and O_b are the first and last $m(i-1)$ rows of O; and i being the number of block rows of the block Toeplitz matrix.

A eigenvalue decomposition of A leads to

$$A = \mathbf{\Psi}\Lambda\mathbf{\Psi}^{-1} \tag{3.26}$$

being Λ an diagonal matrix containing the discrete-time eigen frequencies and modal damping information in terms of the eigen values λ_i, with $i = [1, 2, \cdots, m]$. $\mathbf{\Psi}$ stands for the mode shape matrix. The following derivations shall be done

$$\Omega_i = \frac{ln(\lambda_i)}{dt} \tag{3.27}$$

$$f_i = \frac{|\Omega_i|}{2\pi} \tag{3.28}$$

$$\zeta_i = -\frac{Re(\Omega_i)}{Im(\Omega_i)} \tag{3.29}$$

$$\Psi_i = Re(C)\mathbf{\Psi} \tag{3.30}$$

being Ω_i the continuous-time eigen values; f_i the modal frequency; ζ_i the damping ratio; C is the matrix containing the first m (number of poles) rows of O; and Ψ_i the mode shape vector.

The specific OMA SSI-COV algorithm used, composed of six main routines, will be shortly commented on below, function by function, and their setting for the usage on the given thesis.

1. **Calculation of cross-correlation function -> eqs. (3.20) to (3.22):**
   The function returns the *Impulse Response Functions* (IRF). Using T_s, time lag, for covariance calculation as 8s. Higher values T_s would lead to unwanted computational effort, otherwise small values lead to the non proper identification of system properties. References reviewed in [18] show that the maximum time lag should range from two to six times the longest natural period (0.353Hz $\leftrightarrow$ 2.83s).

   Important to note that a **down-sampling** may be applied to the input acceleration data, in case the desired modes range is significantly lower than the given sampling frequency f_s. At Sec.6.3, the time step is multiplied by a factor of six, for both simulated Av04 FAST and Av07 measured data, without accuracy loss, reducing computational effort.

2. **Build of block Toeplitz matrix and SVD -> eqs. (3.23) to (3.24):**
   Build a block matrix with constant matrices along parallels to the main diagonal [28] from the covariance matrices (IRF). Then, derive its singular value decomposition, simplifying the matrix and making it easier to find interesting properties of the original matrix, as rank and numerical error to a linear system solution.

3. **Modal identification procedure -> eqs. (3.25) to (3.30):**
   Identification of the modal properties of the system, such as *fn*, eigenfrequencies, ζ, damping ratios, and ϕ, mode shapes.

4. **Stability checking procedure -> eqs. (3.25) to (3.30):**
   When identifying great numbers modes of complex structures, automated stability checking is essential. For that, *Stabilization Diagrams* has been created and is being improved over the years [21, 29, 30]. The goal is to distinguish system poles from numerical poles or the so-called spurious poles, setting

accuracy tests in terms of percentage errors on frequency (δ_{freq}), damping ratio (δ_{zeta}) and MAC (δ_{MAC}). A m maximum number of poles (N_{max}) is initially chosen and the algorithm will compare the eigenvalues found by two consecutive numbers of poles in a decreasing routine till a minimum (N_{min}), also defined by the user. The error thresholds are presented in ref.[18]. A pole is considered stable only if all the three above error requirements are satisfied between two consecutive pole numbers set by m.

The appearance of spurious poles is the result of some approximations and limitations in the covariance method as explained in ref.[8]. Between them, it can be mentioned: measurements inaccuracies and coupled noise; usage of finite ranges on the derivation of the correlation; and the non-ideal stationary and linear behavior of the data.

5. **Selection of stable poles:**

   Remove the negative damping (also considered unstable poles) and normalize the mode shapes for post-MAC building.

6. **Cluster Algorithm:**

   Build MAC and construct agglomerative clusters from linkages, based on a criterion $eps_{cluster}$ of 0.2, regarding the euclidean distance (eigen frequency or/and damping ratio) estimations. The clustering routine plays a major role in the OMA SSI-COV automated functionality code by grouping, sorting and averaging modes previously found. Considering that all modes share the same wind conditions (same seed with different tower sensors positions), the routine clusters the stables poles and ignores groups with less than five elements (minor clusters). Finally, it averages the modal parameters inside each major cluster as the resulting eigen frequency, modal damping ratio and mode shape.

4 | FAST model of the AV04 turbine

This chapter exhibit an overview of both the aeroelastic simulations tool in Sec.4.1 and the wind generation software in Sec.4.4, FAST and TurbSim respectively. Besides that, it presents a code comparison and validation project supervised by NREL, so-called OC5, that focused on checking reliable Av04 numerical modeling tools. An extensive and robust methodology based on different Load Cases (LCs) with stepwise increasing complexity was applied to several participant's codes, as shown in Sec.4.2. The same methodology is followed in the given thesis to further tune the FAST model and achieve missing results in Sec.4.3.

Important noting that OpenFAST is the most advanced tool developed by NREL and has been replacing FAST8. One of the main differences is the inclusion of major improvements on *Aerodyn v15*, which includes significant updates to the blade-element/momentum theory (BEMT) solution algorithm. Since the blade *BeamDyn* file for the Av04 was not available due to intellectual property (IP) reasons, such capability was not included. The initial simulations on this thesis were run with FAST8 and later, updated to OpenFAST, with minor and even negligible differences in the outcomes. For this reason, the reference to *FAST* on this thesis includes both FAST8 and OpenFAST tools.

4.1. FAST Overview

FAST (Fatigue, Aerodynamics, Structures and Turbulence) code has been developed by the National Wind Technology Center (NREL) to work as a powerful computer-aided engineering tool for simulating the coupled dynamic response of wind turbines excited by aerodynamics and hydrodynamic loads. The code is capable of predicting both the extreme and fatigue loads [31, 32] of two- and three-bladed horizontal-axis wind turbines (HAWTs), being the last one, the standard design in

Offshore sites all over the globe.
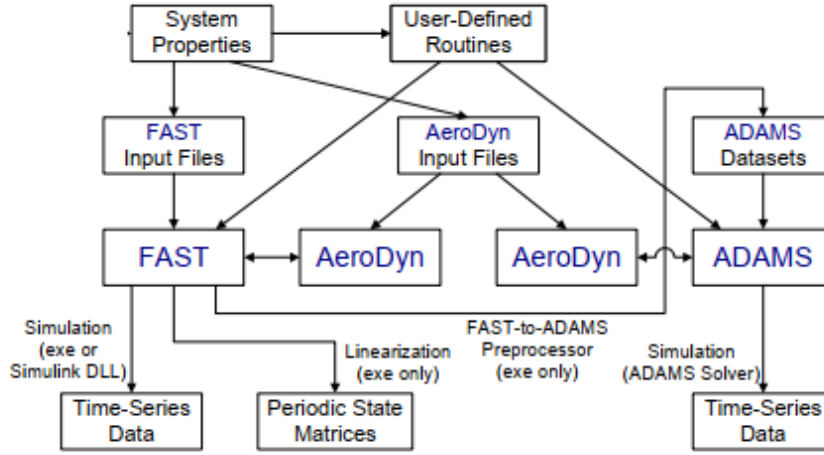
Figure 4.1: FAST Operation Mode.

The first version of FAST was released in 2002. Several modifications, updates and improvements have been made over the years. It can be mentioned for example that at FAST v8.16 or FAST8 (last version), compared to its ancestor v7.02, many features were added [33] such as tower drag loading; quasi-steady and dynamic surface loading; tower and nacelle tuned-mass dampers; and blade-shear, extensional and torsion DOFs. Each one of the above cited regards to main modules presented inside of FAST code block (figure 4.1), corresponding to different physical domains of the coupled aero-hydro-servo-elastic solution. These modules will be briefly described below since they were repeatedly utilized on this thesis work. Note that FAST has also the automated ADAMS routine embedded in its executable, but this functionality was not utilized.

ElastoDyn: which contains the structural description and dynamics of the rotor, drive train, nacelle, tower, and platform. The different DOFs can be set depending on the user's objective, as for blade, generator, tower and platform motions. Initial Conditions (IC) for the same parameters can also be applied. The turbine configuration, mass and inertia values are defined in this section. Moreover, the different blade sections and respective pitch, mass and inertia are included at the *BldFiles.dat*. The same can be said for the tower, in which mass, length, inertia, stiffness and damping are added through the *TwrFile.dat*. This last will have its *FAStTunr(1)* and *SSStTunr(1)* (tower stiffness factors) further

tuned for the better matching of the 1st tower bending modes of the Av04 OWT model with the reference, as shown in section 4.3. Finally, several time series outputs can be chosen as shown and detailed at *OutListParameters.xlsx*, available online, that describe FAST possible outputs for not only ElastoDyn but all its modules.

Inflow: sets the input stochastic wind files. It has several wind type options which do not need external tools as *Steady* and *Uniform*, but also more complex wind types as *Binary TurbSim* and *Binary Bladed-Style*. For the NREL 5MW adapted mode, *Polimi* set a wind mesh composed of 64x32x32 grid points (xyz) with a respective distance between points of 16x3x3 [m], at a reference height of 90m. In order to define the horizontal wind speed, *HWindSpeed* shall be set or time series data for uniform wind field should be provided. As for the case in which on-site wind measures ought to be reproduced, TurbSim is used to generate .wnd files for the Bladed-style full-field files.

AeroDyn: contains the aerodynamic input properties, from both the airfoil (blade) section and tower contribution. Besides that, it defines several flow properties, such as the inflow model *InfModel* which can be *DYNIN* or *EQUIL*, depending on the time lag between wake effect and respective influence in the rotor perceived flow. In this matter, the *IndModel*, induction factor model can also be chosen. It is relevant to say that different airfoil sections can be used throughout the blade length.

ServoDyn: regards the control strategy for pitch angle and generated torque (rotor speed). During this thesis work, *DISCOIN.dll* was replaced for *ROSCO.dll*, to solve some observed faults.

BDBldFile, HydroFile, SubFile, MooringFile, IceFile: these modules will not be over-commented on this thesis, since they were not applied. The Av04 model did not include the foundation flexibility, due to design confidentiality, so it was fixed at the tower bottom from sea level; it did not evaluate the hydrodynamic load contributions; Av04 does not have mooring cables and does not include extreme temperature conditions in the discussion. However, all of those are powerful modules that could be further analyzed for the completeness of Av04 model.

Other parts of FAST features, inputs and outputs will be only commented in

the following sections to avoid needless repetition while sharing contributions from previous OC5 and results of the given thesis.

4.2.   Previous Contributions - OC5 Methodology

NREL has carried out several pioneering projects on the validation of simulation tools for OWTs. One of the last combinations of efforts was driven on the OC5, which focused on the comparison of simulated results to the response data of physical systems, analyzing the Alpha Ventus *Senvion 5MW*, or as already mentioned, the Av04. *Phase III* Part I [7] presents the results of a code-to-code comparison and the subsequent publication Part II [9] narrows the comparison of simulated data against full-scale measurements from Alpha Ventus site (SCADAs, LIDARs, FINO).

A total of 27 participants contributed to Part I, including POLIMI FAST8 model. Each participant was oriented to perform a sequence of simulations aiming to gradually tune its model and by sequence increase the level of complexity of the model while trying to minimize the implementation effort and modeling errors. An OWT model developed by the University of Stuttgart (SWE) was used as a reference model. SWE was the only model that had full access to structural and aerodynamic properties of the real blades, foundation and functional controller documentation provided by *Senvion* and *OWEC Tower*, the jacket substructure manufacturer.

Due to the lack of relevant design parameters for the OC5 participants, it was necessary to: use NREL 5MW reference controller and blades parameters [34] and adapt them to match *Senvion* behavior; build similar quattropod jacket substructure designs closely compared to the Av04 real one; verify and tune the OWT models before their validation; and finally answer if the OWT simplified models were sufficient to describe complex offshore systems.

OC5 defines four groups of Load Cases (LCs) to tune and check the capabilities of the different OWT modeling tools. Each one of them is described below, with a short comment on the FAST model results and its complementary tuning and missing plots, which will be pursued in the following section 4.3.

The chosen statistics tool to measure the performance of all participants and LCs was the non-dimensional root mean square error (NRMSE) 4.1. It is a normalized variable, where lower values indicate less residual variance and therefore better fit. Important to note, that NRMSE overweight high errors so other statistical measures

might fit results even better [7].

$$NRMSE = \frac{RMSE}{X_{SWE,max} - X_{SWE,min}} 100\%$$ (4.1)

where

$$RMSE = \sqrt{\frac{\sum_{t=1}^{n}(X_t - X_{SWE,t})^2}{n}}$$ (4.2)

LC group 1

Concentrated on the mass, resulting vertical load and fore aft and side to side overturning moments. No air was included in those simulations, aiming to validate the structural properties of the models. *Polimi* model met quite well the reference, with an -0.5% at Mass of the RNA and Tower (LC 1A), -3.7% at fore aft overturning moment (LC 1A) and 4.7% at the entire OWT mass including RNA, tower, jacket substructure and foundation piles.

LC group 2

Examined modal properties still in no air conditions. Flexible RNA and tower, with all 6 DOFs constrained at the tower bottom. Unfortunately, the FAST model is not included in the results. Matching the first fore aft global eigen frequency is essential to further analyze OWT damping in operational conditions. The primary objective of the next section 4.3 will be to match the FAST Av04 model with the SWE reference. To identify the eigen frequencies, ICs of 1m were applied in *ElastoDyn* to the top tower in fore aft direction (*TTDspFA*) and in side to side direction (*TTDspSS*). In this way, selected eigen frequencies were determined according to the dominant modes on the frequency domain response of the time series. The Discrete Fourier Transform (DFT) was computed by using the MATLAB Fast Fourier Transform (FFT) algorithm slightly modified to avoid an odd number of points in the time-series FAST output.

LC group 3

Verified controller dynamics and aerodynamics forces, with rigid RNA and tower. Steady deterministic and Stochastic wind seeds were generated and analyzed. For the turbulent scenario, six independent wind seeds, each 10

minutes long, for every single LC in order to get statistically comparable results as recommended in the IEC 61400-1 standard. The FAST model achieved good results for deterministic wind seed, at around 15% (average between participants). However, it presented severe oscillations for the stochastic turbulent seeds, leading to errors higher than 30%. Such behavior highlights a flaw in the controller initially chosen by *Polimi*, the so-called *Discon.dll*. As recommended, *ROSCO.dll* replaced the previous controller. The tuned controller is shown in 4.3.2, in which better results are achieved.

LC group 4

Similar to LC group 3, sought to validate the controller behavior and aerodynamic loads, but this time, including an extra complexity with RNA and tower flexibility. The same comments made for FAST model performance from LC 3 are valid for LC 4.

OC5 LCs do not account for hydrodynamic loads, once the marine environment was disregarded. Subsequent validation of OC5 Phase III shall include waves, tides, currents, buoyancy force, marine growth and flooded elements since all of these can affect the dynamic response of OWT, even though such effect is more perceptive in floating OWTs.
In the end, the majority of the OWT models were verified and presented satisfactory responses to partial and full-loading wind speeds regions.
The given thesis work based its modeling methodology on the work done at OC5 and sought to complete missing validating results from the Av04 FAST model, before running further LCs, to identify modal parameters from the tower.

4.3.   OpenFAST Av04 Model

General technical specifications of the Av04 are presented below.

Technical Parameter	Value	Unit [-]	Observation
Rotor diameter	126	[m]	-
Height of hub	92	[m]	-
Total height above seabed	185	[m]	-
Rated output	5	[MW]	-
Rotor Speed	6.9 - 12.1	[rpm]	-
Cut-in wind speed	3.5	[m/s]	= force 3
Rated wind speed	13.0	[m/s]	= force 6
Cut-out wind speed	30	[m/s]	= force 11
Weight of nacelle without rotor and hub	290	[tons]	-
Weight of nacelle with rotor and hub	410	[tons]	-
Jacket foundation Weight of steel	500	[tons]	-
Tower	210	[tons]	-

Table 4.1: General Design Parameters Av04 (Senvion 5M).

As previously commented, many *Senvion* design parameters were not available. In this sense, the foundation flexibility was not considered in this thesis work due to data confidentiality, and the model was constrained at the bottom for all further simulations, resulting in a isolated tower structural and aerodynamic vibration response. One of the forecasted outcomes assumed would be higher eigen frequencies for the first tower bending modes (fore aft and side to side) against OC5 results and measured data from Alpha Ventus, since no stiffness from support substructure, foundation and soil are being considered in the model.

Prior to running OC5 LCs, the Av04 FAST model had all its structural design properties checked. Dimensions, masses and inertia from the tower and Rotor-Nacelle-Assembly (RNA) were matched with data provided by NREL representatives. A portion of these data is described on table 4.2, additional tower data with sectional wall thickness, fore aft and side to side moment of inertia, density and stiffness were also checked. All these datasets were confidential and available only for OC5 participants. Throughout the checking, no errors were found on the input files of *ElastoDyn*, *AeroDyn*, *ServoDyn* and *Inflow*.

All simulations set a recommended module time step (Δt) equal to 0.01s (sampling frequency $f_s = 100$Hz).

Finally, it is worth mentioning that the given thesis did not have access to OC5 SWE

Parameter	Value	Unit [-]	Description
$I_{nacelle,x}$	-	$[kg.m^2]$	The nacelle inertia moments are provided with respect to the nacelle
$I_{nacelle,y}$	-	$[kg.m^2]$	coordinate system with origin at the interception of tower and shaft axis
$I_{nacelle,z}$	-	$[kg.m^2]$	x-axis: downwards, y-axis "left" when looking downwind, z-axis: downwind
$m_{nacelle}$	-	[kg]	Total nacelle mass including generator, gearbox, transformer, etc
$CG_{nacelle}$	-	[m]	Center of gravity with respect to the tower top coordinate system [xyz]
$H_{nacelle}$	-	[m]	Nacelle canopy height
$L_{nacelle}$	-	[m]	Nacelle canopy length
$W_{nacelle}$	-	[m]	Nacelle canopy width

(a) Nacelle Properties.

Parameter	Value	Unit [-]	Description
H_{hub}	-	[m]	Hub height from MSL
m_{hub}	-	[kg]	Hub mass
CG_{hub}	-	[m]	Center of gravity with respect to the tower top coordinate system [xyz]
I_{hub}	-	$[kg.m^2]$	Hub moment of inertia around low speed shaft
R_{hub}	-	[m]	Hub radius

(b) Hub Properties

Table 4.2: IP - Design Properties of Av04 (Senvion 5MW).

reference data, but only to the graphic results presented at OC5 Phase III Part 1 report [7]. The MATLAB function *grabit.m* provided the means to manually extract data points from the image files.

4.3.1.   LC 2.x - Modal Checking

Even though the model was properly filled in terms of parametric nomination, Av04 FAST performed oddly bad on the determination of the first global fore aft eigen frequency, in other words, the along wind tower bending mode, while running LC 2B (which will be more extensively described below when the final result is presented). An absolute error of 13.8% was achieved, significantly higher than the average of other OC5 participants of 1.9%.

Aiming to reach a better match with the OC5 SWE reference, it was decided to tune the Tower Adjustment Factors (TAF) from the FAST model, on the *Elasto-Dyn_Tower.dat* file. TAF allows modifying modal stiffness and damping from first and second modes of fore aft and side to side individually.

TAF Parameter	Unit []	Standard Value	Tuned Value	Description
FAStTunr(1)	-	1	**0.86**	Tower fore-aft modal stiffness tuner, 1st mode
FAStTunr(2)	-	1	1	Tower fore-aft modal stiffness tuner, 2nd mode
SSStTunr(1)	-	1	**0.86**	Tower side-to-side stiffness tuner, 1st mode
SSStTunr(2)	-	1	1	Tower side-to-side stiffness tuner, 2nd mode
AdjTwMa	-	1	1	Factor to adjust tower mass density
AdjFASt	-	1	1	Factor to adjust tower fore-aft stiffness
AdjSSSt	-	1	1	Factor to adjust tower side-to-side stiffness

Table 4.3: TAF: Standard and Tuned values.

The TAF tuning was not a straightforward process since changing any variable would result in specific drawbacks. *FAStTunr(2)* and *SSStTunr(2)* were not modified since they would not improve by any means the first tower mode responses fore aft and side to side. The variation of the last three factors, *AdjTwMa*, *AdjFASt* and *AdjSSSt*, produced severe distortions on the FFT response near the first flapwise collective eigen frequencies (0.65Hz), which could not be fixed with other parameters. Therefore, the tuning focused on the *FAStTunr(1)* and *SSStTunr(1)*. As shown in 4.2, lowering their values led to a better match of the global first fore aft eigen frequency, however, it worsened the NRMSE of the following LC 4.1. These higher absolute values of NRMSE were expected since the controller would have to be reset for new tower stiffness values, seeking to adapt control gains to achieve desired steady-state response close to OC5. It is better to keep such errors as low as possible, but they do not represent a major flaw. The most important points were to check the proper dynamic behavior of the model with the new TAF values and the least influence on the flapwise collective mode.
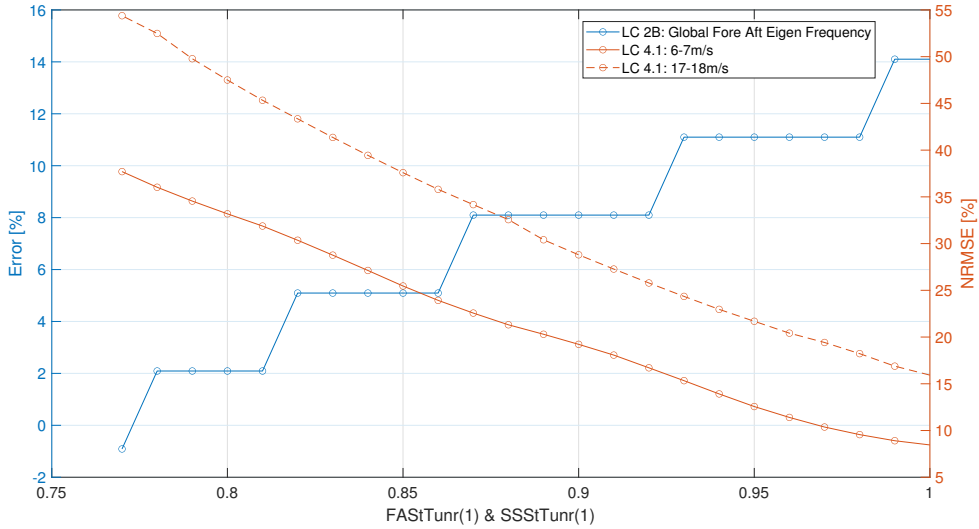
Figure 4.2: TAF Tuning Procedure and Drawbacks.

The final decision was to use both *FAStTune(1)* and *SSStTune(1)* equal to **0.86**, resulting in a final error of **5.1%** for the first global fore aft eigen frequency. Further improvements, resulted in a high effect on the flapwise and edgewise collective modes and the incapability of the FAST controller to match the dynamic response of OC5 SWE in the following LCs.

In the end, Lc 2B was performed as suggested by the OC5, comparing both standard and tuned TAF performances. No air was included, setting *Inflow* with "0" (still air), and ICs were applied to four diverse variables as shown in figure 4.3. Flexible RNA and tower were set. However, OC5 SWE also considers the Transition Piece (TP), jacket substructure elasticity, besides 6 DOFs constrained at lowest astronomical tide (LAT) -29.5m at 4 jackets legs. For this reason, it is forecasted that the eigen frequency from the FAST model shall be higher since it does not include these flexible components, but only RNA and tower as flexible and constrained at the tower bottom.
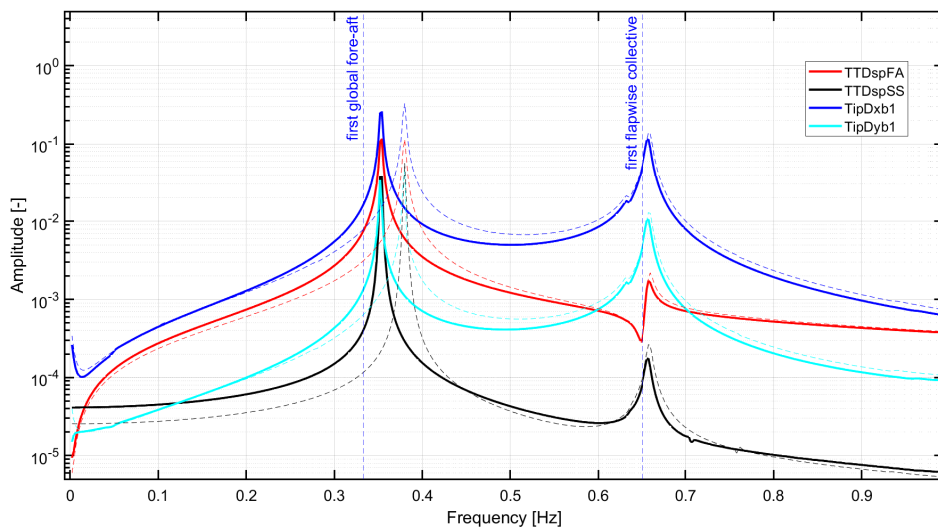
Figure 4.3: LC 2B - FFT of the time-series outputs (dashed lines represent TAF standard).

The final results of eigen frequencies for the two global bending modes, dominated by the tower contribution, are presented in the table below.

	Eigen Frequency	Unit
1st **Global Fore Aft Mode**	0.353	Hz
1st **Global Side to Side Mode**	0.343	Hz

Table 4.4: Av04 Eigen Frequencies Identified with FFT

The FAST model was tuned with the new values of TAF. Subsequently, all simulations will have their OC5 simulations updated. The LCs that had OC5 SWE reference available will be compared below with the FAST Av04 model.

4.3.2.   LC 3.x and LC 4.x - Aerodynamic Response

Now, aerodynamic loads will be inserted into the model. From deterministic (steady wind seeds) to stochastic (turbulent wind seeds) scenarios were taken into consideration.

Steady, deterministic wind was used in *Inflow*, setting *WindType* as 2 (uniform). In this way, an time-variant wind grid was generated varying from $V_{cut-in} = 3m/s$ to $V_{cut-out} = 30m/s$ with increasing 1 m/s each 50s, without wind shear.

Steady Wind simulations of LC 3.1 and LC 4.1 had a simulation total time (T_{max})
set to 700s.

Stochastic wind LCs were analyzed in six seeds each, being the final time series
response to the time domain clustering of them. The hub velocity (V_{hub}) was set
to 16m/s. Wind standard deviations were also supplied by OC5: σ_u, σ_v and σ_z,
2.11m/s, 1.69m/s and 1.06m/s respectively.

Turbulent Wind simulations of LC 3D and LC 4D had a simulation total time (T_{max})
set to 1400s. As mentioned previously, for each LC, six different and independent
seeds were generated. Afterward, the seeds were clustered, achieving longer recording
times and resulting in more robust spectra responses.

To avoid initial nonlinear and transient behavior, a pre-simulation time (T_{pre}) of
400s was set, removing the first portion of the time series. This strategy was applied
to guarantee that the FAST controller was working properly and the output time
series analyzed was in the right region. The T_{pre} was set for both Steady Wind and
Turbulent Wind simulations.

LC 3.1: Steady Wind Simulations - Rigid Tower
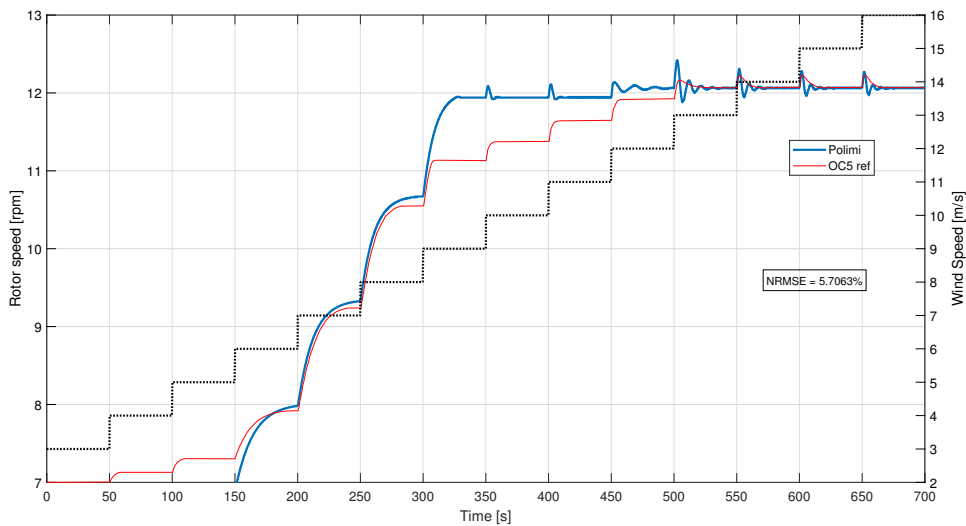
Figure 4.4: LC 3.1 - Rotor Speed as function of Wind Speed (dashed line represents the stepped
wind speed).

It can be noted that *Polimi* reaches the steady-state, or the so-called, rated wind speed, at 9m/s. While OC5 reference shall achieve rated condition at 13m/s as provided by *Senvion* manufacturer. Further tuning of the adapted DTU Wind Energy Controller used in FAST must be done for better matching. However, such procedures are not in the scope of this thesis.
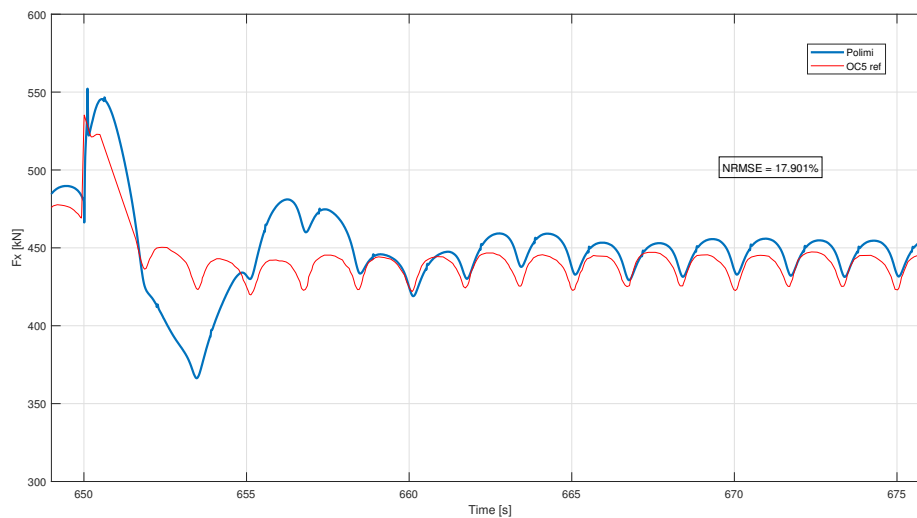
Figure 4.5: LC 3.1 - Tower Top Fore Aft Shear Force - Turbulent Mean Wind Speed of 16m/s.

Same comments can be done for higher wind speeds as in figure 4.5. Where for the transient portion, *Polimi* controller gains have to be further tuned to be able to smooth the amplitude of vibration and by consequence shear forces on the tower for sporadic above rated wind speeds records that can occur on open site.
The average CPU simulation time needed (T_{CPU}) was equal to 120s.

LC 4.1: Steady Wind Simulations - Flexible Tower

Same wind and simulation conditions for the *LC 3.1* are utilized at *LC 4.1*. The crucial difference is the additional flexibility from RNA and tower, increasing the level of complexity of the model.
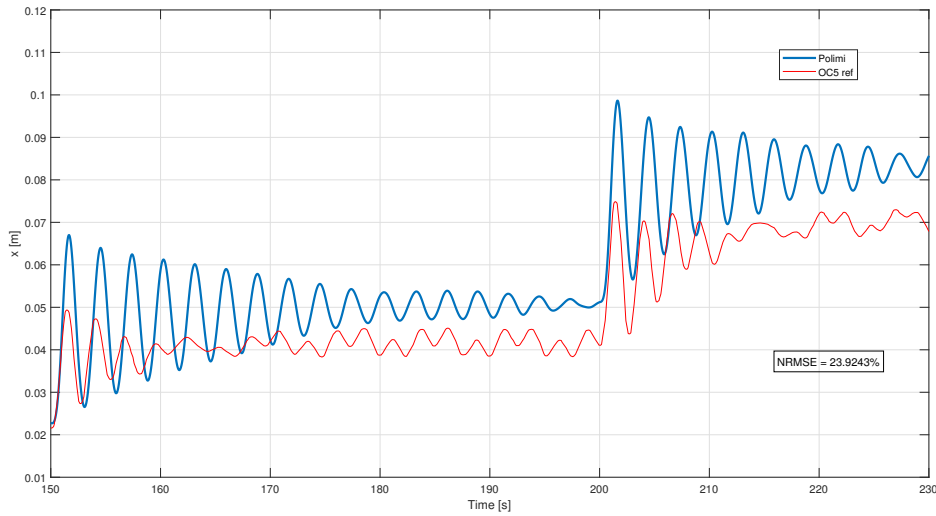
(a) Polimi FAST **biased** response.
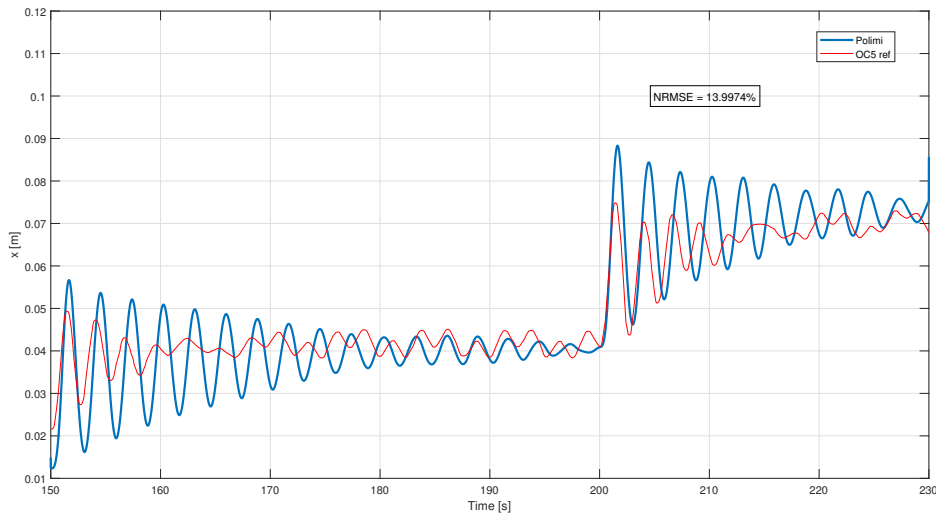
(b) Polimi FAST **detrend** response.

Figure 4.6: LC 4.1: Tower Top Fore Aft Displacement - Deterministic Wind Speeds of 6-7m/s.

It can be noted that there is a shift in the steady-state response generated by the *Polimi* FAST model in Fig.4.6b. The controller should be tuned for the new TAF found (check Tab.4.3), matching the new tower stiffness values and following the OC5 reference. As previously mentioned, tuning the controller is not in the scope of the given thesis. However, a *detrend* response is presented for both LCs Fig.4.6 and Fig.4.7, in order to check the dynamic response performance from the FAST model still using NRMSE as the statistical measure tool. The *detrend* is generated

by subtracting the average *Polimi* and adding the average *OC5* reference to the *Polimi* response. The so-called **biased** response is the one without any alteration. Moreover, *Polimi* model showed to be less damped than the *SWE reference*, with overall greater amplitudes of tower top fore aft displacement for 6-7m/s wind speeds, an initial hint of whether the numerical model is underdamped compared to the real design.
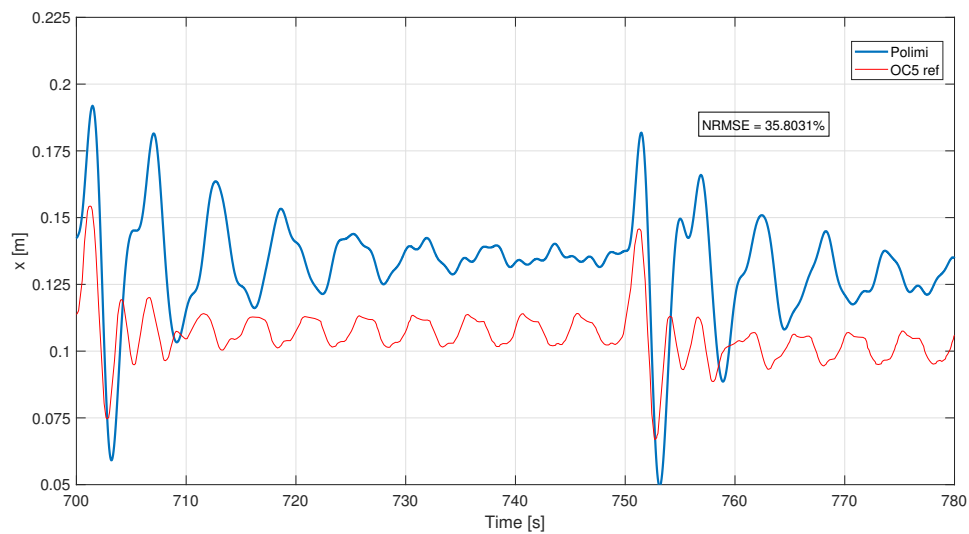
(a) Polimi FAST **biased** response.
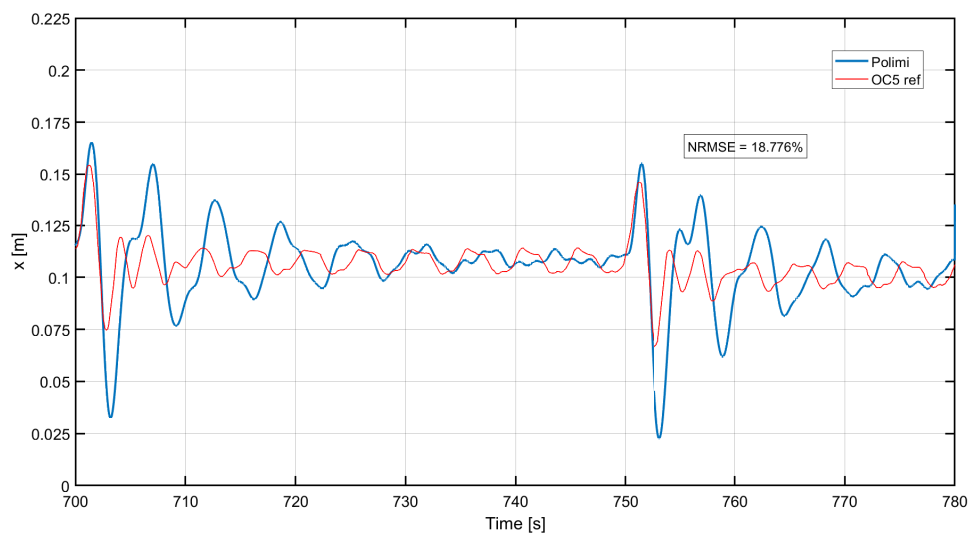
(b) Polimi FAST **detrend** response.

Figure 4.7: LC 4.1: Tower Top Fore Aft Displacement - Deterministic Wind Speeds of 17-18m/s.

Polimi FAST model response of tower top fore aft displacement for higher wind

	Polimi		OC5 Participants Average
	Biased	**Detrend**	
LC 3.1 (fig4.4)	-	**5.7%**	not given
LC 3.1 (fig4.5)	-	**17.9%**	**14.3%**
LC 4.1 (fig4.6)	23.9%	**13.9%**	**14.4%**
LC 4.1 (fig4.7)	35.8%	**18.7%**	**12.6%**

Table 4.5: Polimi (FAST) performance (**NRMSE**) against other participants in OC5.

speeds was not initially included the in OC5 report, due to severe oscillations caused by the controller (NRMSE > 30%). A better result was achieved with the TAF tower tuning and the usage of the new controller *ROSCO.dll* provided by OC5, as shown in figure 4.7.

The T_{CPU} for the flexible tower scenario was slightly different from the rigid tower. An overall performance comparison is presented on table 4.5, checking *Polimi* FAST model performance.

The stochastic analysis of turbulent wind seeds was done by the usage of more suitable tools such as Power Spectrum Density (PSD) and Probability Density Function (PDF). The Welch method was chosen to compute the power of the signal over the specific frequency range by averaging short windowed observations. Welch's periodogram spectrum is able to reduce the computational effort while using discrete Fourier transform (FFT). Moreover, another advantage is that the segmented frequency components, from the periodogram, are averaged, reducing noise in the estimated power spectra. As a drawback, the frequency resolution is reduced. Finally, Hanning windowing is used since it presents less leakage from main lobes to side lobes and better frequency accuracy compared to other techniques such as rectangular, flat-top and exponential. For that reason, Hanning is usually chosen for random signal applications.

LC 3.2D: Turbulent Wind Simulations - Rigid Tower

Using turbulent wind seeds provides a wider spectrum of excitation frequencies to understand whether the simulation tool can properly describe the real turbine's response. *Polimi* controller performed well till 1Hz for the pitch angle response in above-rated wind speed conditions of 16m/s. However, it was not able to highlight subsequent rotor harmonics 6P and 9P, at around 1.20Hz and 1.8Hz respectively, as shown in the PSD of figure 4.8. Furthermore, a pitch angle over-prediction can be

noted for all the frequency range above 1Hz.
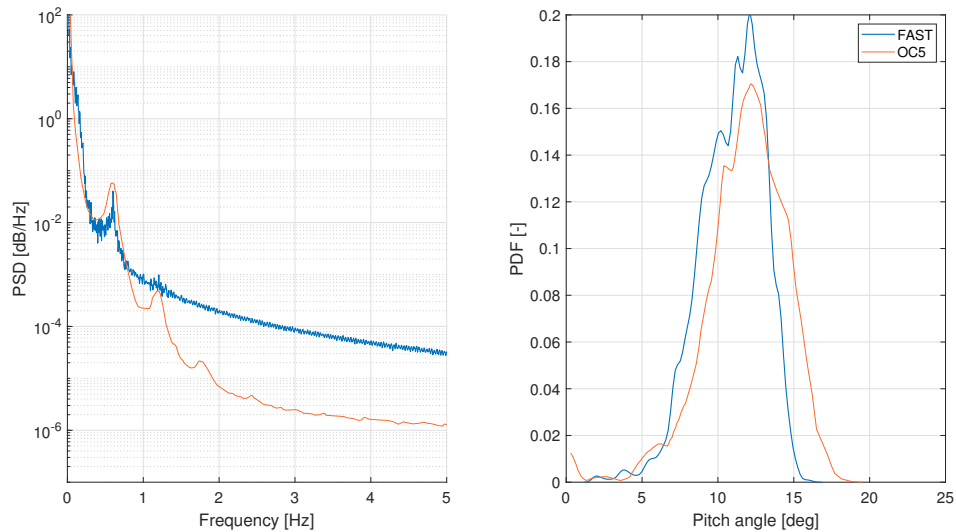
Figure 4.8: LC 3.2D - PSD and PDF of Pitch Angle - Turbulent Mean Wind Speed of 16m/s.

Some discrepancies were visible in PDF plots too. Other OC5 participants presented similar limitations, due to non-optimized controller parameters.
The average T_{CPU} was equal to **850s** for each LC seed.

LC 4.2D: Turbulent Wind Simulations - Flexible Tower

Lastly and more complex, turbulent wind seeds are run including flexible RNA and tower.
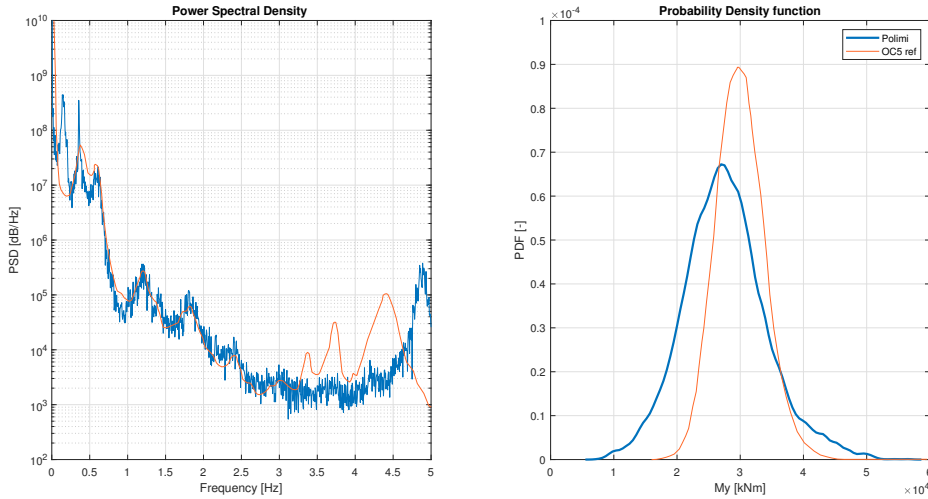
Figure 4.9: LC 4.2D - PSD and PDF of Fore Aft Bending Moment at Tower Bottom - Turbulent Mean Wind Speed of 16m/s.

As commented in the OC5 report, *Polimi* FAST model presents flatter probability distributions compared to other participants and to *OC5* reference. On the other hand, *Polimi* performed better on identifying low and high-frequency modes 3P, 6P and 9P for the fore aft bending moment at tower bottom response. It can be noted that *Polimi* model is not able to reproduce two different second edgewise modes, at 3.4 Hz and 3.7 Hz, since it does not include *BeamDyn* nonlinear FEM-based blade BEM module.

In conclusion, the FAST model showed on average an NRMSE below 20%, which is considered a good match between model and reference. The Av04 FAST model was further tuned and validated to be used as a reliable wind turbine numerical simulator. Special attention can be given to low-frequency modes range, which includes the fore aft and side to side tower bending modes ($\tilde{0}.36$Hz), in which *Polimi* showed an excellent match to the majority of the LCs.

4.4. Use of TurbSim for Wind Grid Generation

Once *OMA* method will be used to analyze the acceleration data from Alpha Ventus Wind Farm (5.4), so should be done for data from the FAST model, seeking a coherent comparison of eigen frequencies and modal damping ratios values. In order

to set new LCs, its is necessary to generate several numerical wind seeds, having the same statistics characteristics as those samples captured by FINO substation (5.3). The turbulence simulation code more used for properly supplying *Inflow* feature in FAST is the *TurbSim* [35]. It is a stochastic inflow turbulence software capable of numerically generating time series of three-component wind speed vectors at points in a two-dimensional vertical rectangular grid that is fixed in space, respecting the proper spatiotemporal turbulent velocity field relationships. As opposed to a physics-based model, *TurbSim* uses a statistical model as a reference.

(a) The inertial frame coordinate systems and planes "marching" along positive X, regardless of flow angles.

(b) Wind field with both flow angles 0°.
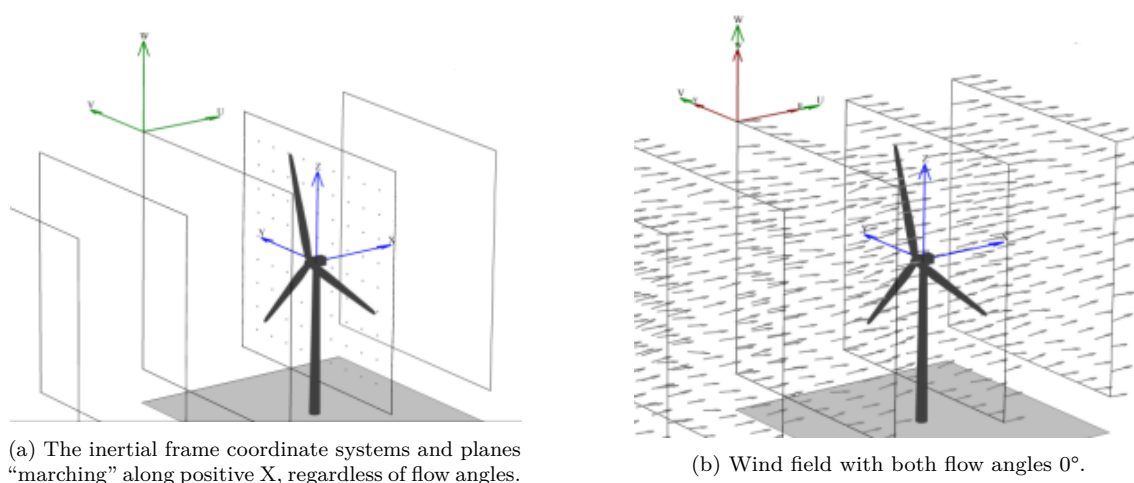
Figure 4.10: Example of TurbSim grids as implemented in AeroDyn (figure from [35]).

In this section, it will be shown how the input files of TurbSim resemble and which parameters were set differently from the OC5 reference.
To avoid over-describing parameters that were not used in the thesis work and that can be found more deeply detailed in ref [35], a short overview of the relevant parameters, as shown in Appendix A, will be held in the following description.

Runtime Options: In order to generate a full-field turbulent time-series data for FAST proper simulation, *WrBLFF* and *WrADTWR* are set to "True", creating a .wnd and a .twr file. Both of them are used by AeroDyn functionality.

Turbine/Model Specifications: Here the parameters are set to meet the dimensions of the AV04 WT analyzed. It was decided to maintain OC5 definitions for minimum vertical and horizontal grid-point matrix dimensions. And concerning the *AnalysisTime*, both 700s and 1800s were simulated, as suggested in ref.[19].

Meteorological Boundary Conditions: As for the turbulence model, Karmal

spectral model is used due to its applicability for onshore and offshore sites. The main variables in the given section were *IECturbc* and *URef*, these were defined for each seed differently based on values presented in Tab.5.2 and Tab.5.3.

Non-IEC Meteorological Boundary Conditions: Since other parameters in this section are rather complex and not accessible (5.3), once again, OC5 standards were used as the "default" option.

Coherent Turbulence Scaling Parameters: This last output definition section has no relevance since is used in case *WrACT* was set to "True".

5 | FINO and SCADA Database

Alpha Ventus is composed of jacket substructure (Av01 to Av06) and tripod type (Av07 to Av12) foundation turbines. In this thesis, it was not possible to access Av04 quality acceleration data to be compared with its respective FAST model. The Av07 showed to be the most well-instrumented OWT and the spatially closer turbine to Av04. The detailed explanation and consequences of such a decision will be exposed in Sec.5.2, together with the strategies to circumvent this issue. Presenting comments on the sensor configuration and quality; the structural designs; and the controller settings of both OWTs.

Anyhow, initially in Sec.5.1, the pioneering Alpha Ventus wind park will be presented and overviewed, highlighting its contributions to the study and design of more efficient OWTs.

At last, the wind seeds (Sec.5.3) and the acceleration time-series (Sec.5.4) are selected from the RAVE database and post-processed, aligned with OC5 methodology.

5.1. Alpha Ventus Wind Farm
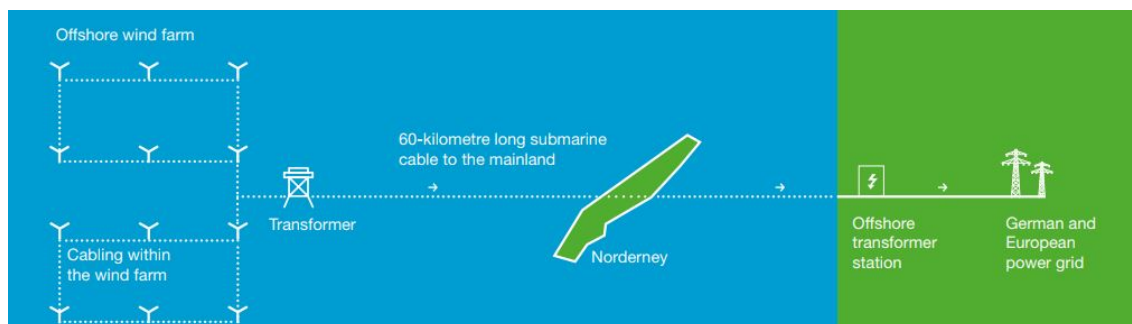
Figure 5.1: Alpha Ventus Grid Connection.

In 2011, one year after its commissioning and official inauguration, Alpha Ventus achieved positive interim results, with power yield higher than expected. The wind park faced positive wind average speeds over the years, producing around 3800 hours of power per year under full load, 50% higher comparable with onshore wind farms. Being the first German OffShore wind park and the first worldwide to be constructed under open sea conditions, 45 km north of the island of Borkum and 60 km from the coast of the mainland, Alpha Ventus became to be a reference and pioneering project. Formed by 6 Senvion-REpower and 6 Adwen both 5MW OWTs, with different foundation configurations, Jacket substructure and Tripod foundation respectively, its size in terms of OWTs quantity can lead to modest undertaking conclusions, since even Vineby Offshore Wind Farm, the first of its kind in the world, operating from 1991 to 2017, presented 11 OWT. However, never before have such huge designs of 5MW been used in offshore installations. The blade tip of a REpower cuts through the air at over 300 km/h under full load. The 2019 annual average gigawatt-hours of power into the grid generated could supply electricity for approximately 57000 average households (3500kWh) in the north of Germany. Besides that, located so far from the coast, meant to aware of 60 km of long submarine cables connecting Alpha Ventus Substation to Onshore installations (5.1), containing output signals of 30000 volts to 110000 volts. The project led to great achievements and gained experience on Offshore Wind Farms, which were still to be designed, financed and commissioned.

To truly perform a great influence on future projects, a fundamental singularity of Alpha Ventus was the great attention aimed at the instrumentation and data acquisition on the OWTs and substructures 5.2.
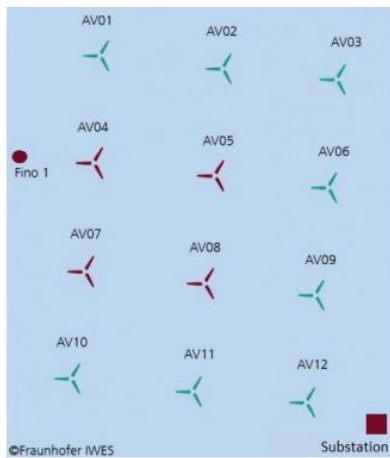
(a) Map representation of instrumented OWTs.

(b) FINO1 substation in front of Av04.

Figure 5.2: Alpha Ventus Sensors Capabilities.

The Research at Alpha Ventus (RAVE) is responsible for carrying out development work at Alpha Ventus since 2019 and the data archive is operated by Federal Maritime and Hydrographic Agency (BSH) and, in some cases, by the turbines manufacturers. There were more than 1200 measurement channels of data installed in all the wind park facilities (OWTs, FINO1 and Transformer substations). Supervisory Control And Data Acquisition (SCADA) acts as a computerized and centralized system for remote and real-time monitor-control of industrial and wind energy applications. It acquires information on the state of operating OWT, sending coded signals on dedicated communication lines so that the OWT can be perceived and controlled remotely in a secure way.

Unfortunately, not all of them are still available due to short-term individual research campaigns and harsh offshore conditions. Out of the 12 OWTs, Av04, Av05, Av07 and Av08 were massively instrumented at the commissioning (5.4). The Av04 and Av07 are widely more equipped and maintained and have the advantage of being the closest turbines to FINO1. This last one is the designed and built substation aiming to acquire a vast range of different parameters, such as wind speed and direction at 30m and 100m above sea level.

In the interest of performing OMA, acceleration records come to be the main input. And by so, it's important to note that only Av07 has accelerometers placed in the blades of the turbine. This fact is to be taken into consideration in cases of further studies for example on the coupling and decoupling of the first blade flapwise mode and the first tower fore-aft motion, and their respective damping contributions.

Furthermore, the Av07 has five pairs of accelerometers on different height tower levels whereas the Av04 has only two single accelerometers on different height points. In the first one, it is possible to average the two available signals to remove the torsional component and reduce measurement noise.

For these reasons and further feedback from current employees working with Av04 accelerometer maintenance, it was decided to use Av07 as the principal wind turbine for analyzing operational data, even though it presented significant design differences with Av04 and, by so, with Av04 OpenFAST model.

5.2.   Alpha Ventus OWTs - Av04 and Av07

Despite a large number of sensors and consequent data being recorded on the Alpha Ventus site (FINO substation and OWTs), as already mentioned in 5.1, one of the biggest challenges in the data analysis is to pick and access reliable datasets, in terms of NaN values and right sensor documentation. In other words, incomplete sensor documentation (such as direction and position) and the lack of consistent maintenance and replacement of invalid pieces from the beginning of the farm operation in 2010, made the selection of which sensor and time series to be used for analysis, not a trivial task.

Unfortunately, for the AV04 OWT, the acceleration data in parallel to wind data available was not as solid as for the AV07. Serving as a source of proof, for two different month seeds, April 2016 and November 2015, it was not possible to distinguish the damping ratios for the so-called *cross wind* and *along wind* motions of the OWT tower [36], which were correctly identified on AV07. Sources working at the Alpha Ventus site reported that sensors on AV04 may not be well placed and so a new set of acceleration sensors was installed later on. However, neither had improved results for the described analysis.
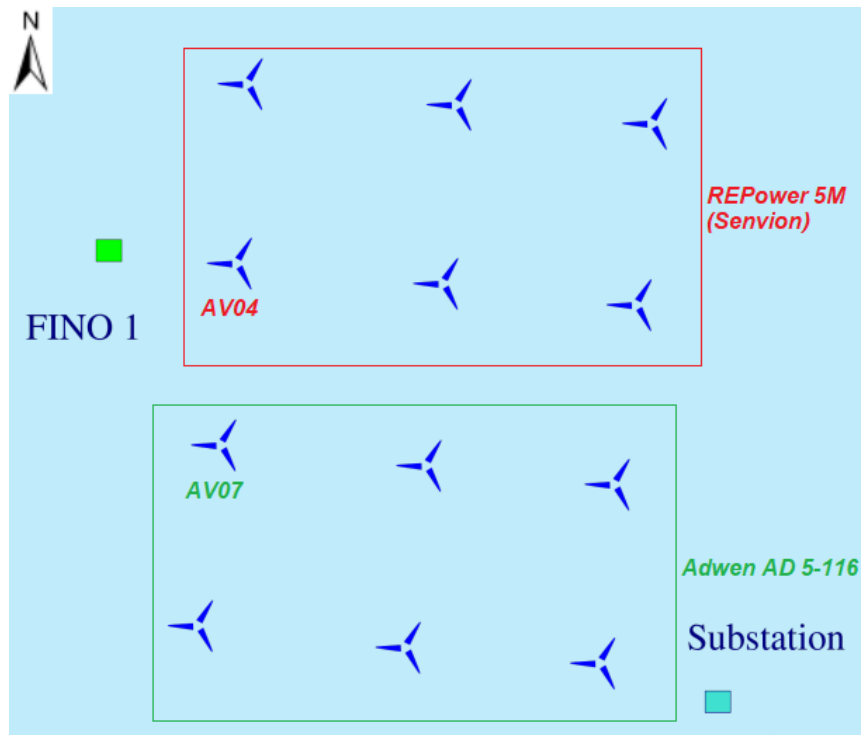
Figure 5.3: Alpha Ventus Site Representation: Two Different Wind Turbine Manufactures.

The influence of the AV07 control algorithm on the tower eigenfrequencies, when the wind speed becomes close to the rated speed, was seen clearly. The same behavior was not clear in AV04. Because of an evident quality gap between the two OWTs measurements, it was chosen to use the AV07 as a reference to the simulated output from *FAST*. Important to note that the main difference between the two cited OWTs designs is the bottom foundations, AV07 has a tripod structure and Av04 has a jacket quattropod substructure, as shown in 5.4. The Alpha Ventus layout and OWTs positioning are shown more evidently in 5.3.
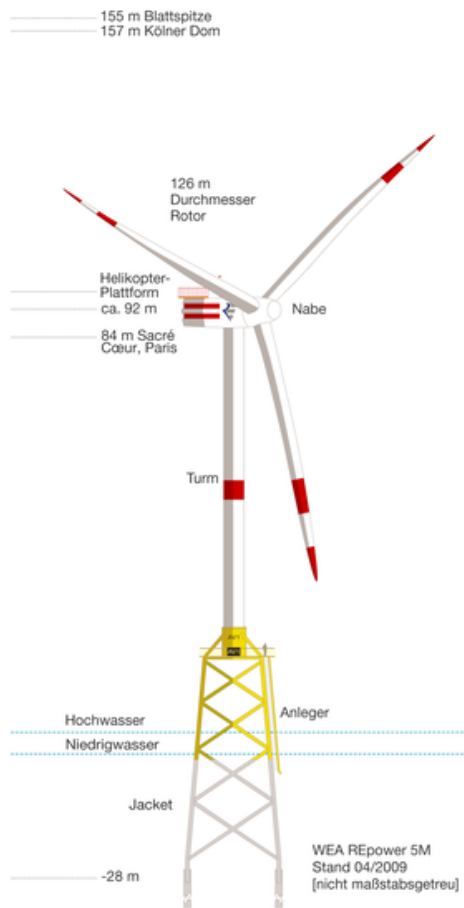
(a) Senvion OWT wide view.
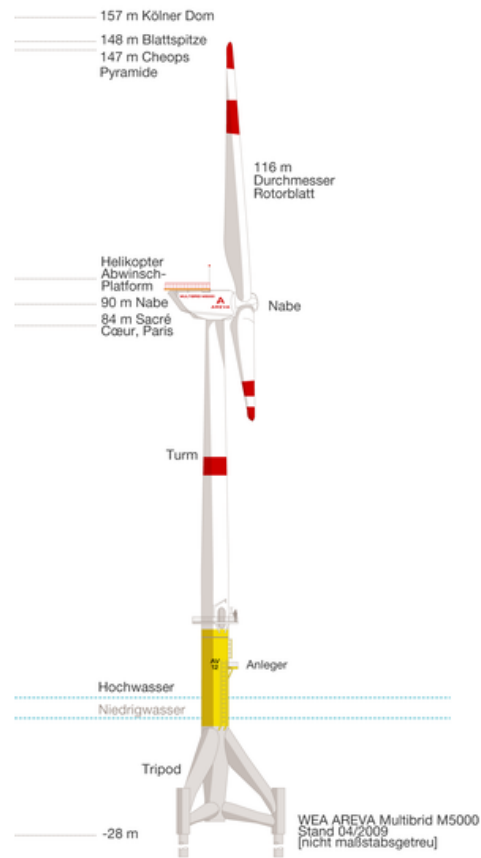
(b) Adwen OWT wide view.

Figure 5.4: Both AV04(left) and AV07(right) technical drawings.

Information on the blade design (i.e. airfoils) and controller response of the Av07 were not available, which introduced extra uncertainty to the modal identification comparison to the simulated FAST Av04 model. One way found to attenuate such lack of information was to check the operating response of the Av07, in terms of rotor speed and blade pitch, and compare it with the same steady-state parameters used by the Av04 controller (presented in Sec.6.1). The whole month of November 2015 of Av07 was scattered in Fig.5.5 together with the Av04 FAST model values.
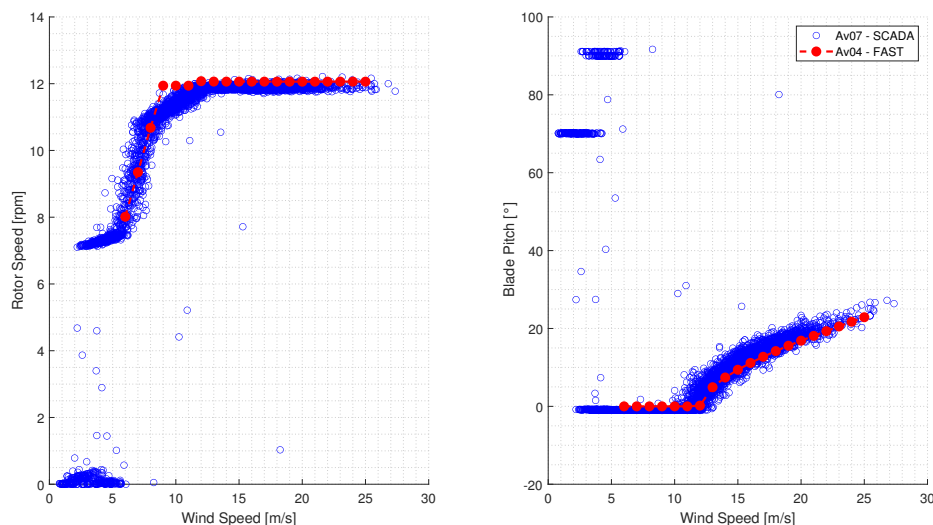
Figure 5.5: Av07 and Av04 Controller Settings.

A promising match can be seen between both OWT controllers. Anyhow, a quantitative comparison of the modal parameters extracted should be still avoided mainly due to differences in the rotor diameter and blade design.

Moreover, in this thesis work, all the simulations were done setting an AV04 fixed-bottom condition, aiming to avoid unwanted complexity and considering a lack of manufactures foundation design parameters. Having measured data and simulated data from different OWTs present significant differences in the modal properties.

Understanding the foundation weight on the values of modal frequencies, damping ratios and the dynamic response as a whole shall be a great source of work for future developments on Alpha Ventus OWT tower bending modes (fore aft and side to side).

5.3.   Wind Data - November 2015

As mentioned previously, one of the most complete wind seeds found in the Alpha Ventus open-source data was the one of November 2015. It derives from a sonic anemometer placed 80 meters above sea level in the FINO substation. The seed is composed of wind speed time-series with sampling frequency f_s equal to *20Hz*. The *averaging time* used to define all main properties was *30-minute*, as suggested in [19]. In this way the final matrix size was *1440x36000*, matching 2 half-hour x 24 hours x 30 days = *1440*; and each column an progression of 0.05 s (1/*fs*) matching

30 minutes x 60 seconds/min x fs = *36000.*

Before starting to extract relevant turbulent characteristics from the data available, a quality check was pursued by comparing the mean wind speed extracted from the given data in front of other instruments also placed in FINO, such as cup anemometers and wind vanes at the same 80 meters height, 5.6. Sonic and ultrasonic anemometers are known for generating more accurate wind speed and direction measures. Although being a more expensive technology, sonic sensors tend to replace the so-called mechanical solutions or cup anemometers. These last ones have moving parts, which present a higher maintenance cost and do not operate as efficiently in extreme atmospheric conditions (freezing weather) as the ultrasonic wind sensors.
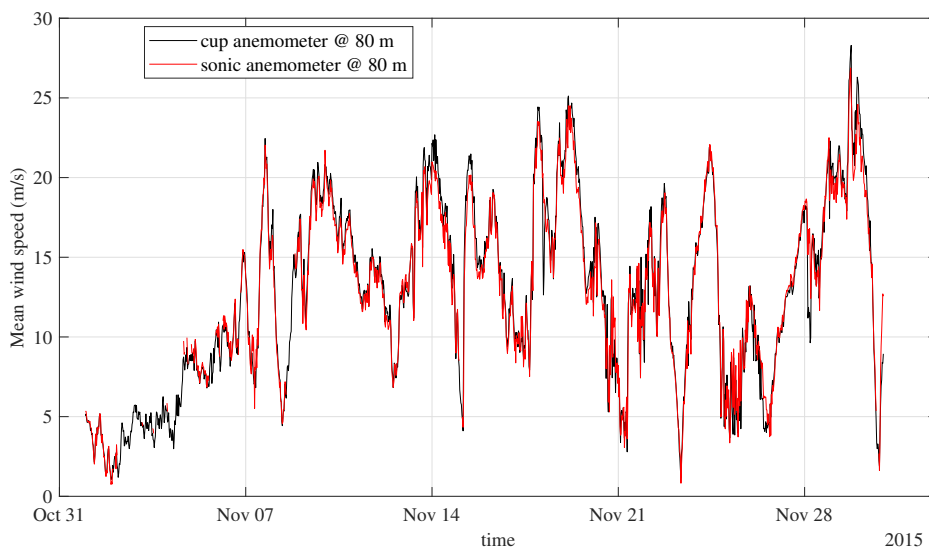
Figure 5.6: Mean Wind Speed Time-Series and Quality Check.

The tight agreement between two different measuring sources was taken as one of the quality checks. Parallel to that, the 30-minute average standard deviation of the wind speed is shown in 5.7a, the values tend to oscillate between 0.5 o 2.5 (m \s) for the whole month of November.
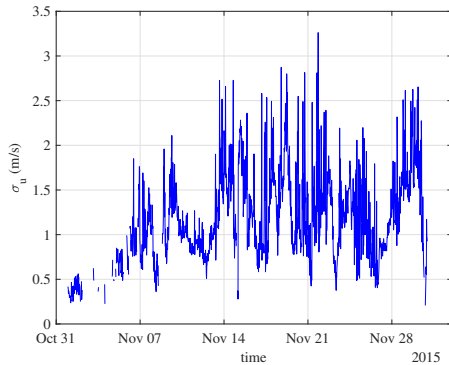
(a) Standard Deviation of the Wind Speed Record.
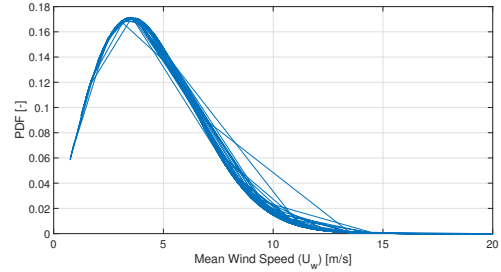
(b) Probability Density Function of Mean Wind Speed.

Figure 5.7: Standard Deviation and PDF of the Wind Speed Record.

Moreover, November 2015 seed presented interesting values regarding atmospheric stability (5.1). The classes are based on the dimensionless height ζ, found by applying the *Monin-Obhukov* similarity theory. The total number of samples is equal to 1440 (30-minute averaged values on a time window of 30 days).

Category	Range	Share of Data
Very Stable	$5 > \zeta > 2$	
Stable	$2 > \zeta > 0.2$	26.7%
Neutral	$0.2 > \zeta > -0.2$	
Unstable	$-0.2 > \zeta > -2$	70.7%
Very Unstable	$-2 > \zeta > -5$	

Table 5.1: Classification of atmospheric stability.

In order to achieve reliable calculations and analysis, it is desirable to use a neutral to a very stable range of values. This statement is made since there is an influence of the different atmospheric classes on, for example, the fatigue load spectra of blade root and tower base loads [37]. Once again, the period of November 2015 performed well (Fig.5.8). The southeastern sector of the wind rose is the mast shadow portion of the turbine, where contributions were neglected.
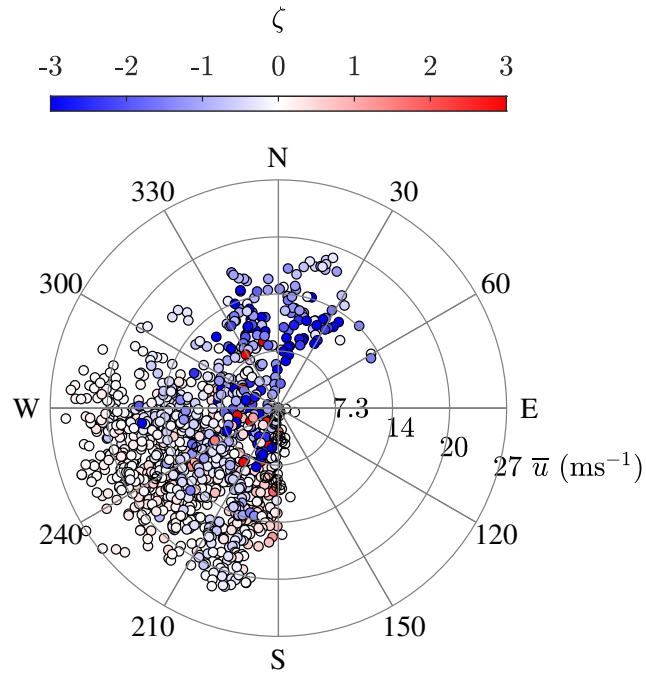
Figure 5.8: Wind Rose & Atmospheric Stability.

One of the last statistical characteristics extracted from the wind speed time-series was the fundamental scaling velocity *u**, resulting from the square root of the ratio between surface stress and air density.

Relevant to comment that the usage of different modeling tools, such as inertial dissipation and eddy, forecast a proportional dependence between friction velocity and wind speed ([38]), as expected by theoretical calculations. Such a relationship is also clearly seen in November 2015 seed (Fig.5.9).
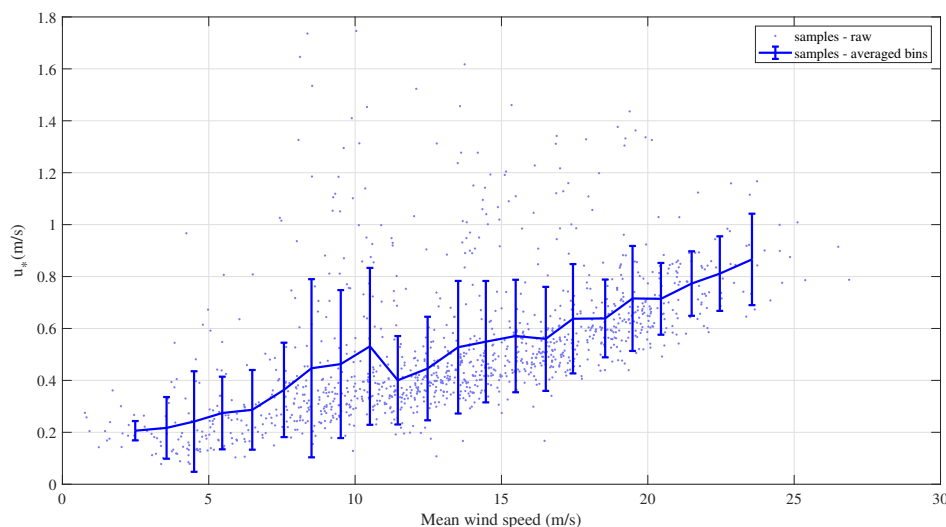
Figure 5.9: Friction Velocity 30 min averaging of November 2015.

In the end, once the wind speed time-series data were checked to ensure the November 2015 seed quality, the main stochastic wind characteristics could be extracted so to be used in *TurbSim* to generate the wind fields (explained in more detail on Sec.4.4).

In the following items, two LCs of OC5 Phase III Part 2 [9] were selected as references to extract meteorological properties from the measured Av07 data and allow the generation of a twin wind simulated grid to be used in Av04 FAST model. The two different operating conditions of the OWT represent relevant scenarios, one below and one above the rated wind speed. In this way, the influence of controller response and aerodynamic loading are visualized. For each of the LCs, six seeds were extracted for the sake of subsequent clustering and proper analysis of stochastic phenomena.

- **LC2.1x: Power production below rated wind speed**

  The six wind seeds selected were run in TurbSim setting stochastic wind field and Kaimal Spectrum model. The target was matching the wind speed at the hub, in the LC with V = 8 ms^{-1}. The optimum November 2015 seed values extracted and their respective Turbulence Intensity (TI) factors are shown below.

	Unit	Seed 1	Seed 2	Seed 3	Seed 4	Seed 5	Seed 6
Mean Wind Speed	[m/s]	7.99	8.00	8.01	8.01	8.01	7.97
Turbulence Intensity Factor	[-]	0.12	0.16	0.11	0.15	0.09	0.08
Time Period	$[day-hour/minute]$	20-21h30	20-13h00	23-14h00	25-15h00	5-4h00	7-4h30

Table 5.2: Wind Seeds for OC5 Load Case 2.1x.

- **LC2.3x: Power production above rated wind speed**
  As for LC2.1x, the six wind seeds selected were run in TurbSim setting stochastic wind field and Kaimal Spectrum model. But now matching the LC with V = 19 ms^{-1}. The optimum November 2015 seeds values extracted and their respective Turbulence Intensity (TI) factors are shown below.

	Unit	Seed 1	Seed 2	Seed 3	Seed 4	Seed 5	Seed 6
Mean Wind Speed	[m/s]	18.99	18.98	19.01	19.02	19.97	19.04
Turbulence Intensity Factor	[-]	0.08	0.05	0.08	0.08	0.11	0.09
Time Period	$[day-hour/minute]$	29-00h30	7-16h00	18-22h30	19-10h30	15-8h00	22-18h00

Table 5.3: Wind Seeds for OC5 Load Case 2.3x.

Important to note that in OC5 Phase III Part 2 simulation time *Ts* was set to 600s. In Ch.6, *Ts* used was 1800s, improving the output data reliability (ref.[19]), which will be commented afterwards.

5.4.   Accelerometer Data of Av07 - November 2015

The acceleration records for the month of November 2015 were taken from the Av07 Hub-Nacelle and from five Tower spots. As for the wind data, the acceleration data was organized into daily events with a duration of *30 min*. A significant difference is that for the acceleration response, the *fs* was equal to *50 Hz*. And so, for each of 30 min, vectors were sizing *1x90000*. Several pairs of accelerometers are positioned in Av07 hub guaranteeing the identification of *fore-aft*, *side-side* and *axial* acceleration response. In this thesis work, the first two motions will be studied. An issue that shall be mentioned is the limitation of accelerometers to properly record low-frequency contributions. However, it seems to be negligible for modes with frequencies above 0.1Hz [39], and then, not a problem for first tower bending modes identification.

It is important to comment that Av07 database for the nacelle acceleration was

available in four main outputs: **ahx**, **ahz**, **avx** and **avy**. Due to non-reliable documentation confirmed by RAVE employees, distinguishing the real orientation of the sensors and by so, which were representative of fore aft and side to side motion, was not a straightforward procedure. The separated response shown in this section is the outcome of an initial "detective" work performed in all the nacelle sensors using OMA for single accelerometers, extracting meaningful insights. In section 3.2, not only Av07 modal parameters identification is performed but also, before that, nacelle sensors direction checking.
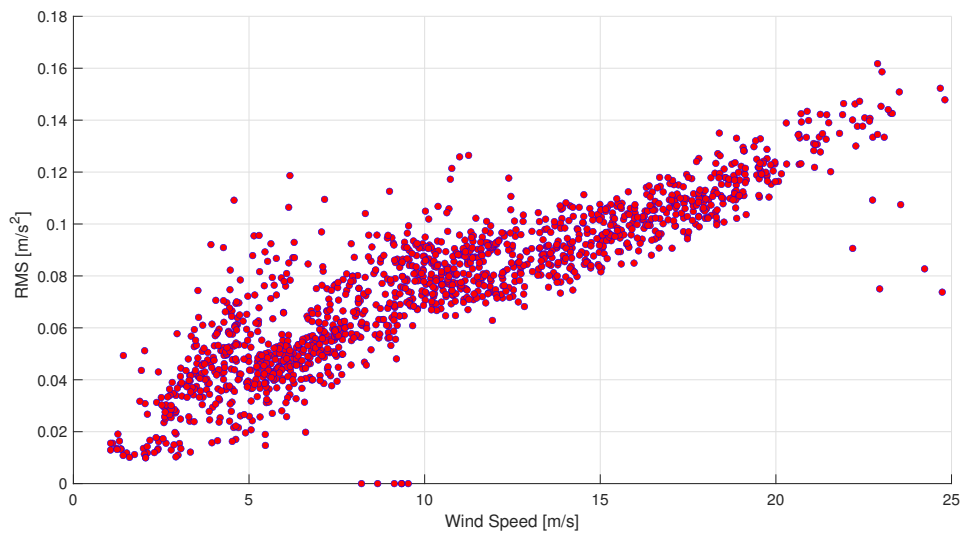
Figure 5.10: Fore-Aft RMS of Nacelle Acceleration Response as function of Mean Wind Speed.
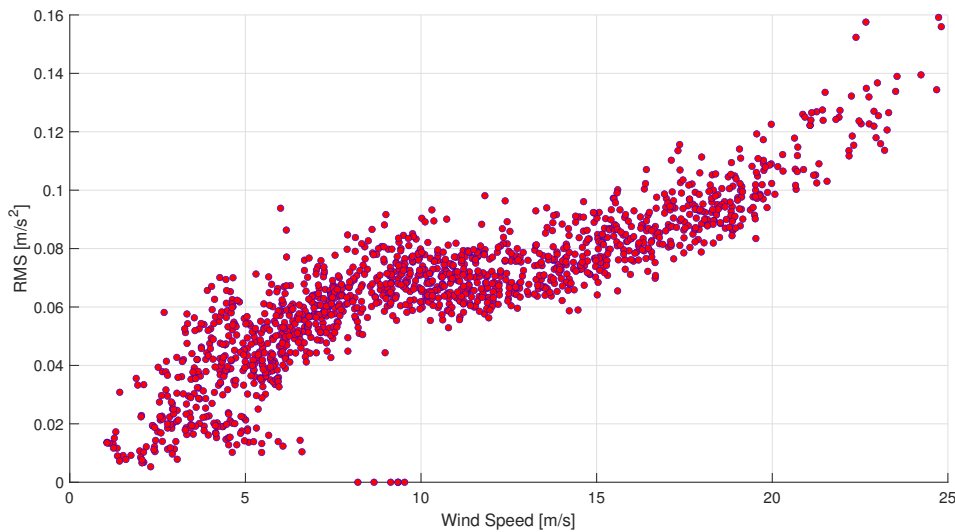
Figure 5.11: Side-Side RMS of Nacelle Acceleration Response as function of Mean Wind Speed.

Commonly applied to the analysis of suspended bridge's motion to cross wind excitation, the validation of Finite Element (FE) models might be pursued by studying the relationship between the standard deviation of acceleration response and the mean wind speed. The paper [40] focuses on the effect of high wind speeds on vibration responses and modal parameters variation for a unique sea-crossing cable-stayed bridge, Donghai Bridge. While doing so, it found a quadratic curve fitting the vertical acceleration RMS and the absolute crosswind speed. Similar behavior can be seen in [41], where the buffeting response of a suspension bridge in complex terrain is studied based on full-scale data from Lysefjord Bridge. The increasing RMS value of the bridge deck response at mid-span in parallel to the mean wind speed occurs both in the computed model and the measured data.

Even though being rarely used for WT analysis (e.g. [36]), such behavior was seen through scatter plots Fig.5.10 and Fig.5.11. Each dot represents a 30-minute length observation. The coherent results may be derived from the buffeting aerodynamic forces that influence the motion of the tower linearly for higher wind speeds.

- **LC2.1x: Power production below rated wind speed**
  The acceleration time-series record seeds for the power production below rated wind speed, $U_w = 8 \text{ ms}^{-1}$, were checked one by one in order to avoid seeds presenting non logical values, such as null or extreme high peak values. Both

fore-aft and *side-side* responses presented no undesired behavior.

- **LC2.3x: Power production above rated wind speed**
  As for the below rated, the 6 acceleration response seeds for power production above rated wind speed, $U_w = 19$ ms^{-1}, were equally checked.

6 | Results and Discussion

This chapter presents the obtained modal identification results on both the simulated Av04 FAST model and the Av07 measured data. Results are followed by relevant comments and analysis.

First, in Sec.6.1, a classic logarithmic decay method is applied to specific simulations of FAST Av04, seeking to have a quantitative source of comparison with the following OMA methodologies.

Two different OMA tools are used. One partially (Sec.6.2) and one fully automated (Sec.6.3) solution. Both can properly identify the fore-aft and side-to-side tower bending modes, with good eigen frequency accuracy and contrasting damping behaviors for each mode. However, OMA-SSI appears to overestimate the along wind damping for the majority of wind conditions, while presenting higher variability. Further comments will be done on this matter throughout the chapter.

6.1.   Mean Logarithmic Decay Method

The first modal extraction tool used on the Av04 FAST model is the Mean Logarithmic Decay Method (MLD). It provides an extra reference for the following OMA tools.

The schematic of how MLD was applied is illustrated in fig.6.1. The main goal was to identify the damping contributions coming exclusively from the tower structure and aerodynamic loading.

The simulations are done with the turbine operating at steady-state conditions: Steady wind, fixed rotor speed, fixed blade pitch and controller off. In addition, an initial condition is imposed to the tower deflection. The turbine's steady-state operating conditions are found with a wind step simulation and are represented in Fig.6.2.
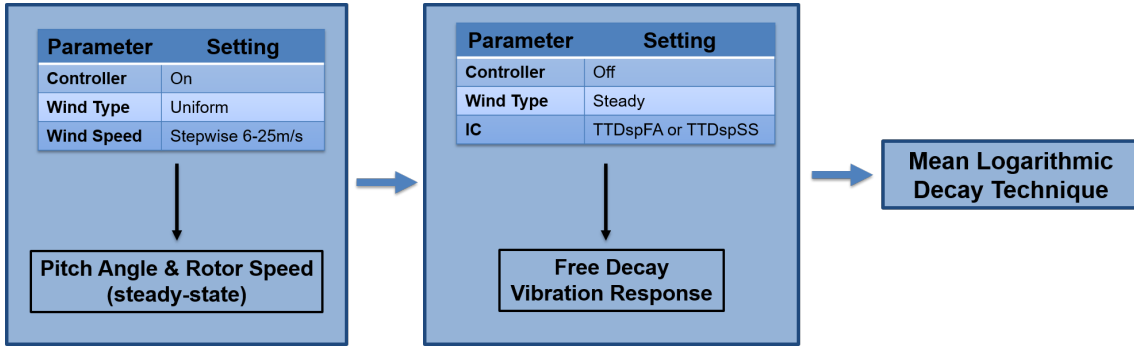
Figure 6.1: Logarithmic Decay Methodology Schematic by blocks.

The first simulation block was set with the controller activated and a stepwise unitary increase in the wind speed from 6 to 25m/s, each step lasting for 200s. The total simulation time was equal to $4000s$ ($dt = 0.01s$). The FAST outputs *RotSpeed* and *BlPitch1* were stored and for each wind speed, only the last 500 records ($5s$) of each were averaged, representing the steady-state value for that given wind speed. This was done to avoid the transient behavior derived from the instantaneous wind speed step increase.
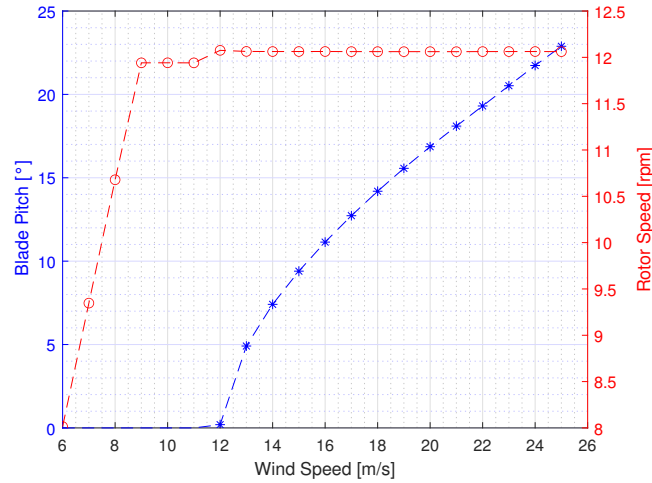
Figure 6.2: Pitch-to-feather controlled system of the AV04 turbine as a function of the wind condition.

Once the steady-state values of each wind speed set by the controller are known, the second simulation block can be configured. The simulation time was equal to $800s$ ($dt = 0.01s$) for each of the 20 seeds (6 to 25m/s).

All seeds were run for $IC = 1m$ separately applied on *TTDspFA* (fore aft or along

wind) and *TTDspSS* (side to side or cross wind), resulting in 40 simulations. Some of the free decay vibration response can be seen in Fig.6.3 and Fig.6.4. Besides the highlighted peaks as small blue circles, for each of the free decay vibration responses, two vertical green lines represent the linear range of decay. Only the peaks inside the linear range are selected to compute the mean logarithmic decay technique, and the subsequent eigen frequencies and damping ratios, as derived in eqs. (6.1) to (6.3).

(a) $6m/s$ (b) $12m/s$

(c) $18m/s$ (d) $24m/s$
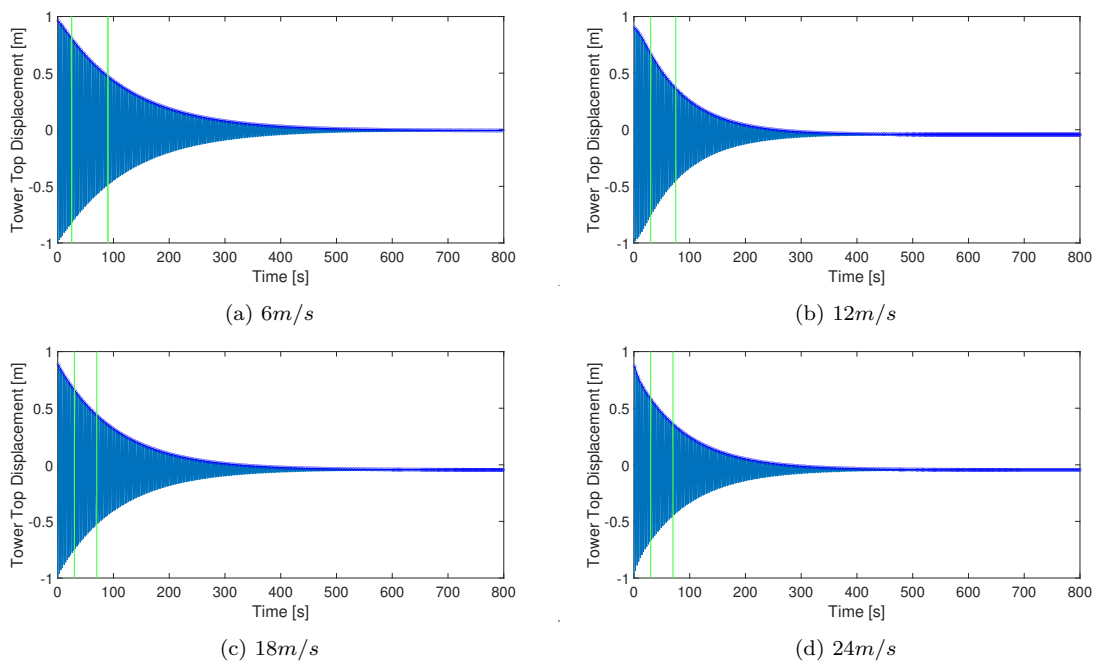
Figure 6.3: Cross Wind Free Decay Responses with IC applied to *TTDspSS*.

(a) $6m/s$

(b) $12m/s$

(c) $18m/s$

(d) $24m/s$
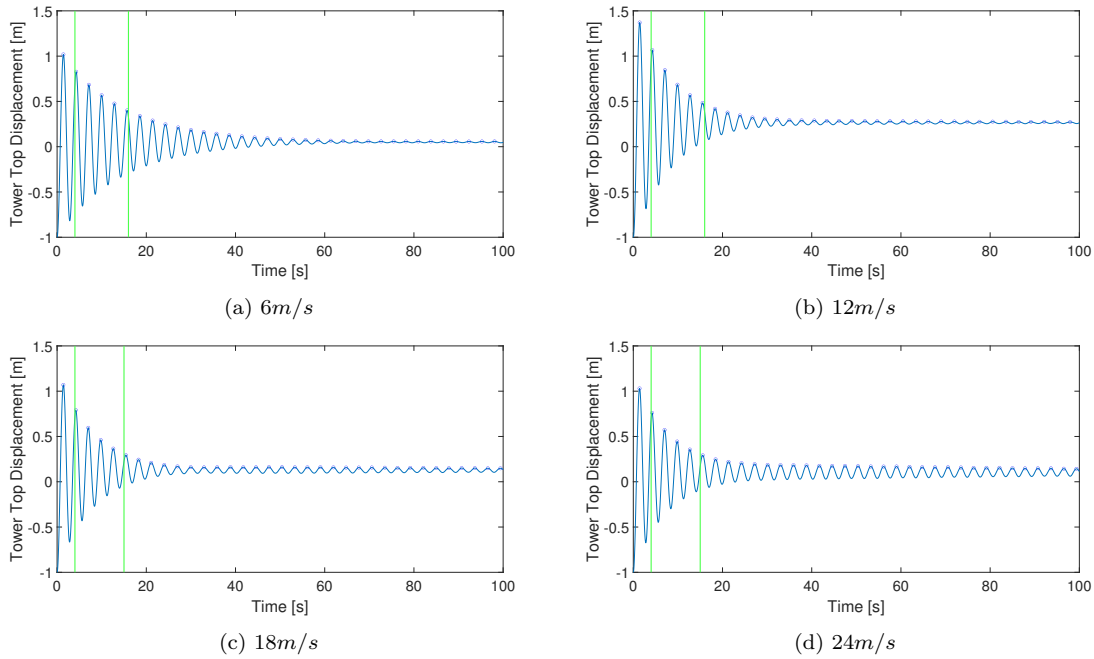
Figure 6.4: Along Wind Free Decay Responses with IC applied to *TTDspFA*.

The equations used to calculate the eigen frequencies and damping ratios are shown below. The number of peaks selected to be averaged was $n = 10$ for the cross wind and $n = 5$ for the along wind seeds.

$$\Delta t_{kk} = \frac{(loc_{kk+1} - loc_{kk})}{dt} \tag{6.1}$$

where *loc* represent the time instant vector position of a given peak and dt the simulation time step. As previously commented, $kk = [1, 2, \cdots, n]$. The eigen frequency is found by

$$f_{kk} = (\frac{1}{\Delta t_{kk}}) \tag{6.2}$$

And the modal damping ratio by

$$\delta_{kk} = \ln(\frac{pks_{kk}}{pks_{kk+1}})$$
$$h_{kk} = \frac{1}{\sqrt{1 + (\frac{2\pi}{\delta_{kk}})^2}} \tag{6.3}$$

where the *pks* is the amplitude of a given peak. The h_{kk} stands for the local damping ratio.

The final eigen frequency and damping ratio were found by averaging the stepwise f_{kk} and h_{kk} as follow

$$f_n = \frac{1}{n}(\sum_{kk=1}^{n} f_{kk})[Hz]$$

$$h = \frac{100}{n}(\sum_{kk=1}^{n} h_{kk})[\%]$$

(6.4)

These procedures were applied for each wind speed, for fore aft and side to side motions.

Results for the modal properties of the FAST Av04 are presented in Fig.6.5
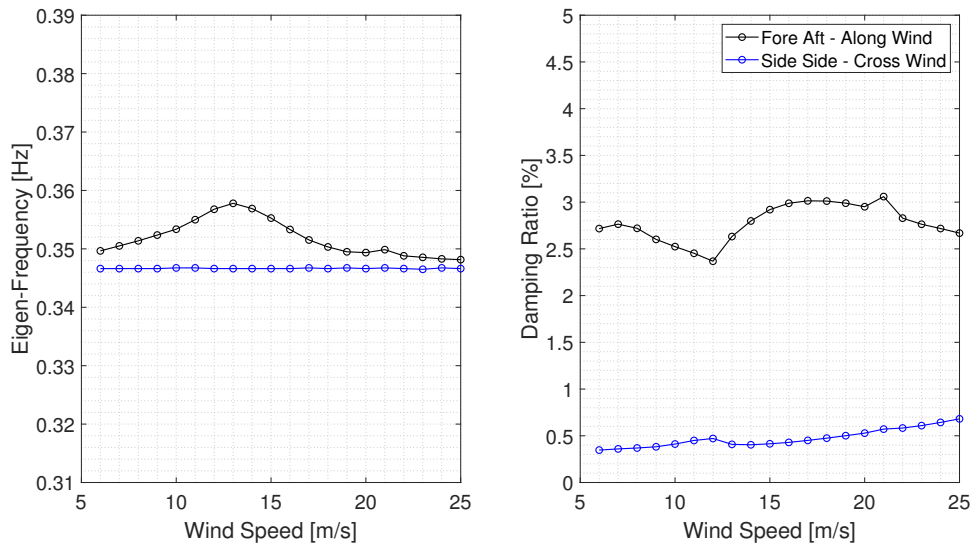
Figure 6.5: Modal Parameters (eigen frequency left and damping ratio right) of the Av04 using MLD.

The eigen frequencies are independent of the wind speeds for the cross wind motion; a slight effect can be observed in the along wind motion.

On the other hand, damping for the along wind is at least three times higher than the cross wind for any given wind speed. Such a difference highlights the influence of the aerodynamic damping on the final response. For the cross wind, it is assumed that damping derives almost exclusively from tower structural damping. Moreover, the controller settings used in the below- and above-rated wind regions, included by means of the steady-state values used, can be visualized for both motion around $Wind_{speed} = 12m/s$, where blade pitch reaches non null values (Fig.6.2). Av04 is regulated by a variable-speed pitch-to-feather control strategy. Large pitch changes are applied to compensate for higher wind speed aerodynamic forces, maintaining

constant rotor torque. In this way, the controller probably has a significant effect on the damping ratio but it is challenging to know its exact description.

6.2.   OMA Single Accelerometer

As commented in chapter 5, it was chosen to keep following OC5 methodologies, by generating meaningful LCs, while using OMA Sing and OMA SSI-COV. For the sake of completeness, besides the below rated wind speed (LC 2x1: 8 ms^{-1}) and above wind speed (LC 2x3: 19 ms^{-1}) seeds, extra two wind speed scenarios were selected, at 13 ms^{-1} and 23 ms^{-1}, allowing a better visualization and analysis of the modal parameters as a function of the wind conditions.

Before presenting the OMA Sing final results and relevant capabilities, it was necessary to investigate Av07 sensors' real direction since the first operational modal identification, using RAVE documentation as a reference, provided oddly results. The Av07 sensors validation was performed by applying OMA-Sing to the 8 ms^{-1} and 19 ms^{-1} seeds. The eigen frequencies and damping ratios led to a quantitative and qualitative analysis of the absolute values and their trend. The pursued investigation concluded that **avy** stands for **Along Wind** recordings and **avx** for **Cross Wind** recordings.
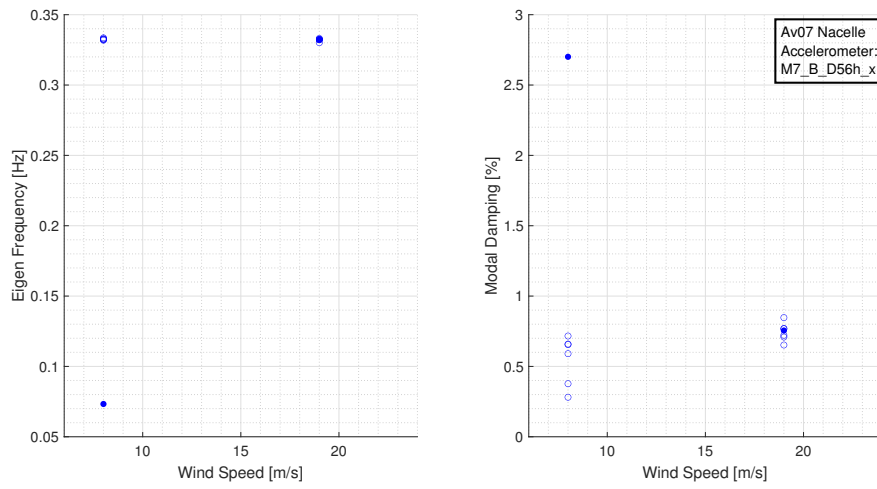
(a) **ahx**
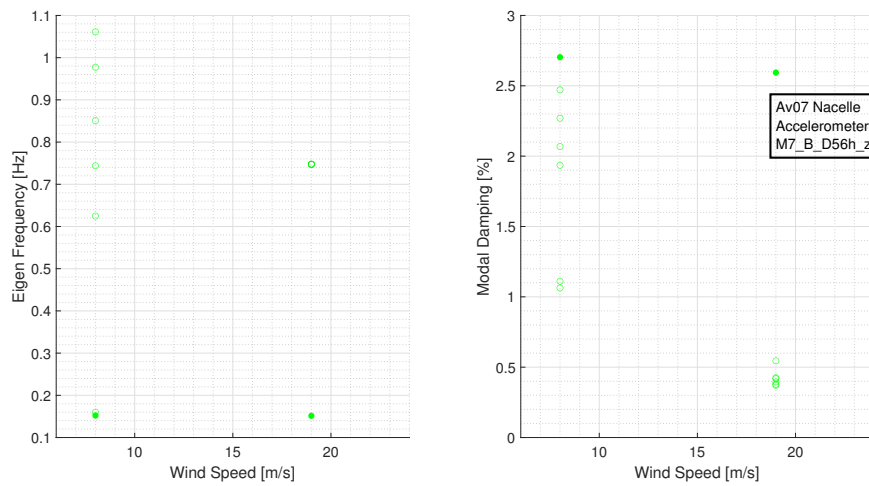
(b) **ahz**
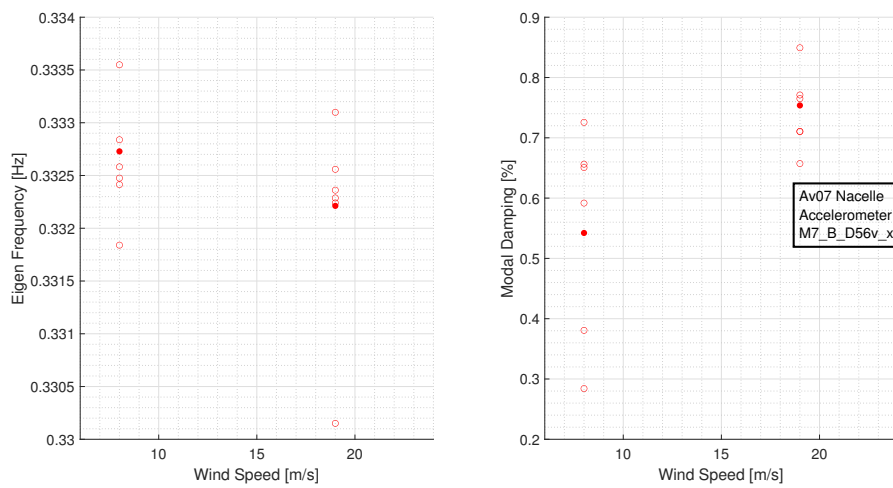
(c) **avx**

Figure 6.6: Av07 RAVE sensors direction check using OMA-Sing.

(d) **avy**
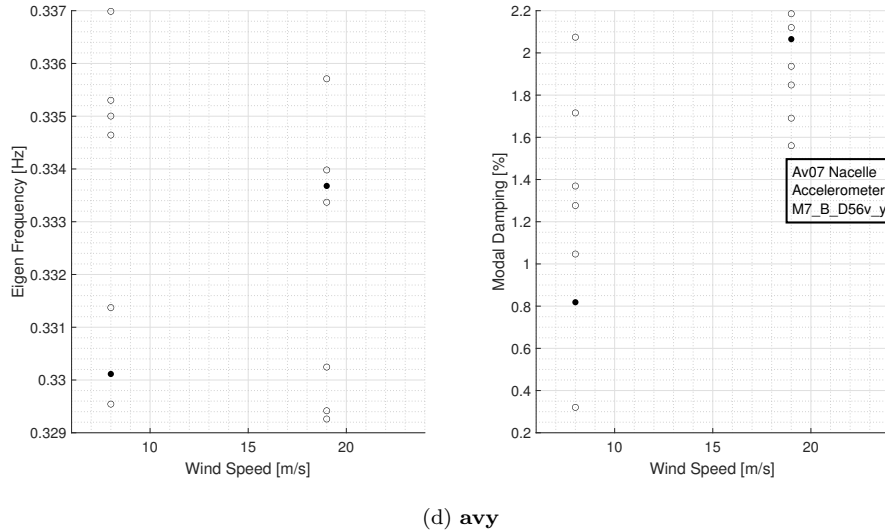
Figure 6.6: Av07 RAVE sensors direction check using OMA-Sing (cont.).

Note that for each wind speed, six seeds were selected plus one seed representing the time-series clustering of those (fulfilled circles).
What could be deduced is

- Figure 6.6(a) suggests that **ahz** output is the vertical motion sensor. As eigen frequencies varied a lot depending on the seed and an oddly damping estimation was found, with decreasing trend for higher speeds.

- The **ahx** and avx output have very similar results and trends, as shown in Fig. 6.6(b) and Fig. 6.6(c). However, for the ahx, OMA Sing was not able to find the predicted 1st fore-aft eigen frequency (around 0.32Hz), for the time clustered point (fulfilled circle). Tuning OMA Sing parameters was tried, using manual peak picking, but no improvements were achieved.

- The **avx** output presents the smallest variability for the eigen frequency on each seed and increasing trend of damping with a maximum around of 0.8%. So, it was assumed as being **Cross Motion** (Side to Side) sensor direction.

- Finally, as shown in Fig. 6.6(d), **avy** is concluded to be the **Along Motion** (Fore Aft) motion output, since it presents bigger variability for the eigen frequency for each seed compared to avx. As for the damping, higher values overall with a steeper increasing trend, reaching around 2.2%.

The along wind (avy) and Cross wind (avx) accelerometers were assumed to be

switched with respect to RAVE documentation, which were suggested as the transverse to nacelle direction and in the nacelle direction accelerometers, respectively. Once Av07 measured data and the Av04 simulated data were available, OMA Sing was applied following the seeds standards of OC5 Phase III Part 2.

Acceleration seeds of Av07 and Av04 were 30 minutes recording long with a $f_s = 50Hz$ and $f_s = 100Hz$, respectively. Resulting in 90,000 and 180,000 data points.

6.2.1.   Av04 - FAST Data Output

OMA Sing was applied to *NcIMUTAxs* and *NcIMUTAys* outputs from FAST simulations, for better matching with Av07 data, as the Av07 RNA in operation is assumed to be aligned to the wind direction and a rotational matrix is not needed to recover the along wind and cross wind motions from the accelerometers.

The first results were achieved by maintaining f_s as $100Hz$, the same value used in OC5 Phase III. However, OMA Sing had a poor performance for the identification of the low-frequency tower modes (around 0.34Hz). As shown in Fig. 6.7, OMA Sing is not able to identify, for *Seed 1*, *Seed 2* and *Seed 4*, any mode around the first tower bending mode for along wind motion at 8 ms^{-1}. The lowest identified mode was around 0.55Hz. Same for the cross wind motion, in which from Seed 1 to Seed 5, OMA Sing is not able to identify any mode with a frequency range close to the side to side tower bending motion, presented in 4.4.
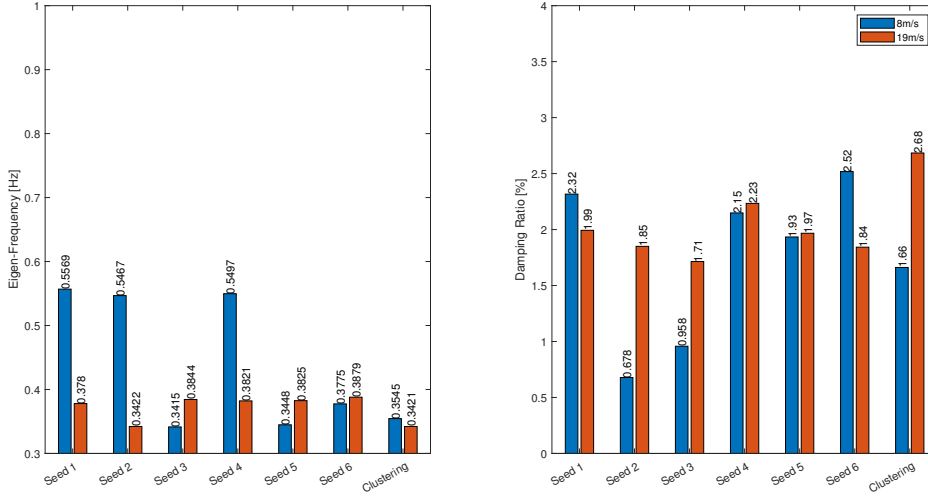
(a) Along Wind
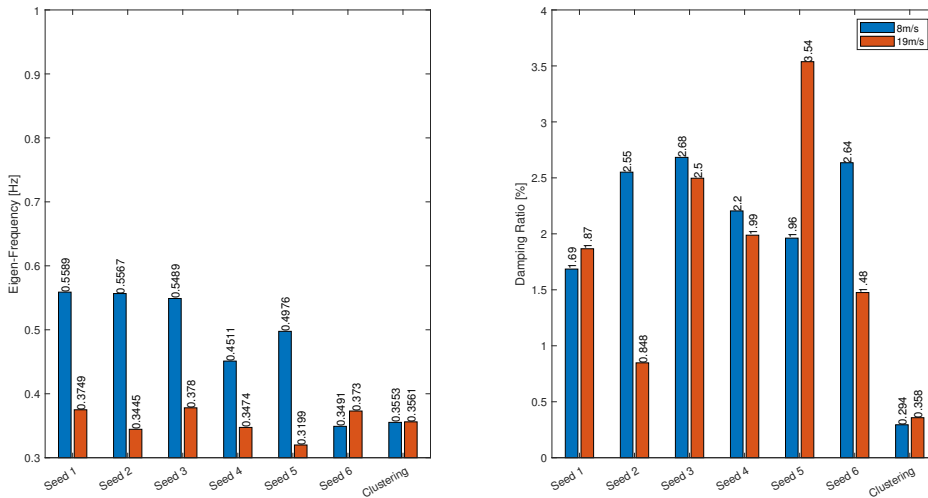
(b) Cross Wind

Figure 6.7: Modal Parameters Av04 using OMA-Sing with $fs = 100Hz$.

In order to better identify low modes of vibration, a down sampling of the FAST output was pursued. When using $f_s = 50Hz$, the automated peak picking method was able to extract the tower bending modes for the majority of the seeds, except for *Seed 2* and *Seed 4* along wind at 19 ms^{-1}, which had to be manually chosen. It may be mentioned that these two seeds had no odd condition in comparison to the remaining seeds, presenting Turbulence Intensity (TI) factors slightly below the seeds' average (Tab. 5.2). No particular reason was found to justify such behavior.
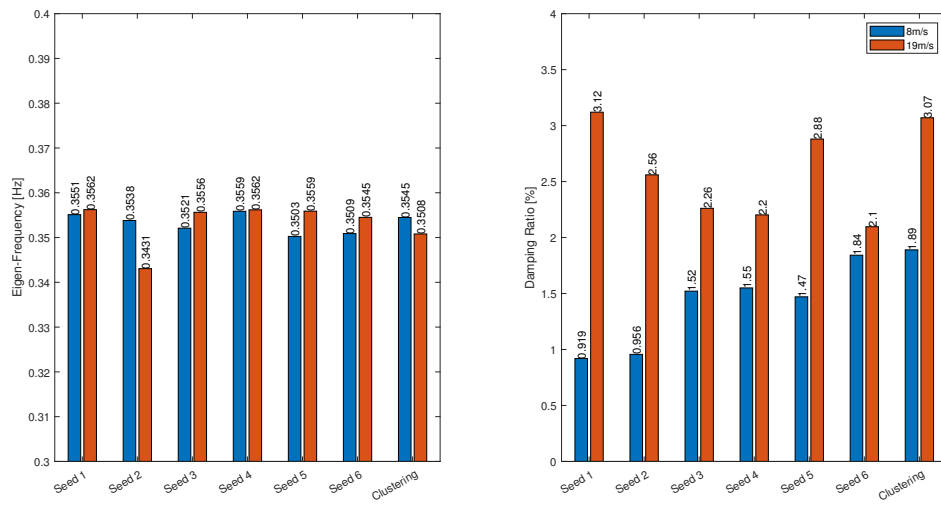
(a) Along Wind
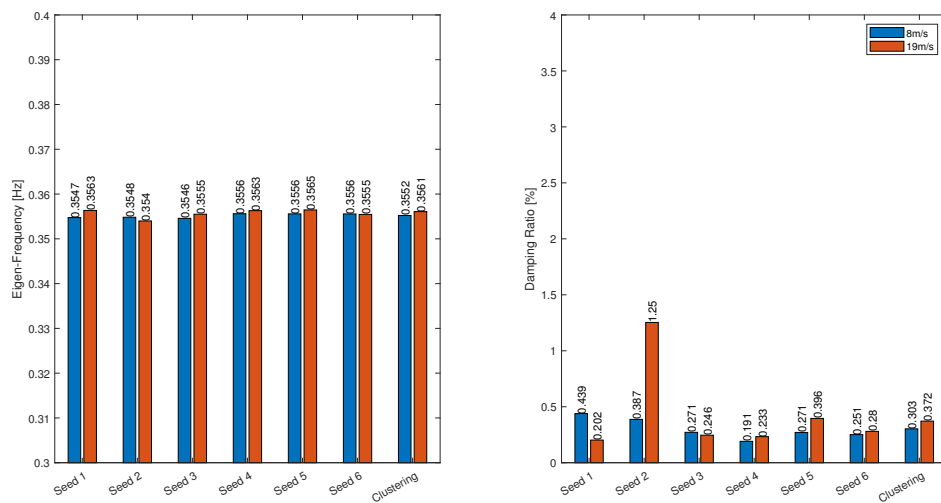
(b) Cross Wind

Figure 6.8: Modal Parameters Av04 using OMA-Sing with $fs = 50Hz$.

A further down sampling ($f_s = [25, 15, 10, 5]$ Hz) was performed seeking to improve identification and computational time. Nevertheless, the performance of OMA-Sing did not become more accurate, presenting non-straightforward correlation with f_s. Studying such iterations could be a great source of future work.

Figure 6.9 presents the mid steps from the OMA-Sing routine for the LC 2x1 and LC 2x3. In the left portion of the subfigures, a band pass filter is applied to each of the *Nmodes* identified with the peak picking routine. The blue lines stand for the

acceleration PSD and the red lines to the spectrum filtered at a given eigen frequency, highlighting the specific mode contribution. In the right side, the respective IRFs are found applying the covariance methodology, as shown from Eq. 3.20 to Eq. 3.30, but for a simpler system with one accelerometer ($M = 1$). The black lines stand for the IRF computed of each mode and the red line for the best fitting modified exponential decay function. All these plots regard the **clustered seeds**.
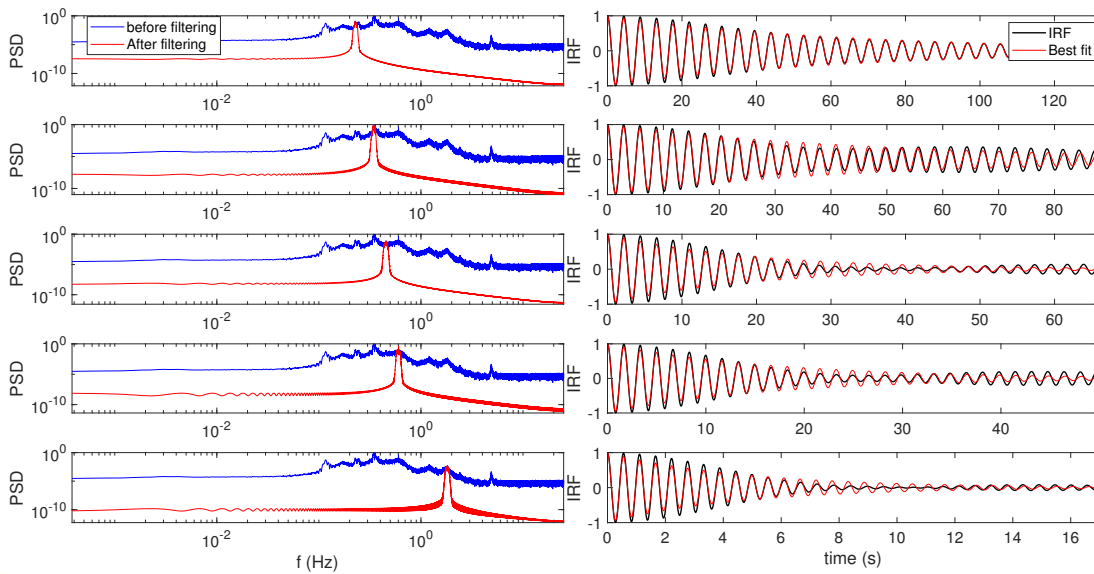
(a) LC 2x1 - 8m/s
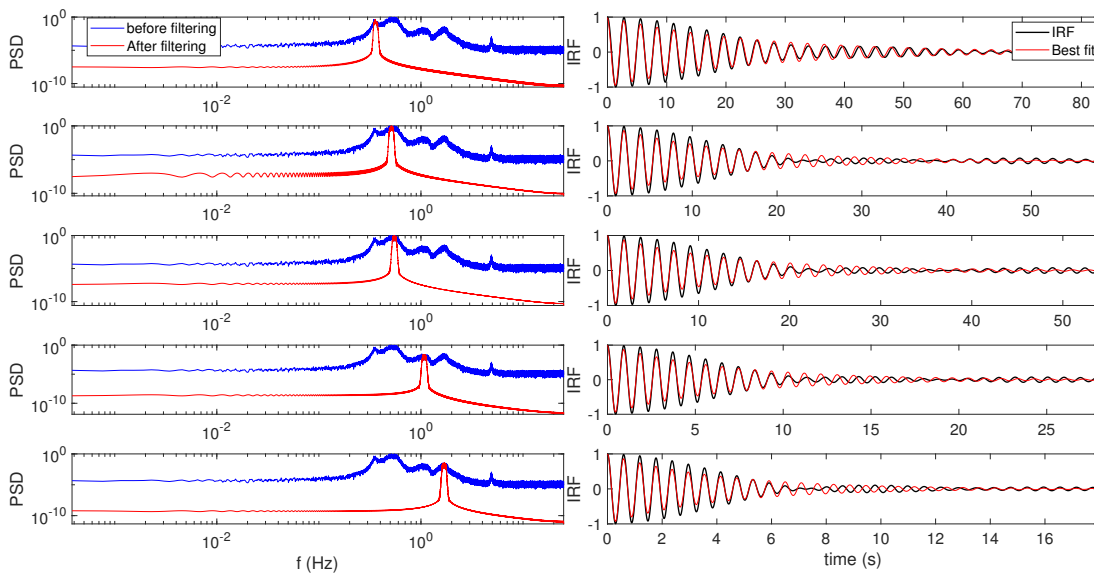
(b) LC 2x3 - 19m/s

Figure 6.9: Av04 **Seed Clustered** OMA-Sing (mid steps results) Band Pass Filter and IRF fitting - **Along Wind**.

In Fig.6.9, the fore aft tower bending mode is the second-lowest mode. This suggestion is based only on the frequency value of the found mode. Different from OMA SSI-COV, OMA Sing is not able to recover the mode shapes since it would require more than one acceleration sensor. The final damping ratio result should be another source of proof of whether the correct mode has been selected. For the sake of completeness, the extra wind condition ($13m/s$ and $23m/s$) seeds results will be also shared below.
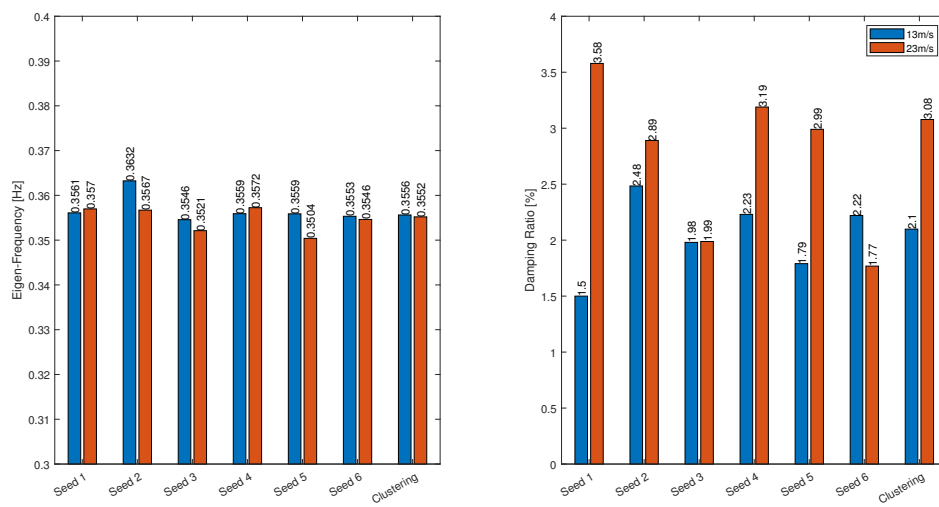
(a) Along Wind
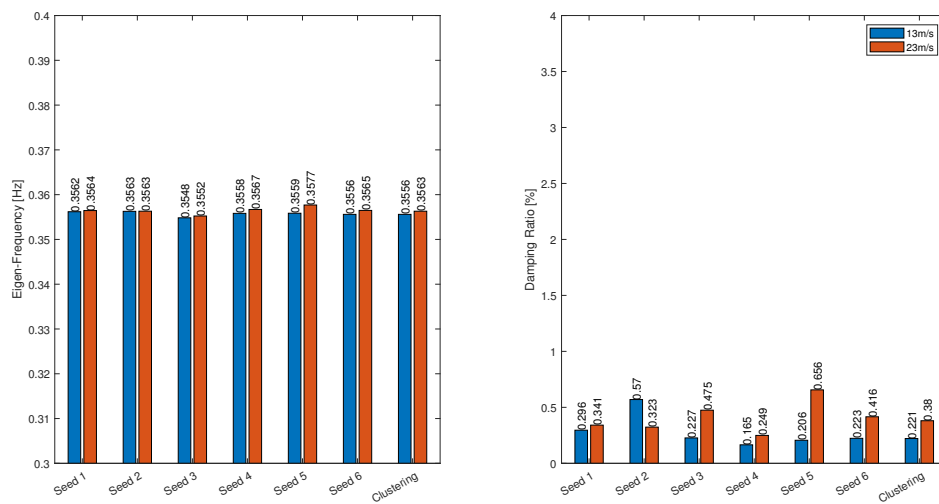
(b) Cross Wind

Figure 6.10: Modal Parameters Av04 using OMA-Sing with $fs = 50Hz$ (extra).

6.2.2. Av07 - Full Scale Data Output

As followed in Av04, OMA-Sing was applied to all previously selected seeds of Av07 (sec.5.4). For the measured data, OMA-Sing automated peak picking worked properly for all seeds, different from FAST Av04 seeds, in which manual peak picking was necessary.
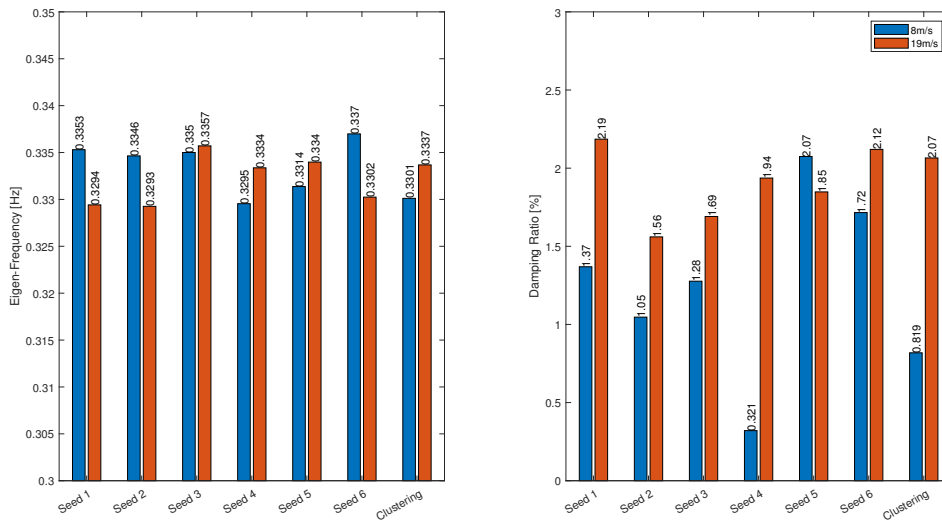
(a) Along Wind
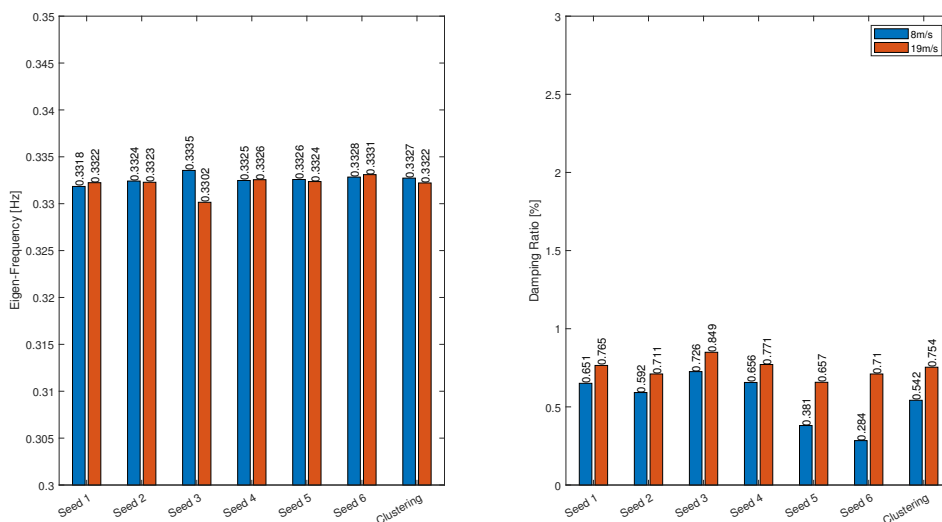
(b) Cross Wind

Figure 6.11: Modal Parameters Av07 using OMA-Sing with $fs = 50Hz$.

The OMA Sing routine for the Av07, Fig. 6.11, properly identified the tower

bending modes eigen frequencies for all considered seed. A smaller variability is seen for the cross wind motion when compared to the along wind motion. Same happened for the Av04 identification in Fig. 6.8.
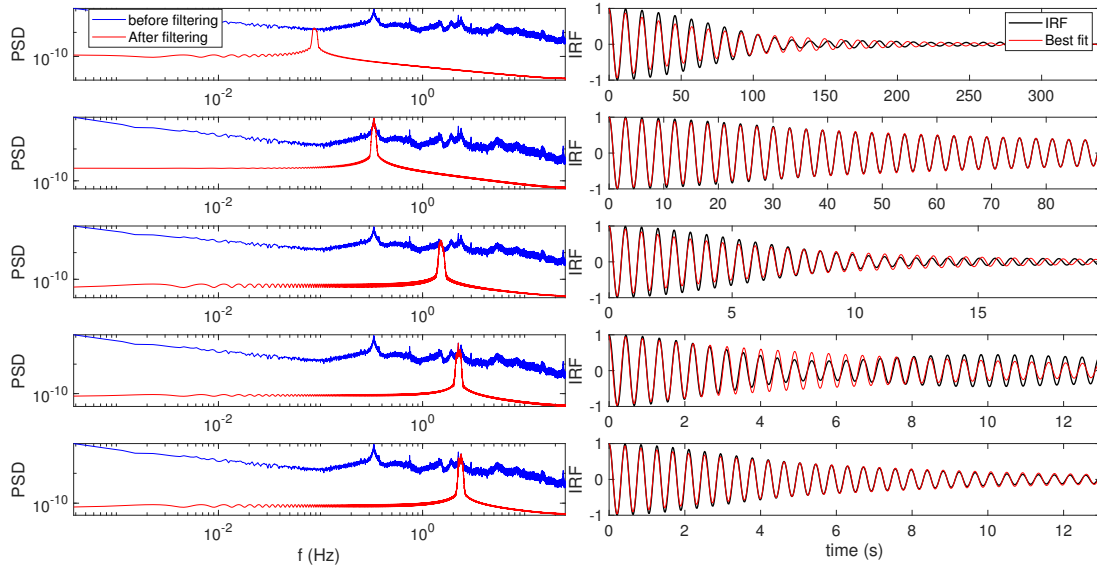
(a) LC 2x1 - 8m/s
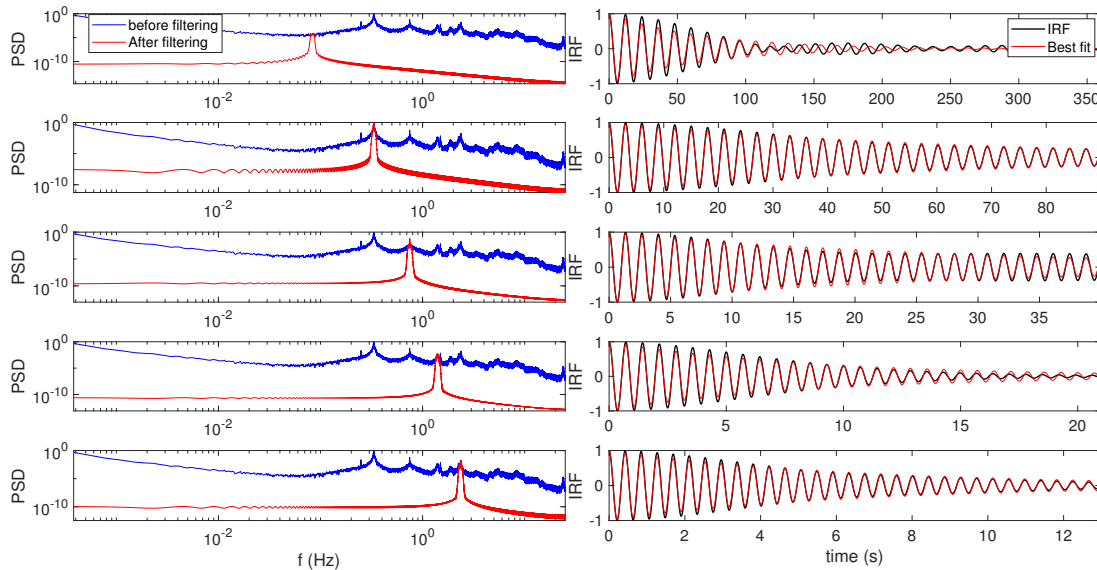
(b) LC 2x3 - 19m/s

Figure 6.12: Av07 **Seed Clustered** OMA-Sing (mid steps results) Band Pass Filter and IRF fitting - **Cross Wind**.

Besides that, along wind damping ratio presented higher trend to the increasing wind speed against cross wind damping ratio. Comparing the wind speeds of 8 ms^{-1} and 19 ms^{-1}, the damping ratio increase was of 152.7% and 39.1% for the along

wind and cross wind motion respectively. For Fig.6.12, cross wind tower bending mode is the second-lowest mode identified by OMA-Sing. Both along wind and cross wind tower bending modes can be distinguished from the other modes since they are the only peaks in the PSD spectrum around 0.35Hz, as expected from the MLD results shared at Tab. 4.4. The closest and fairly spaced mode generally identified is at around 0.6Hz, suggesting to be the 3P rotor harmonic, as seen in Fig. 4.8. As done for Av04, the extra seeds modal extraction results will be attached below.
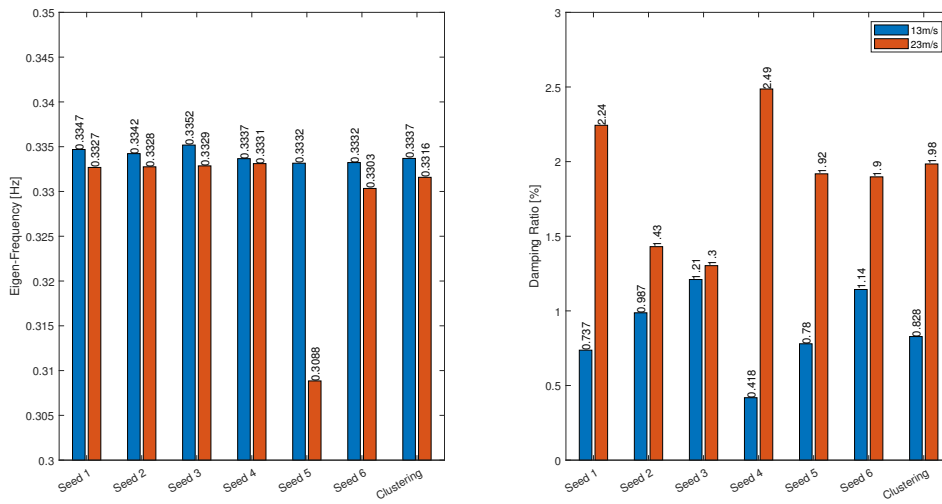
(a) Along Wind
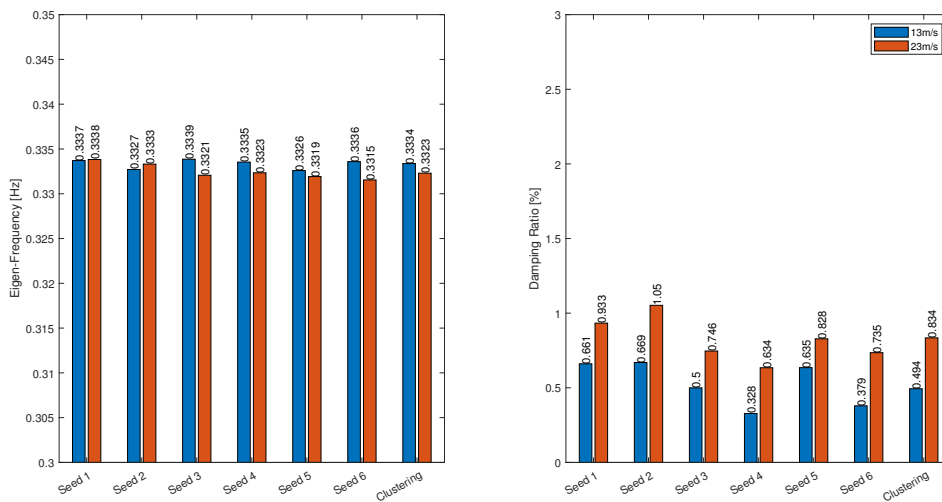
(b) Cross Wind

Figure 6.13: Modal Parameters Av07 using OMA-Sing with $fs = 50Hz$ (extra).

6.2.3. Comparison of OMA Sing results

Results of the previous sections are compared in this one to understand whether OMA Sing presented different performances between the FAST model and the full-scale measured data. Moreover, discuss the differences in the along wind and cross wind modal parameters extraction. It was chosen to use error bar plots, which facilitate the visualization of the mean response and its variability.
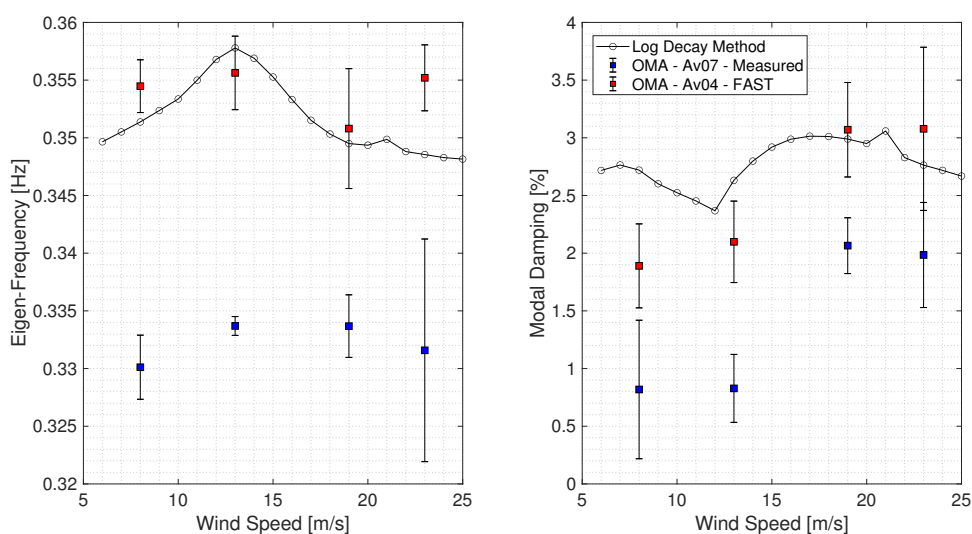
Figure 6.14: Error Bar Plot of OMA-Sing Along Wind Results against Log Decay.

The along wind motion eigen frequencies of the Av04 were properly identified, with great accuracy. Almost the same outcome for the Av07, with slightly higher uncertainty for the highest wind speed, still lower than 4% of variability.

For damping, the simulated Av04 presented a similar variability to Av07, which was not expected since the first one has significantly fewer liabilities compared to full-scale measurements as noise, sensors malfunctioning and non-stationary wind time-series. For the Av04 along wind motion identification at 23 ms^{-1}, two seeds (3 and 6) had to use the OMA Sing manual pick peaking routine. The manual solution provided values more distant from the reference MLD, as shown in Fig. 6.10. This might be one source of variability for the Av04 modal extraction. This could also be suggesting that the loading conditions have a lower effect on the OMA Sing performance when compared to highly damped responses' identification.

Anyhow, the highest damping difference between MLD and OMA Sing for the Av04 along motion was 29.5% for 8 ms^{-1}. On the other hand, the high variability for

the Av07 identification at 8 ms^{-1} could be the outcome of the higher TI factors of its seeds, when compared to the 19 ms^{-1} seeds (see Tab. 5.2 and Tab. 5.3). Such behavior suggests that higher TI introduces higher damping ratio uncertainty to OMA Sing identification on full-scale data.

For both Av04 and Av07, it was possible to visualize two distinct controller setting regions: the first one, below rated wind speed, where rotor speed increases with higher wind speeds; and the second, above rated wind speed, where the fixed-speed variable-speed (FS-VP) mode of operation continuously adjust the pitch angle to maintain a constant power generation for above rated wind speeds. In particular, for Av04 and Av07, the power limitation is pursued by a pitch-to-feather regulation, where the aerodynamic thrust force decreases as wind speed arises, with a significant lift coefficient drop and remaining low drag coefficient. In this way, as seen in Fig. 6.14, damping at above rated wind speeds (19 ms^{-1} and 23 ms^{-1}) do not increase as sharply due to limited aerodynamic contributions, but presents rather a smooth trend compared to values between 8 ms^{-1} and 19 ms^{-1}. In summary, OMA Sing is able to illustrate such a phenomenon while identifying the modal damping ratios.
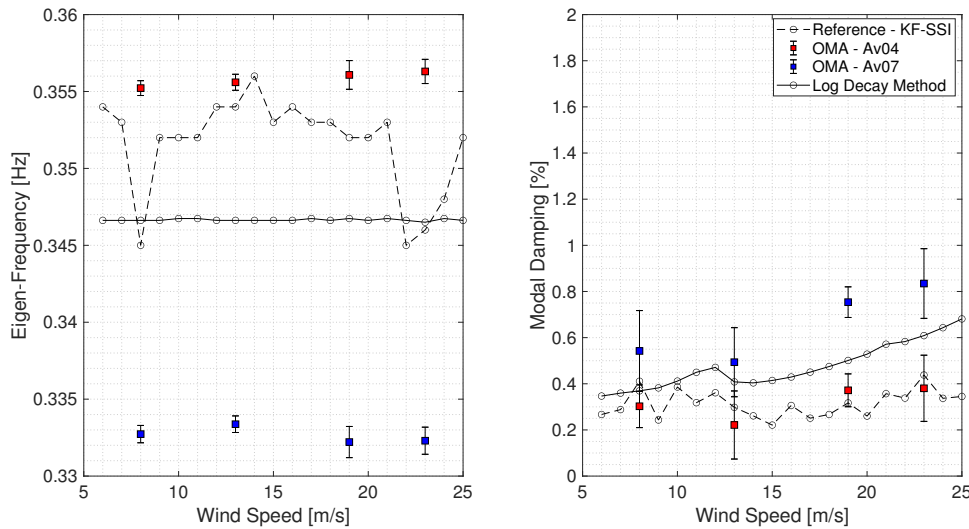
Figure 6.15: Error Bar Plot of OMA-Sing Cross Wind Results against Log Decay and Reference ([42]).

The cross wind eigen frequencies are identified for both Av04 and Av07 with better accuracy (lower variability). The cross wind damping ratio of Av04 is smaller than the MLD reference, with a maximum difference of 35% for 23 ms^{-1}. Moreover, it showed a very similar behavior compared to validated data from [42], where the

OMA KF-SSI is applied to a 6 MW operational OWT at the Dudgeon wind farm. OMA Sing was able to properly distinguish along and cross wind modal parameters even though being very closely spaced modes. It presented very different damping ratio orders of magnitude for the orthogonal tower modes, highlighting the aerodynamic contribution over the structural. Moreover, the controller regions could be seen on along wind motion's identification for both simulated Av04 and full-scale Av07.

6.3.   OMA SSI-COV

The same OC5 LCs methodology followed by the OMA-Sing was set for OMA SSI-COV.

A significant difference, from the given tool to the previous already discussed, is that it was applied in a fully automatized way. The automated "behavior" can be divided into two principal steps: firstly, inside the OMA SSI-COV code, as described in items *4* to *6* on Sec.3.3; secondly on the post-processing of modal parameters found for all the seeds analyzed. The last one was pursued by applying a second clustering routine. Wind conditions could not be assumed constant for the second routine and had to be assigned for each mode. As previously, a hierarchical-agglomerative clustering or linkage clustering was chosen, however, this time, based on the frequency (eps_{freq2}) and neglecting minor clusters ($\geq min\_clust\_size = 10$).

Moreover, a further down sampling was applied to the Av04 and Av07 acceleration data. SSI-COV is a more complex tool and computational effort must be reduced. A down sampling factor of six was applied, leading to a final $d_t = 0.06s$.

The Stabilization Diagram accuracy thresholds were set to: $\delta_{freq} = 0.01$, $\delta_{zeta} = 0.05$ and $\delta_{MAC} = 0.005$, based on [18]. The δ_{MAC} was lowered compared to the reference and still a good behavior was found in the diagrams, where the number of poles with a stable frequency and stable damping did not over-prevail.

6.3.1.   Av04 - FAST Data Output

OMA SSI-COV was applied to FAST outputs *TwHt1ALxt* to *TwHt5ALxt* for the along wind motion and *TwHt1ALyt* to *TwHt5ALyt* for the cross wind motion. They represent the tower acceleration at five equally separated height levels on along wind and cross wind directions respectively. The stabilization diagram of two wind conditions (8 ms^{-1} and 19 ms^{-1}) is firstly shown providing the necessary tools to

analyze the performance of OMA SSI-COV.

(a) Along Wind

(b) Along Wind - Limited Range

(c) Cross Wind - Limited Range
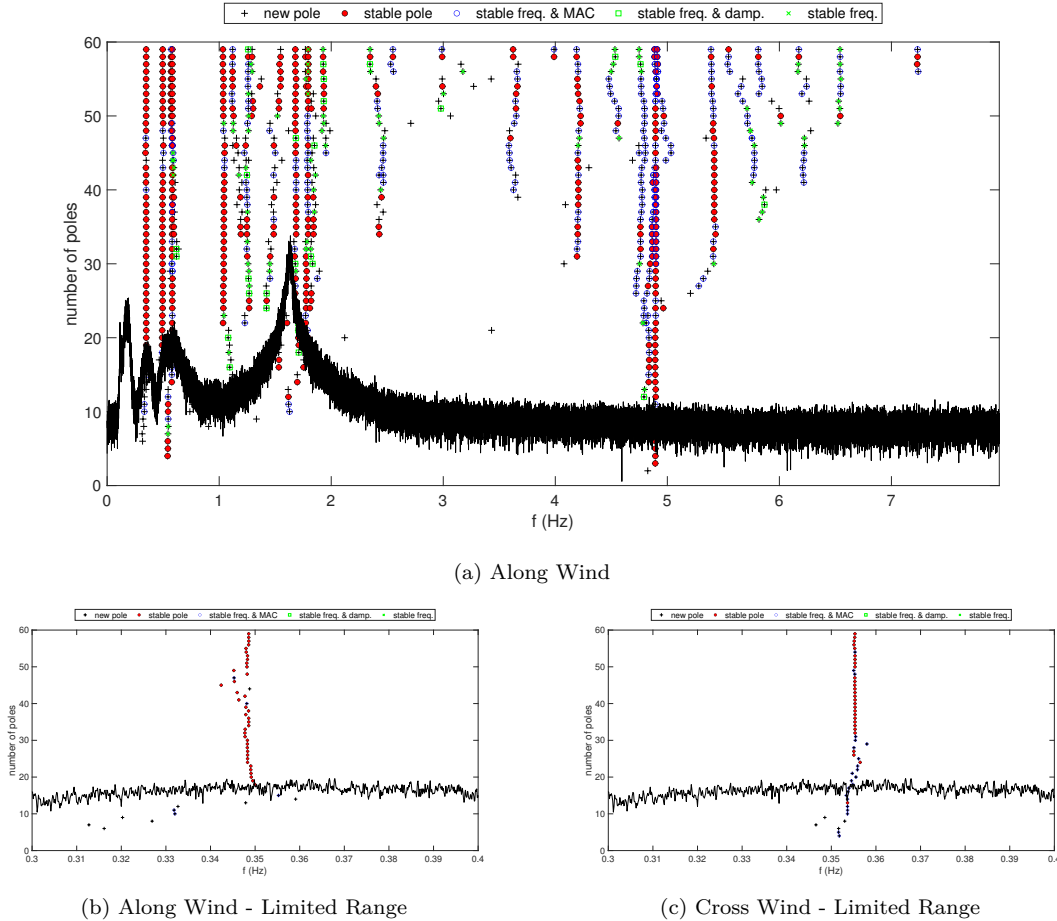
Figure 6.16: Av04 OMA-SSI Stabilization Diagram for **Seed Clustered - 8m/s**.

Figure 6.16 illustrate the Stabilization Diagram for the 8 ms^{-1} wind speed. For the low wind speed, both along and cross motions have a good identification accuracy for the first tower bending modes (around 0.35Hz), with many stables poles identified. However, along wind motion presents less concentrated modes for the same accuracy parameters compared to cross wind motion. The dispersion of modes for closely spaced poles in the along wind (limited range) suggests the presence of spurious modes in between structural modes, as explained on item 4 in Sec.3.3. The overall Stabilization Diagram, Fig.6.16(a), also shows that higher frequency modes can only be identified with a higher number of poles.

(a) Along Wind

(b) Along Wind - Limited Range

(c) Cross Wind - Limited Range
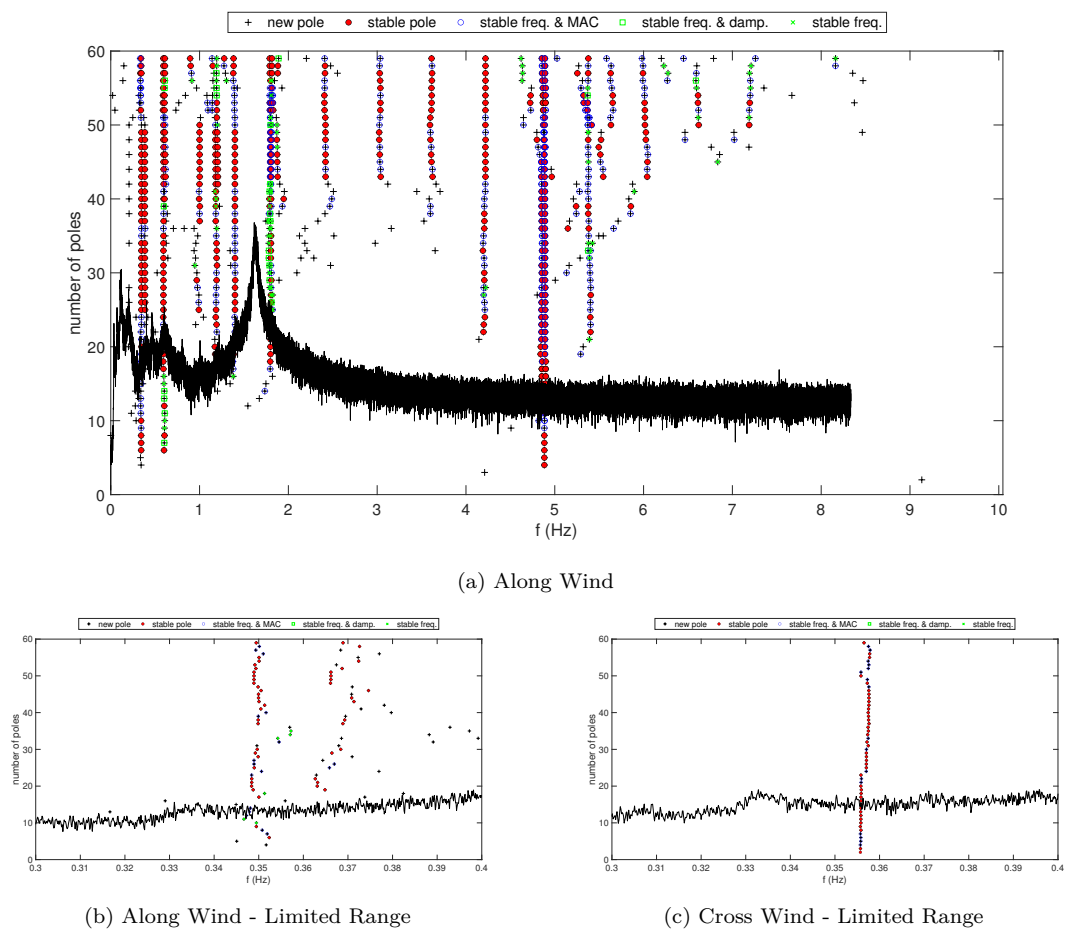
Figure 6.17: Av04 OMA-SSI Stabilization Diagram for **Seed Clustered - 19m/s**.

Differently from the below rated wind speed, the along wind identification for 19 ms^{-1} should provide less reliable results, since many modes are spread in the frequency range of interest (Limited Range). The poor identification performance for any range of poles' numbers in Fig.6.17(b), partially avoids the hypothesis that spurious modes arise due to an over-estimation of the system order [30]. Furthermore, the higher acceleration standard deviations for higher wind speeds, as shown for Av07 full-scale measures at Fig.5.10, may suggest that OMA-SSI could present lower performance not only for highly damped system's identification but also when unsteady aerodynamic contributions increase. The cross wind modes are still very well extracted with several stable poles closely spaced.

(a) Along Wind
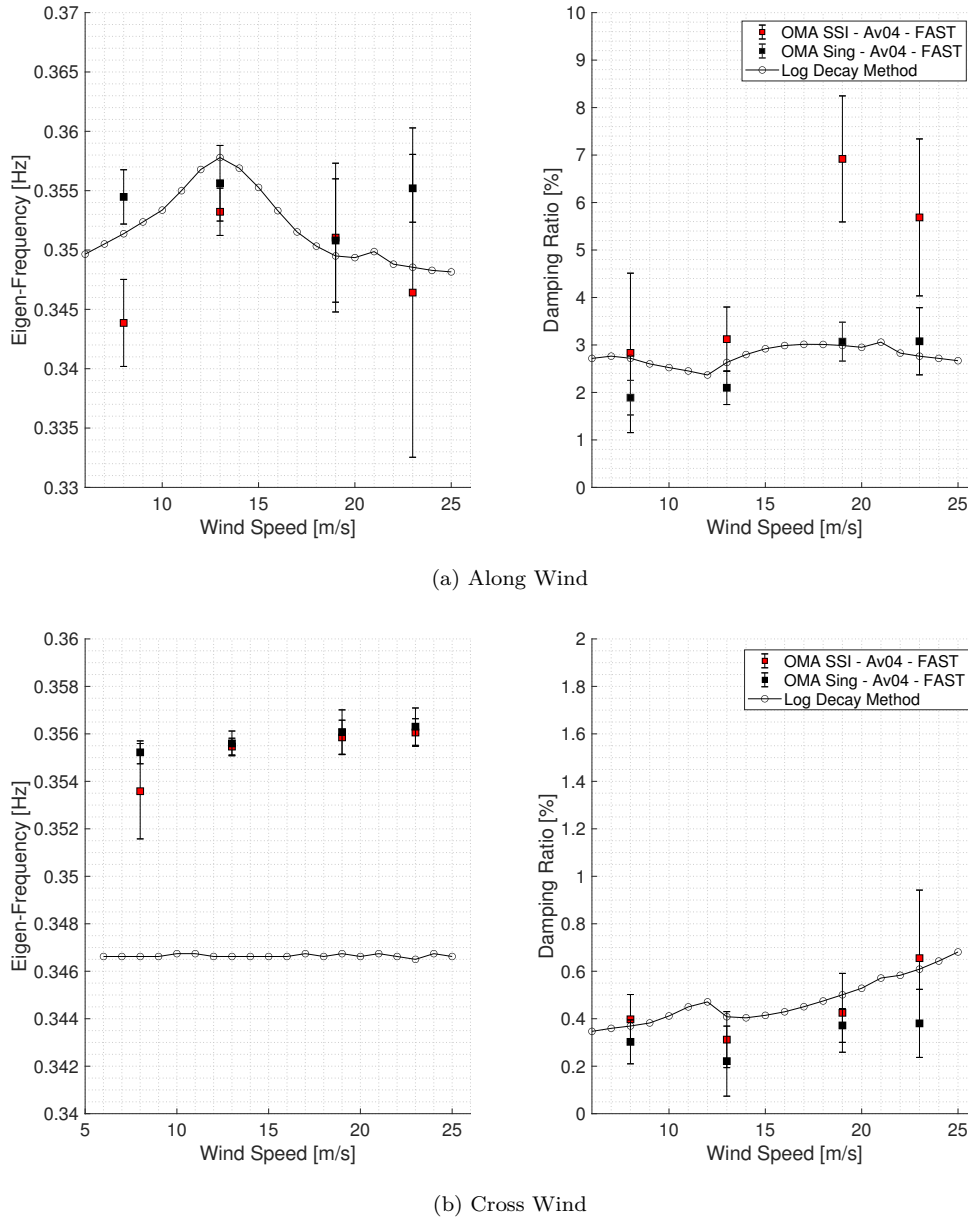
(b) Cross Wind

Figure 6.18: Error Bar Plot of Av04 OMA SSI-COV Modal Parameters for all seeds against OMA Sing and MLD.

As expected by analyzing Fig.6.16 and Fig.6.17, OMA SSI-COV has a great performance for the cross wind motion. The damping ratio of the cross wind or side to side tower mode had a good match with the MLD reference, better than compared to OMA Sing. Either modal parameters had better identification accuracy.

On the other hand, in the along wind motion identification, there is a big over prediction of the damping ratio for above rated wind conditions, in parallel with very

high variability. The accuracy of the mode identification in terms of eigen frequency is also negatively affected by higher wind speeds for the OMA SSI-COV. Since the stationarity and white noise loading assumptions are satisfied for the FAST model, one remaining feature that could be influencing the OMA SSI-COV performance is the higher levels of damping, above 3%.

Nevertheless, it must be mentioned that OMA SSI-COV can distinguish the orthogonal modes, along wind motion and cross wind motion. Even though being closely spaced modes, the eigen frequencies were identified with high accuracy and the damping ratios had a visible different order of magnitude.

Before aiming for a conclusion on the tool's capabilities and limitations to identify modal parameters, OMA SSI-COV is applied in the full-scale Av07 data, to further check its performance.

6.3.2. Av07 - Full Scale Data Output

Due to unsure documentation, the exact location of the five pairs of accelerometers in Av07 tower was not precise, in terms of height and direction. Regarding the first uncertainty, a big advantage of OMA SSI-COV is that knowing the sensor's height position is not necessary.

Concerning the second uncertainty, Av07 had two pairs of accelerometers at a given height, each pair at diametrically opposite points (90° and 270°). This allowed averaging the respective signals as the resultant acceleration record, removing the torsional component and reducing the measurement noise from both along and cross wind motions. But still, the direction was a meaningful issue.

The unsure sensors positioning due to ongoing documentation and unreliable wind direction data requested the application of a novel methodology. The principal component analysis (PCA) was applied to retrieve the linearly uncorrelated along wind and cross wind variables with respect to the wind excitation. On the OMA Sing, the nacelle accelerometer is parallel to the wind excitation at every instant, whereas for tower sensors, this is rarely the case. The PCA algorithm identify orthogonal projections of a data onto lower-dimensional space, by building the covariance matrix from the input data and decomposing it (SVD). In many cases, PCA is used to reduce the dimension of a dataset, but at this thesis, it was applied to recover the uncorrelated orthogonal tower motions, where the initial 2-D data dimension remained.

As done for Av04, relevant stabilization diagrams are discussed. Afterward, the modal

parameters extraction results of the tower bending modes using OMA SSI-COV will be presented.

(a) Along Wind

(b) Along Wind - Limited Range

(c) Cross Wind - Limited Range
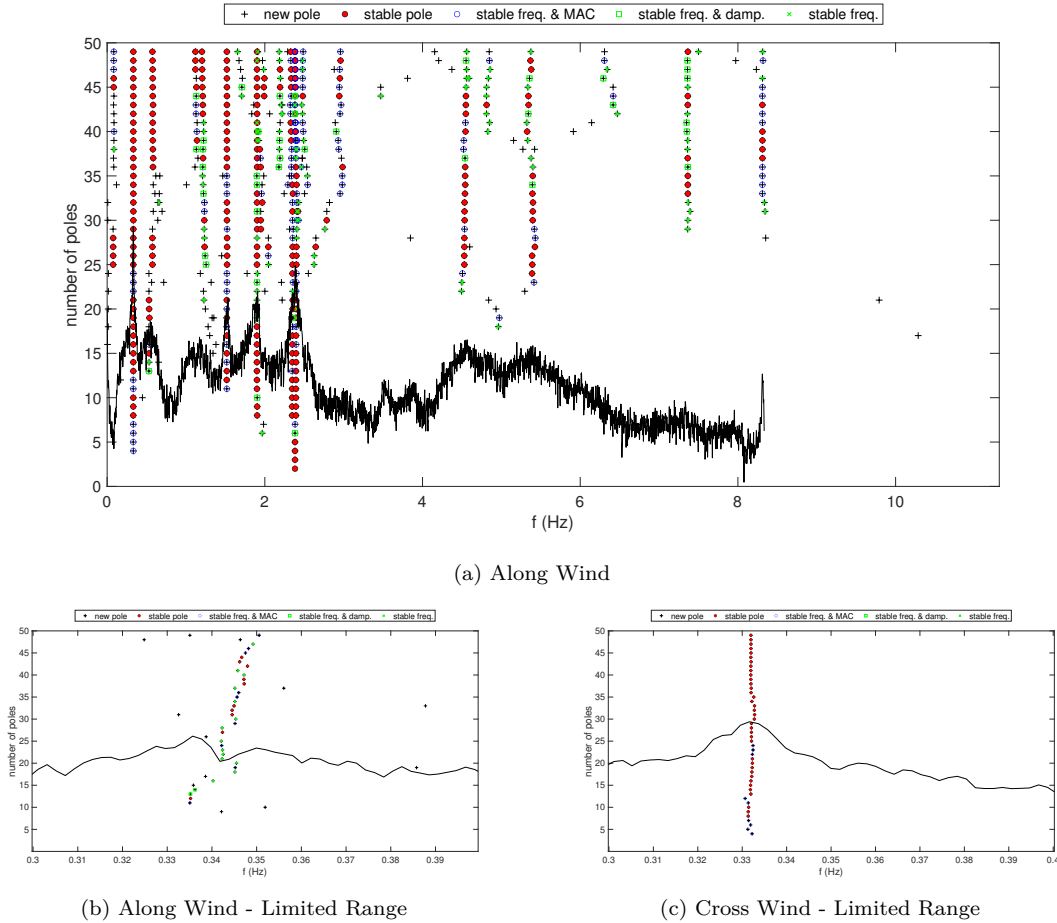
Figure 6.19: Av07 OMA-SSI Stabilization Diagram for **Seed 8m/s**.

OMA SSI-COV identified several stable poles for the cross wind motion. On the other hand, the along wind mode identification presented very spread results even for below rated operation conditions and a low amount of stable modes. Spurious modes prevailed over structural modes for all the range of pole's values. A very similar behavior is seen in Fig.6.20. This suggests that OMA SSI-COV is not able to easily catch the modal parameters from full scale along wind motion. However, it is not possible to confirm this statement without a larger number of samples for a more robust analysis, considering several wind conditions, such as atmospheric stability, turbulence intensity and wind speed. Such analysis will be initially performed in Sec.6.3.3.
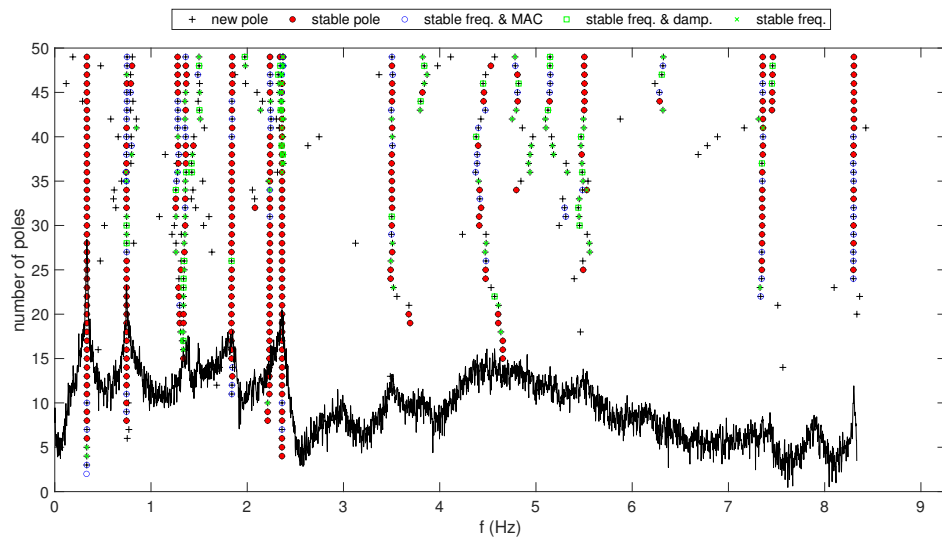
(a) Along Wind
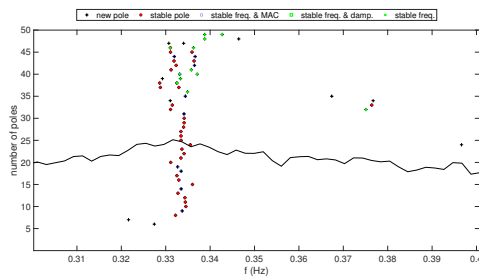
(b) Along Wind - Limited Range
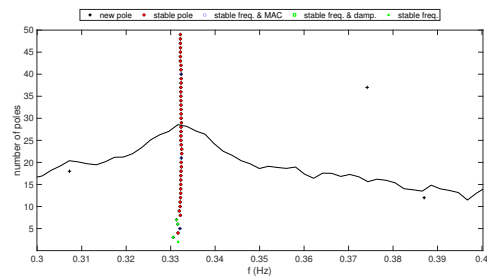
(c) Cross Wind - Limited Range

Figure 6.20: Av07 OMA-SSI Stabilization Diagram for **Seed 19m/s**.

OMA SSI-COV again exhibited in Fig.6.20 very discrepant identification performance for above rated wind speed depending on the orthogonal tower mode. The along wind motion identification is rather dispersed for the whole range of pole's order, highlighted for a number of poles greater than 30.

The cross wind identification, as shown in Fig.6.20(c), is still very promising for above rated wind speeds. The cross wind tower bending mode is properly identified with a predominance of stable modes, indicating once again that the OMA SSI-COV is mainly influenced by the damping order of magnitude rather than the wind loading conditions.

Final Av07 modal parameters identified by using OMA SSI-COV are shared below.
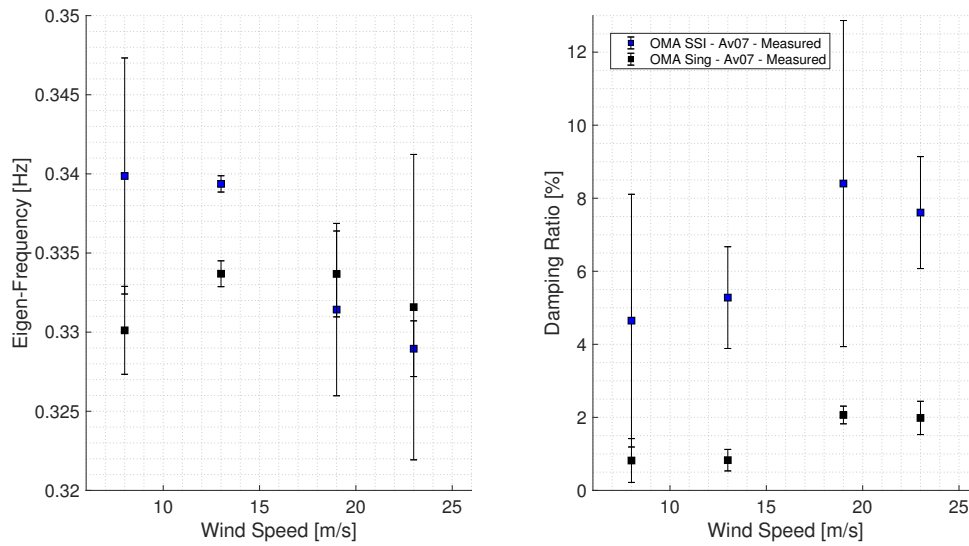
(a) Along Wind
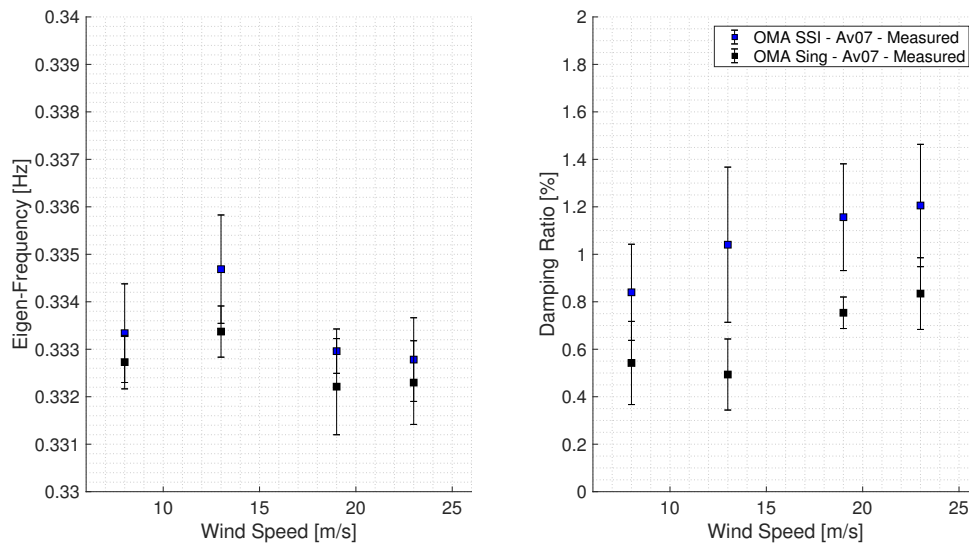
(b) Cross Wind

Figure 6.21: Error Bar Plot of Av07 OMA SSI-COV Modal Parameters for all seeds against OMA Sing.

The overall performance of the OMA SSI-COV is well predicted by the analysis of the mid-step automated stabilization diagrams.

The along wind motion identification of the Av07 full-scale data using OMA SSI-COV is challenging. The eigen frequencies extracted and shown in Fig.6.21(a) are uncertain and point in large subsequent damping ratio's identification, in terms of absolute value and standard deviation.

Diversely, for the cross wind motion, OMA SSI-COV presented a good performance. The variability of the eigen frequency values is as accurate as for the already validated OMA Sing. Besides that, damping ratio identification showed a more visible trend to wind speed. The absolute damping ratios are higher than OMA Sing technique results. A wider amount of seeds should be selected to validate the cross wind damping ratio values.

Aiming to further verify the different performances of OMA SSI-COV depending not only on the vibration response damping order, but also on different operating and meteorological conditions, the whole month of November will be analyzed. All available 30-minute average seeds are considered in the following section.

6.3.3. Atmospheric conditions' effect on the OMA SSI-COV results

OMA SSI-COV presented higher damping ratio values for both along and cross wind motions identification in comparison to MLD and OMA-Sing. For the along wind (Fig.6.21), even the eigen frequencies had larger uncertainty and the damping variability was large.

Analyzing a bigger database should be a good strategy to verify whether OMA SSI-COV performance is being affected by specific operations conditions. Otherwise, highlight OMA SSI-COV limitations or poor tuning.

Instead of only identifying six particular seeds for four different wind speeds, the whole month of November 2015 was analyzed. A total of 1440 dataset were analyzed ($2\frac{seeds}{hour}$ x $24\frac{hours}{day}$ x $30\frac{days}{month}$).

The second clustering routine was tuned for a bigger dataset. The linkage function was more rigorous, including frequency and damping in the distance criterion. In this way, the tower bending modes should be properly identified, each with a significant number of points.
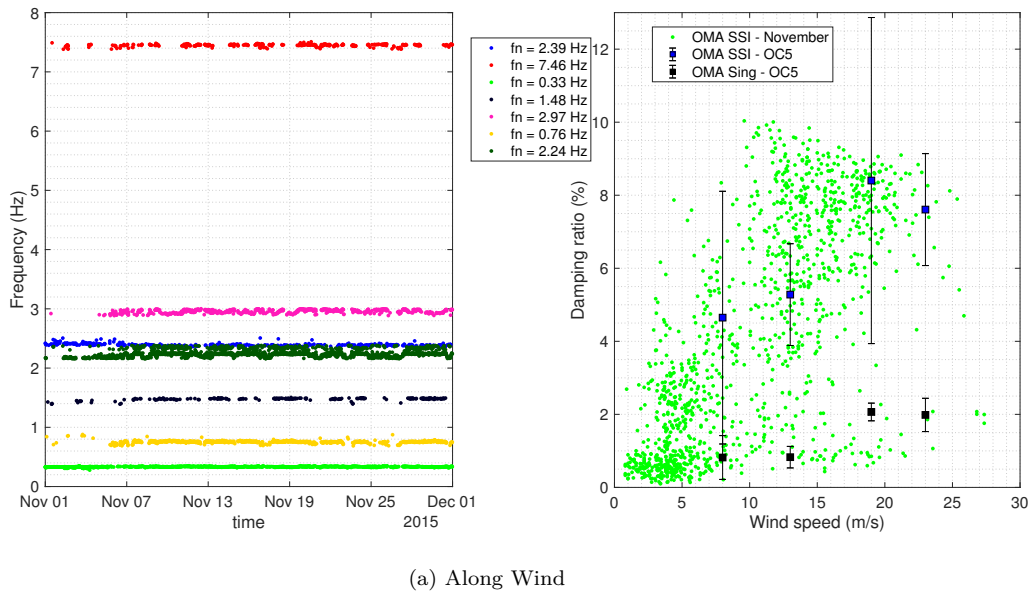
(a) Along Wind

Figure 6.22: Av07 OMA SSI Eigen Frequency and 1st Tower Mode Damping Ratio.

(a) Cross Wind
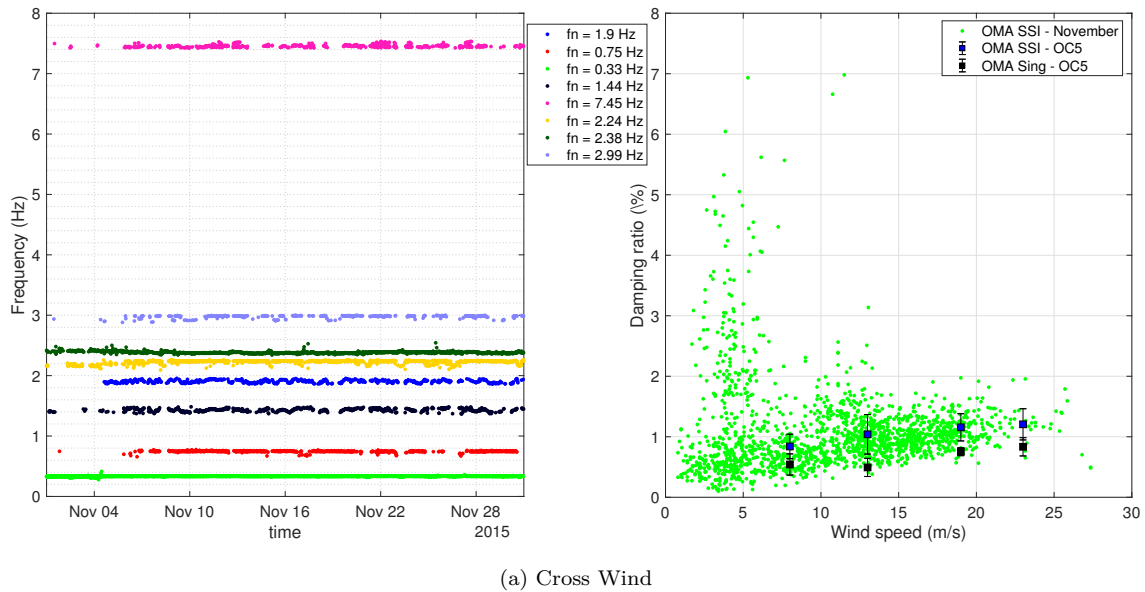
Figure 6.23: Av07 OMA SSI Eigen Frequency and 1st Tower Mode Damping Ratio

The damping ratio for the along wind motion has a large variability for almost all the wind speed range, even though the eigen frequency ($0.33Hz$) is properly identified throughout the whole month of November (green color). The damping ratio for the cross wind motion is significantly more accurate compared to OMA Sing. However, from 2 to 7 ms^{-1}, some samples presented damping ratio values around

and above 3%, which is higher than expected by MLD and OMA Sing.

Because of these inconsistencies, November 2015 Av07 damping ratio results were filtered with respect to different meteorological, operational and structural-response conditions, trying to find possible features that could be biasing the damping identification and setting unreal absolute high values, up to 13% for along wind, and variability.

The main goal is to understand whether there are noise spurious modes prevalence in Fig.6.23 and if they are the outcome of physical conditions, such as the TI factor or the mean yaw direction, rather than driven by numerical OMA tool's limitations.

Sensibility Analysis - Cross Wind Damping Ratio

A sensibility analysis of the main operating conditions is done in this section trying to understand the presence of a correlation of modal damping ratios with atmospheric conditions for wind speeds from 2 to 7 ms^{-1}.

(a) Nacelle Mean Yaw (°)

(b) Turbulence Intensity (%)

(c) Blade Pitch (°)

(d) Generator Speed (rpm)

(e) Acceleration RMS (m/s²)
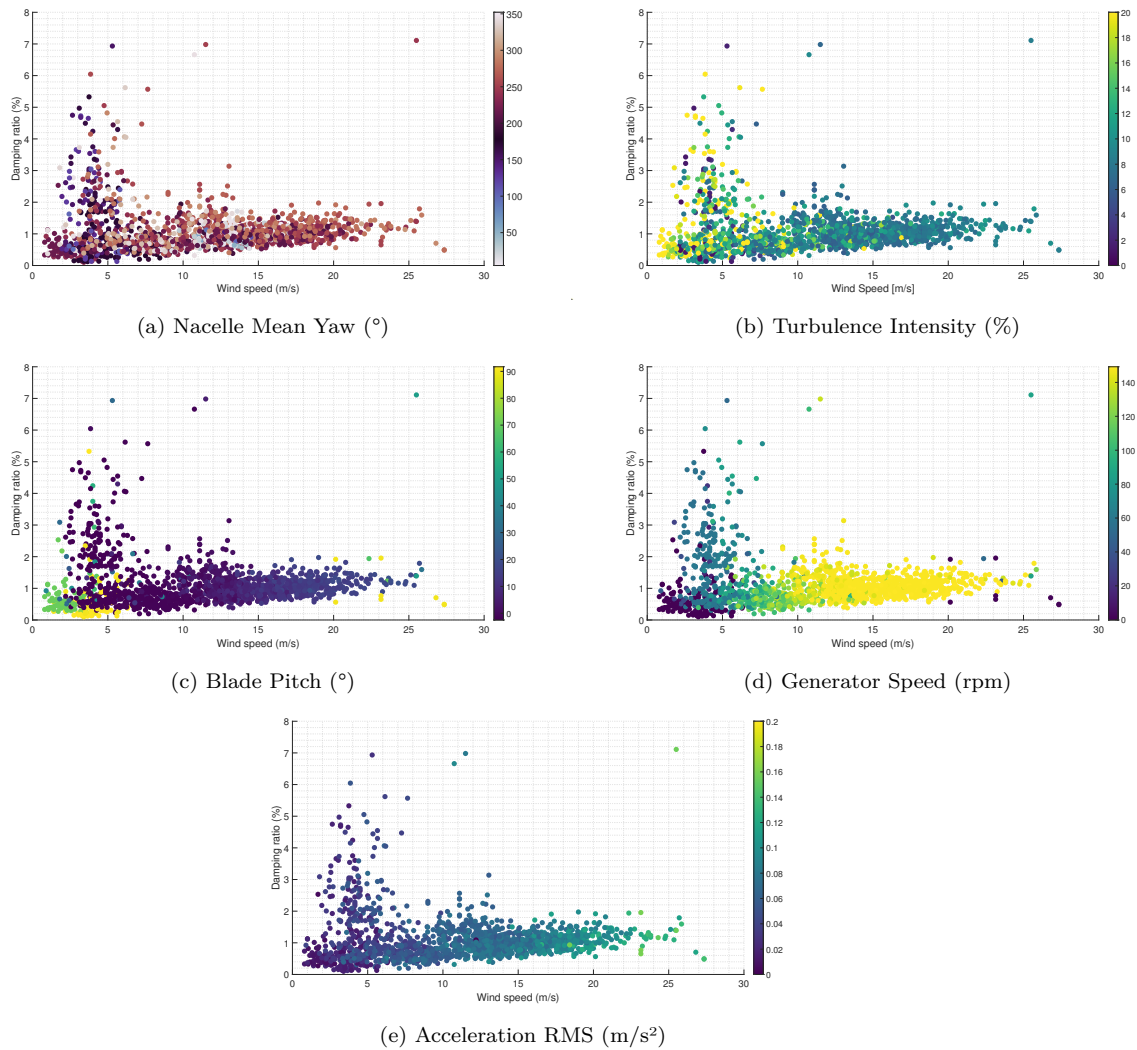
Figure 6.24: Cross Wind Damping Sensibility Analysis for Av07 OMA SSI-COV.

It is possible to visualize a correlation between the scatter damping ratio and the mean nacelle yaw. In Fig.6.24(a), there is a range between 100° and 150°, in which the identification is worsened, with high damping ratio variability and spread points. A work of 2014 on the wake effect in the Alpha Ventus Wind Farm [43] highlighted a lower generation efficiency for partial loads when 3 OWTs and 4 OWTs were in a row, at around 90° and 180° respectively. This could be a hint for the worsening effect of the nacelle mean yaw influence on the cross wind damping ratios, when Av07 is in the wake of other turbines. A similar correlation can be seen with the TI factors in Fig.6.24(b). The scatter for low wind speeds is mainly related to TI factors higher than 18%.

The remaining parameters, blade pitch, generator speed and acceleration RMS are

shared for the sake of completeness. They validate the proper operation of the Av07 OWT for the analyzed samples, however they did not guide conclusions on the damping ratio variability.

Sensibility Analysis - Along Wind Damping Ratio

Significant correlation parameters are shown in Fig. 6.25. Sub figures (b) and (c) illustrate that the controlled blade pitch and generator speed did not directly affect the OMA SSI-COV results for the along wind identification, since there is a high variability for almost all the range of controller operating regions: from 0° to 20° of blade pitch and from 40 rpm to 140 rpm of generator speed.

Concerning the turbulent stochastic flow impact on the OMA SSI-COV performance to identify the along wind tower modal damping, there is a slight worsening effect for low wind speeds, between 2 to 8 ms^{-1}, when TI factors are larger than 18%. However, for higher wind speeds, the majority of the seeds presented no correlation between OMA variability and TI values.

Other sensitivities tests were pursued, including the effect of the mean nacelle yaw direction, acceleration RMS, wave direction and atmospheric instability, but no clear relationships with the modal damping ratio were observed.

The sensibility analysis pursued in this section indicates that the OMA SSI-COV performance is worsened in the presence of highly damped vibration responses, with greater than 3% modal damping ratios.

(a) Turbulence Intensity (%)

(b) Blade Pitch (°)

(c) Generator Speed (rpm)
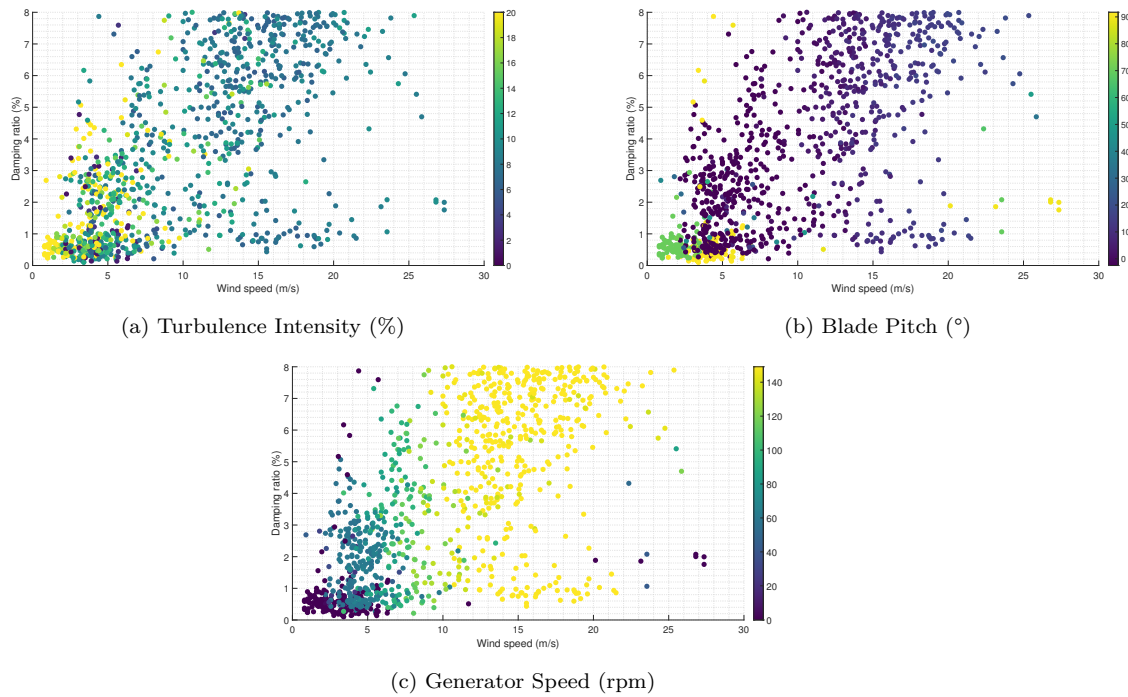
Figure 6.25: Along Wind Damping Sensibility Analysis for Av07 OMA SSI-COV.

The scatter plot of Fig.6.23(a) for the highly damped along wind motion should be caused by numerical uncertainty related to the OMA SSI. As discussed in [5], extracting the damping ratio from highly damped modes is a challenging task for many system identification methods.

In theory, longer lengths of acceleration data may lead to increased accuracy of the OMA SSI-COV identification, mainly for high damping modes. However, the identification of the FAST model along wind response, using 30-minute datasets, also showed poor performance of OMA SSI-COV (check Fig.6.18(a)). Longer time lengths might not provide better OMA SSI-COV performance but increase the computational effort and the uncertainty of the meteorological conditions from real wind park data. In parallel to that, as previously commented, the OMA SSI-COV algorithm has been applied in the study of the vehicle-induced vibration response of the Lysefjord Suspension Bridge [26]. The loading excitation was non-stationary, which does not respect the white-noise zero-mean assumption. However, OMA SSI-COV still produced good results in terms of modal damping identification.

Ultimately, the along wind larger damping variability found using OMA SSI-COV suggests that the tool has a limitation, not related to the meteorological or operating conditions, to identify highly damped modes.

7 | Conclusions and Future Developments

This thesis work sought to address two major objectives: validate two different OMA methodologies on OWTs, applying them to both full-scale data from Av07 and FAST data from Av04; and verify the identification and behavior of the first tower bending modes, along wind and cross wind, modal parameters.

The methodology presented in the Sec.4.2 has been consistently applied during the given thesis. Initially, the Av04 FAST model was validated after a tower modal stiffness tuning and performed well in terms of NRMSE.

Even though different numerical model and full-scale OWTs were considered in this thesis, the methodology generated to validate the OMA tools aimed to be applicable in a generic OWT.

The main conclusive pieces from this thesis unfolded from the research questions and objectives presented in Sec.1.1.

Concerning the two OMA tools validation

- OMA Sing and OMA SSI-COV were able to distinguish the closely spaced orthogonal tower modes. The eigen frequencies identified for the Av04 FAST model matched well the MLD reference for all wind conditions, with an average and maximum difference of 3% and 4% respectively.

- The OMA techniques were able to identify the along wind and cross wind distinct damping ratio behaviors, for both simulated and full-scale data. In the second case, the white noise excitation assumption is not fully respected due to inevitable non-stationary meteorological conditions in a real wind park and yet the OMA tools showed to be robust.

Afterward, the OMA tools had their performance analyzed in terms of variability in the modal damping ratio's identification, while quantitative along wind and cross

wind damping meaningful results were chased.

- The along wind modal damping ratios were significantly higher than the cross wind case for all methods applied. This highlights the aerodynamic contribution to the overall OWT tower's damping. New simulation standards could aim to settle the different orthogonal tower damping ratios.

- OMA SSI-COV presented a better match with MLD reference than OMA Sing for the cross wind tower mode, assumed as lightly damped. Besides that, the OMA SSI-COV performance appears to be worsened, for the cross wind damping identification, when higher TI factors are revealed.

- The identification of the along wind damping showed to be challenging. A significant limitation was seen for the more complex OMA SSI-COV automated solution. The meteorological and controller condition did not appear to have a clear relationship to this behavior. This suggested that OMA SSI-COV has marked limitations on the identification of highly damped modes, which were not observed for the OMA Sing limited samples.

The mathematical features that might lead to a poor OMA SSI-COV damping identification performance for highly damped modes should be addressed in future works. Besides that, new OMA techniques have been recently classified based on nine different suitability criteria [44] for damping identification. Several transmissibility-based OMA tools showed to be strong participants and could be used to identify Av04 and Av07 datasets.

Concerning OWT tower designs, tuned mass dampers (TMD) may be optimized for the lightly damped cross wind tower mode, improving the structure fatigue lifetime [6].

In this thesis, the OMA tools identified only the tower bending modes of vibrations. Further works could aim to validate their modal analysis in other pivotal modes of the OWTs, such as the blade flapwise collective and edgewise modes, verifying their performance on a broad range of frequencies.

A research limitation of the given thesis that should be re-mentioned is that, due to the lack of quality acceleration records and tower instrumentation, it was not possible to rely the OMA results on simulated and real data from the same OWT design. Such limitation impeded quantitative comparison between simulated and full-scale modal analysis. Future campaigns could work on improving the real Av04 instrumentation and data analytics or in the validation of an Av07 numerical model.

Data Availability Statement

Bibliography

[1] Vahid Valamanesh and Andrew Myers. Aerodynamic damping and seismic response of horizontal axis wind turbine towers. *Journal of Structural Engineering*, 140:04014090, 11 2014. doi: 10.1061/(ASCE)ST.1943-541X.0001018.

[2] Hansen M H Baumgart A Larsen, G C and I Carlen. Modal analysis of wind turbine blades. Feb 2002.

[3] Dmitri Tcherniak, Shashank Chauhan, Michele Rossetti, Iciar Font, Jon Basurko, and Oscar Salgado. Output-only modal analysis on operating wind turbines: application to simulated data. In *Proceedings of European Wind Energy Conference*, pages 1–10, 2010.

[4] Jesús María Pinar Pérez, Fausto Pedro García Márquez, Andrew Tobias, and Mayorkinos Papaelias. Wind turbine reliability analysis. *Renewable and Sustainable Energy Reviews*, 23:463–472, 2013. ISSN 1364-0321. doi: https://doi.org/10.1016/j.rser.2013.03.018. URL https://www.sciencedirect.com/science/article/pii/S1364032113001779.

[5] Muammer Ozbek, Fanzhong Meng, and Daniel Jean Rixen. Challenges in testing and monitoring the in-operation vibration characteristics of wind turbines. *Mechanical Systems and Signal Processing*, 41:649–666, 2013.

[6] Ramtin Rezaei, Paul Fromme, and Philippe Duffour. Fatigue life sensitivity of monopile-supported offshore wind turbines to damping. *Renewable Energy*, 123:450–459, 2018. ISSN 0960-1481. doi: https://doi.org/10.1016/j.renene.2018.02.086. URL https://www.sciencedirect.com/science/article/pii/S0960148118302301.

[7] Wojciech Popko, Matthias L Huhn, Amy Robertson, Jason Jonkman, Fabian Wendt, Kolja Müller, Matthias Kretschmer, Fabian Vorpahl, Torbjørn Ruud Hagen, Christos Galinos, et al. Verification of a numerical model of the offshore

wind turbine from the alpha ventus wind farm within oc5 phase iii. In *International Conference on Offshore Mechanics and Arctic Engineering*, volume 51319, page V010T09A056. American Society of Mechanical Engineers, 2018.

[8] Bart Peeters. System identification and damage detection in civil engineering. 01 2000.

[9] *Validation of Numerical Models of the Offshore Wind Turbine From the Alpha Ventus Wind Farm Against Full-Scale Measurements Within OC5 Phase III*, volume Volume 10: Ocean Renewable Energy of *International Conference on Offshore Mechanics and Arctic Engineering*, 06 2019. doi: 10. 1115/OMAE2019-95429. URL https://doi.org/10.1115/OMAE2019-95429. V010T09A065.

[10] Gayathri Prakash and Harold Anuta. A global energy transformation paper. *International Renewable Energy Agency*, 2019. URL https://www.irena.org/-/media/files/irena/agency/publication/2019/oct/irena_future_of_wind_2019.pdf.

[11] Thomas Carne and George James. The inception of oma in the development of modal testing technology for wind turbines. *Mechanical Systems and Signal Processing*, 24:1213–1226, 07 2010. doi: 10.1016/j.ymssp.2010.03.006.

[12] Morteza Ghalishooyan and Ahmad Shooshtari. Operational modal analysis techniques and their theoretical and practical aspects: A comprehensive review and introduction. *6th International Operational Modal Analysis Conference, IOMAC 2015*, 01 2015.

[13] A. Cunha, E. Caetano, F. Magalhães, and C. Moutinho. Recent perspectives in dynamic testing and monitoring of bridges. *Structural Control and Health Monitoring*, 20(6):853–877, 2013. doi: https://doi.org/10.1002/stc.1516. URL https://onlinelibrary.wiley.com/doi/abs/10.1002/stc.1516.

[14] Doyoung Kim, Byung Kwan Oh, Hyo Seon Park, Hak Bo Shim, and Jiyoung Kim. Modal identification for high-rise building structures using orthogonality of filtered response vectors. *Computer-Aided Civil and Infrastructure Engineering*, 32(12):1064–1084, 2017. doi: https://doi.org/10.1111/mice.12310. URL https://onlinelibrary.wiley.com/doi/abs/10.1111/mice.12310.

[15] Yanchun Ni, Xilin Lu, and Wensheng Lu. Operational modal analysis of a high-

rise multi-function building with dampers by a bayesian approach. *Mechanical Systems and Signal Processing*, 86:286–307, 2017. ISSN 0888-3270. doi: https://doi.org/10.1016/j.ymssp.2016.10.009. URL `https://www.sciencedirect.com/science/article/pii/S0888327016304101`.

[16] Wójcicki, Zbigniew, Grosel, Jacek, Belostotsky, Alexander, Akimov, Pavel, and Sidorov, Vladimir. Oma research of sky tower in wroclaw, poland. *MATEC Web Conf.*, 117:00177, 2017. doi: 10.1051/matecconf/201711700177. URL `https://doi.org/10.1051/matecconf/201711700177`.

[17] F. Magalhães, A. Cunha, and E. Caetano. Vibration based structural health monitoring of an arch bridge: From automated oma to damage detection. *Mechanical Systems and Signal Processing*, 28:212–228, 2012. ISSN 0888-3270. doi: https://doi.org/10.1016/j.ymssp.2011.06.011. URL `https://www.sciencedirect.com/science/article/pii/S0888327011002330`. Interdisciplinary and Integration Aspects in Structural Health Monitoring.

[18] Etienne Cheynet. *Wind-induced vibrations of a suspension bridge: A case study in full-scale.* PhD thesis, 12 2016.

[19] Anela Bajrić, Jan Høgsberg, and Finn Rüdinger. Evaluation of damping estimates by automated operational modal analysis for offshore wind turbine tower vibrations. *Renewable Energy*, 116:153–163, 2018. ISSN 0960-1481. doi: https://doi.org/10.1016/j.renene.2017.03.043. URL `https://www.sciencedirect.com/science/article/pii/S0960148117302355`. Real-time monitoring, prognosis and resilient control for wind energy systems.

[20] J BogunovićJakobsen and Erik Hjorth-Hansen. Determination of the aerodynamic derivatives by a system identification method. *Journal of wind engineering and industrial aerodynamics*, 57(2-3):295–305, 1995.

[21] Rune Brincker and Carlos Ventura. *Introduction to operational modal analysis.* John Wiley & Sons, 2015.

[22] E. Cheynet. Operational modal analysis with single sensor, 2021. URL `https://zenodo.org/record/4487060`.

[23] Technical report.

[24] E. Cheynet. Operational modal analysis with automated ssi-cov algorithm, 2020. URL `https://zenodo.org/record/3774061`.

[25] Etienne Cheynet, Jónas Snæbjörnsson, and Jasna Jakobsen. *Temperature Effects on the Modal Properties of a Suspension Bridge*, pages 87–93. 06 2017. ISBN 978-3-319-54777-0. doi: 10.1007/978-3-319-54777-0_12.

[26] Etienne Cheynet, Nicolò Daniotti, Jasna Jakobsen, and Jónas Snæbjörnsson. Improved long-span bridge modeling using data-driven identification of vehicle-induced vibrations. *Structural Control and Health Monitoring*, 27, 06 2020. doi: 10.1002/stc.2574.

[27] Moritz Häckell and R. Rolfes. Monitoring a 5 mw offshore wind energy converter—condition parameters and triangulation based extraction of modal parameters. *Mechanical Systems and Signal Processing*, 40:322–343, 10 2013. doi: 10.1016/j.ymssp.2013.04.004.

[28] Albrecht Bottcher and Bernd" Silbermann. *Block Toeplitz Matrices*, pages 185–219. Springer New York, New York, NY, 1999.

[29] Lammens S. Heylen, W. and P. Sas. *Modal Analysis Theory and Testing*. Katholieke Universiteit Leuven, Faculty of Engineering, Dept. of Mechanical Engineering, Division of Production Engineering, Machine Design and Automation, 1998.

[30] Chunli Wu, Hanbing Liu, Xuxi Qin, and Jing Wang. Stabilization diagrams to distinguish physical modes and spurious modes for structural parameter identification. *Journal of Vibroengineering*, 19:2777–2794, 06 2017. doi: 10.21595/jve.2017.17629.

[31] Jason Mark Jonkman, Marshall L Buhl, et al. *FAST user's guide*, volume 365. National Renewable Energy Laboratory Golden, CO, USA, 2005.

[32] Samuel J Edwards, Matthew Collette, and Armin Troesch. Wind and wave environments that lead to extreme loads on offshore structures. In *OCEANS 2019-Marseille*, pages 1–6. IEEE, 2019.

[33] Bonnie Jonkman and Jason Jonkman. Fast v8. 16.00 a-bjj. *National Renewable Energy Laboratory*, 2016.

[34] Jason Jonkman, Sandy Butterfield, Walter Musial, and George Scott. Definition of a 5-mw reference wind turbine for offshore system development. Technical report, National Renewable Energy Lab.(NREL), Golden, CO (United States), 2009.

[35] B. Jonkman and Buhl Jr. Turbsim user's guide. 01 2007. doi: 10.2172/15020326.

[36] Etienne Cheynet. Influence of the environmental conditions on the acceleration response of the tower/hub structure of the av07 wind turbine. RAVE Workshop 2021: Presentation 10, 2021. URL https://rave-offshore.de/en/rave-workshop-2021.html.

[37] Matthias Kretschmer, F Schwede, R Guzmán, S Lott, and Po Wen Cheng. Influence of atmospheric stability on the load spectra of wind turbines at alpha ventus. *Journal of Physics: Conference Series*, 1037:052009, 06 2018. doi: 10.1088/1742-6596/1037/5/052009.

[38] B. J. Huebert, B. W. Blomquist, M. X. Yang, S. D. Archer, P. D. Nightingale, M. J. Yelland, J. Stephens, R. W. Pascal, and B. I. Moat. Linearity of dms transfer coefficient with both friction velocity and wind speed in the moderate wind speed range. *Geophysical Research Letters*, 37(1), 2010. doi: https://doi.org/10.1029/2009GL041203. URL https://agupubs.onlinelibrary.wiley.com/doi/abs/10.1029/2009GL041203.

[39] Etienne Cheynet, Jasna Jakobsen, and Jónas Snæbjörnsson. *Wind-induced vibrations monitoring with satellite navigation*, pages 57–64. 09 2016. ISBN 978-1-5108-3590-0.

[40] Etienne Cheynet, Jasna Bogunović Jakobsen, and Jónas Snæbjörnsson. Buffeting response of a suspension bridge in complex terrain. *Engineering Structures*, 128:474–487, 2016. ISSN 0141-0296. doi: https://doi.org/10.1016/j.engstruct.2016.09.060. URL https://www.sciencedirect.com/science/article/pii/S0141029616307660.

[41] Yi Zhou and Limin Sun. Effects of high winds on a long-span sea-crossing bridge based on structural health monitoring. *Journal of Wind Engineering and Industrial Aerodynamics*, 174:260–268, 2018. ISSN 0167-6105. doi: https://doi.org/10.1016/j.jweia.2018.01.001. URL https://www.sciencedirect.com/science/article/pii/S0167610517309091.

[42] Aemilius Vondelen, Alexandros Iliopoulos, Sachin Navalkar, Daan van der Hoek, and J. W. Wingerden. Damping identification of an operational offshore wind turbine using enhanced kalman filter-based subspace identification, 01 2022.

[43] Annette Westerhellweg, Beatriz Cañadillas, Friederike Kinder, and Tom Neu-

mann. Wake measurements at alpha ventus – dependency on stability and turbulence intensity. *Journal of Physics: Conference Series*, 555:012106, dec 2014. doi: 10.1088/1742-6596/555/1/012106. URL `https://doi.org/10.1088/1742-6596/555/1/012106`.

[44] Aemilius A. W. van Vondelen, Sachin T. Navalkar, Alexandros Iliopoulos, Daan C. van der Hoek, and Jan-Willem van Wingerden. Damping identification of offshore wind turbines using operational modal analysis: a review. *Wind Energy Science*, 7(1):161–184, January 2022. doi: 10.5194/wes-7-161-2022.

List of Figures

List of Tables